12-27-2013

Development of a Resource Manager Framework for Adaptive Beamformer Selection

Jeremy P. Stringer

Follow this and additional works at: https://scholar.afit.edu/etd

DEVELOPMENT OF A RESOURCE MANAGER FRAMEWORK FOR ADAPTIVE BEAMFORMER SELECTION

DISSERTATION

Jeremy P. Stringer, Major, USAF

AFIT-ENG-DS-13-D-01

DEPARTMENT OF THE AIR FORCE
AIR UNIVERSITY

AIR FORCE INSTITUTE OF TECHNOLOGY

Wright-Patterson Air Force Base, Ohio

AFIT-ENG-DS-13-D-01

DEVELOPMENT OF A RESOURCE MANAGER FRAMEWORK FOR
ADAPTIVE BEAMFORMER SELECTION

DISSERTATION

Presented to the Faculty

Graduate School of Engineering and Management

Air Force Institute of Technology

Air University

Air Education and Training Command

in Partial Fulfillment of the Requirements for the

Degree of Doctor of Philosophy

Jeremy P. Stringer, BSEE, MSEE

Major, USAF

December 2013
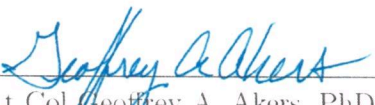
AFIT-ENG-DS-13-D-01
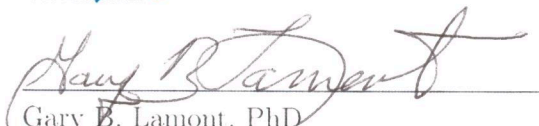
DEVELOPMENT OF A RESOURCE MANAGER FRAMEWORK FOR ADAPTIVE BEAMFORMER SELECTION

Jeremy P. Stringer, BSEE, MSEE
Major, USAF

Approved:

_____
Lt Col Geoffrey A. Akers, PhD
Chairman

6 December 2013
Date

_____
Gary B. Lamont, PhD
Member

9 DEC 2013
Date

_____
Mark E. Oxley, PhD
Member

9 Dec 2013
Date

_____
Julie A. Jackson, PhD
Member

9 Dec. 2013
Date

_____
Lihyeh L. Liou, PhD
Member

09 Dec 2013
Date

Accepted:

_____
Adedeji B. Badiru, PhD
Dean, Graduate School of Engineering
  and Management

9 Dec 2013
Date

AFIT-ENG-DS-13-D-01

Abstract

Adaptive digital beamforming (DBF) algorithms are designed to mitigate the effects of interference and noise in an radio frequency (RF) environment encountered by modern electronic support (ES) receivers. Traditionally, an ES receiver employs a single adaptive DBF algorithm that is part of the design of the receiver system. If the ES receiver is desi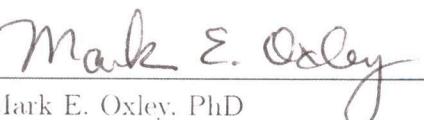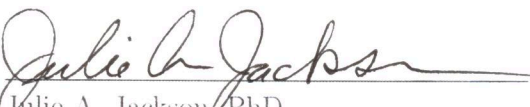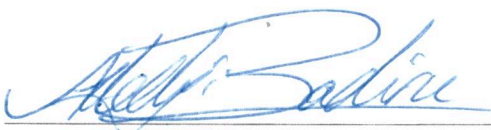gned to form multiple independent beams, the same adaptive DBF algorithm is applied in each beam. Traditional receiver design is effective and works when system processing power is limited. Modern computer technology allows improvements over traditional receiver design, where a receiver is able to change the implemented algorithm based upon system usage. This dissertation provides a new ES receiver framework that attempts to make better use of the available computing resources by adaptively selecting the most efficient DBF algorithm for each beam that is able to meet system requirements. The framework contains a resource manager (RM) that facilitates adaptive algorithm selection through the use of a look-up-table (LUT). The RM estimates parameters of the RF environment, to include the number of signals present in the environment, whether the signals are wideband or narrowband, and their respective directions-of-arrival (DOAs). The parameters of signal relative bandwidth and the number of signals in the environment are used to select an adaptive DBF algorithm from the LUT. The resource manager also contains a method to detect signals-of-interest (SOIs) in the RF environment and to estimate their respective DOAs for use in adaptive DBF implementation. The SOI detection method also indicates the number of independent simultaneous beams the receiver is required to form.

Implementation of the proposed framework requires the development of the adap-

tive DBF LUT. Creation of the LUT requires selecting a set of adaptive DBF algorithms, determining their sensitivity to different environmental parameters, and choosing the *best* algorithm for each member of a selected set of RF environments. The RF environment parameters with the highest sensitivity are used to create the set of RF environments. This dissertation focuses on development and characterization of the RM but provides a representative LUT creation for demonstration purposes. Future users of the framework are required to formulate their own LUT. The methods of the RM, however, are designed to be used intact from the research and implemented with a user generated LUT.

Acknowledgements

All endeavors have a beginning. At the end of this endeavor I would like to remember and thank all who have helped and encouraged me through this process. First thanks goes to my Lord Jesus Christ who being both Alpha and Omega, brought me into this program and has seen me through to the end. A most gracious thanks goes to my wife who agreed to my attending AFIT knowing the long nights and weekends of effort that if required on my part to complete. She has been overly patient with me and I could not have even made it through coursework, much less completed a dissertation without her support.

I also owe a great deal to my advisor Lt Col Akers and Dr. Gary Lamont who mentored both my advisor and myself through the PhD process. Without them this research effort would not exist. I also owe thanks to the remainder of my research committee for their input and guidance at various times throughout the process. All comments and questions helped guide me through the research and produce refunded dissertation represented herein.

I would also like to thank AFRL sensors directorate, not only for their funding of this research and the data they provided, but for their insights and knowledge imparted throughout the last three years. I hope the finished product will be of good use for their future work.

Jeremy P. Stringer

Table of Contents

List of Figures

x

List of Tables

DEVELOPMENT OF A RESOURCE MANAGER FRAMEWORK FOR

ADAPTIVE BEAMFORMER SELECTION

I. Introduction

1.1 Introduction

Designing radio receivers for signal interception and collection, whether for nefarious purposes or good, has been ongoing since Marconi transmitted the first radio signals in the late 1890s [66]. In the "early days" of radio the spectrum was uncrowded and intercepting signals of interest did not require complex processing. Today, the radio frequency spectrum is crowded with competing interests vying for every last Hertz of available bandwidth. The increased number of signals in the available spectrum complicates interception and collection of radio signals. Adaptive digital beamforming (DBF) algorithms counter the increasing spectral complexity by using measurements of the environment to formulate filter weights capable of reducing the effect of interference on signal collection [35, 70, 114]. Even so, the ability to detect and collect low-power sources in a crowded electromagnetic environment, referred to as the "Needle-in-a-Haystack" scenario, is difficult at best [114].

This dissertation proposes a new electronic support (ES) receiver framework, diagrammed in Figure 1, capable of autonomously selecting a *best* adaptive DBF algorithm from a set of adaptive DBF algorithms known to the receiver. The chosen DBF is considered the *best* available algorithm based upon an estimate of the radio frequency (RF) environment intercepted by the receiver's array and available computational resources. The receiver framework selects the best adaptive DBF algorithm
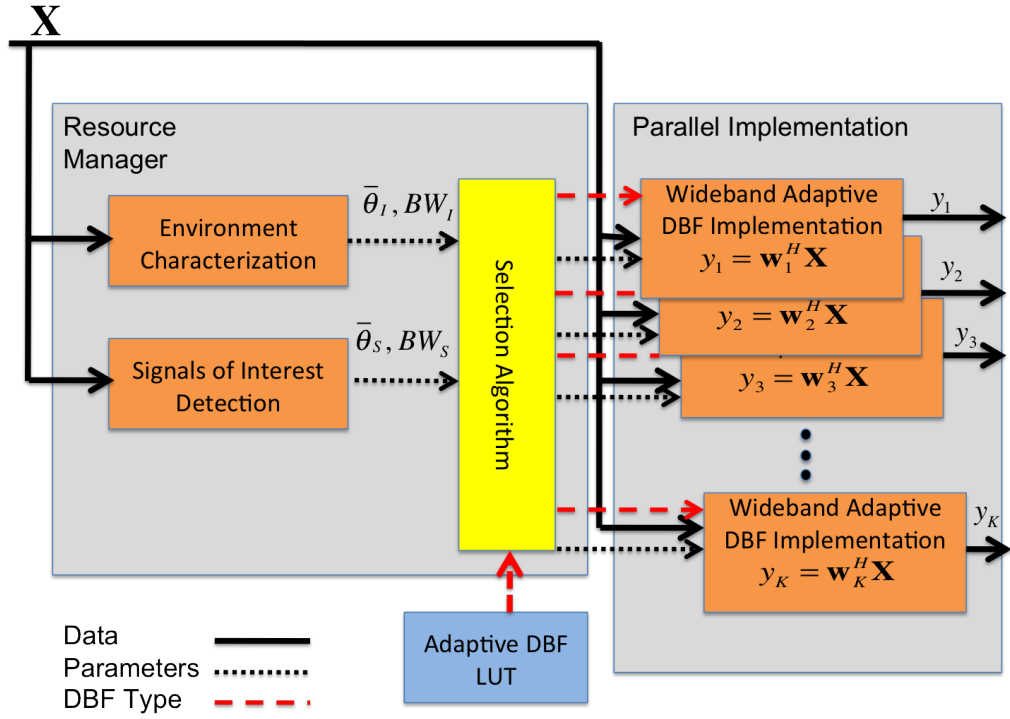
Figure 1. Signal collection receiver structure where X is a matrix of digitally sampled baseband array channel data used by the RM to determine the appropriate adaptive DBF weights

using a resource manager (RM). The RM estimates a set of parameters that characterize the RF environment and selects the adaptive DBF algorithm considered *best* for the environment characterized by the estimated parameters. The choice of what makes an adaptive DBF algorithm *best* for a given scenario is dependent upon the desires of the receiver designer. The RM and the adaptive DBF selection techniques are designed to be reused directly from the framework; however, the implementer is required to choose a set of adaptive DBF algorithms and RF environments and populate a look-up-table (LUT) of adaptive DBF algorithms from which the framework chooses the algorithm based upon the estimated environment parameters. To demonstrate the full function of the ES receiver framework this dissertation creates a LUT of adaptive DBF algorithms based upon their signal-to-interference-plus-noise ratio (SINR) improvement and computational complexity.

The demonstration algorithm selection criteria of computational complexity is from the proposed receiver framework goal of efficient receiver computer resource usage. Using this desire the rule for choosing adaptive DBF algorithms for the LUT is to select the adaptive DBF algorithm that first meets an SINR improvement threshold and has the lowest computational complexity of all algorithms in the chosen set that meet the desired threshold. This decision rule is just one of an infinite number of decision rules based upon receiver designer requirements and is practicable, not necessarily intended to be an optimal decision rule.

The proposed receiver framework expands the current methodologies of adaptive DBF selection while acting as a precursor for future intelligent designs. Adaptive DBF algorithms are chosen for receiver implementation based upon known algorithm performance against different electromagnetic (EM) environments. Classically, the choice of an algorithm is made once during receiver design. Future intelligent systems are likely to implement Haykin's perception-reaction cycle [31]. A static algo-

rithm does not allow for receiver reaction to changing environments such that the *best* algorithm for the environment is being applied. This research presents the first receiver framework to select an adaptive DBF algorithm through perceiving the environment[1]. Furthermore, this receiver framework is the first to consider a second parameter, computational complexity, in the algorithm selection such that the chosen algorithm uses the receiver's resources efficiently. Efficient use of computer resources in the proposed receiver framework is predicated on the use of parallel processing.

1.2 Background

Traditionally ES receivers intercept, detect, characterize, classify, and identify emitters in the electromagnetic environment [18]. The ES receiver design has paralleled the progression of communications systems from narrowband systems to wideband systems and from analog to digital implementations. The transition from narrowband to wideband was necessary as the ES systems adapted to intercept and process the wideband communication signals transmitted by the new communication systems. Also, digital implementation provides access to digital signal processing (DSP) techniques allowing for more sophisticated characterization and classification algorithms [77].

There are two primary types of ES receivers. The ES receiver type most commonly thought of is the radar warning receiver (RWR). The RWR technology is used in combat aircraft to detect enemy integrated air defense system (IADS) threat radars and warn the pilot of incoming anti-air missiles or artillery fire. Primitive RWR detected radar transmissions and provided the direction of the incoming threat radar signal [71, 112]. Modern RWR are more sophisticated and can determine the type of threat radar by measuring the radar's transmission frequency, pulse repetition

---

[1]Perception in the proposed receiver architecture is analogous with measuring/estimating environment parameters.

rate, pulse length, and other characteristics [112]. In this manner RWRs become intelligence gathering instruments as well as providing threat radar data to the pilot. Emitter classification is performed by using DSP to characterize the received radar waveforms in terms of the aforementioned transmission frequency, pulse repetition rate, and pulse length. The RWR forms a pulse descriptor word (PDW) for each pulse and makes classification decisions based upon the PDW.

The second type of ES receiver is the signal collection receiver. Signal collection receivers are applicable to all communications signals in the RF environment [112]. While the receiver can characterize the signal with respect to signal parameters similar to formation of a PDW, such receivers are also designed to decode the transmitted communication signal to collect the information transmitted in the signal. Signal collection receivers often deal with lower power signals-of-interest (SOIs), and therefore must handle signals with lower SINR than the RWR. The difference is due to radar systems using high power transmitters to overcome reflection and round trip losses associated with radar detection [97] and communication SOI employing low probability of intercept techniques. Transmission of low power communication SOIs in a crowded RF environment results in the "needle-in-a-haystack" scenario.

Like the RWR, the signal collection receiver may have to receive, detect, and exploit multiple signals of interest at the same time. There are two ways for an ES receiver to collect multiple signals at the same time, both referred to as forming multiple independent beams. The term "beam" is based on the ability of an array to use constructive and deconstructive interference from multiple antenna array elements to increase the received signal power over a narrow range of receive angles while decreasing the received signal power from all other directions [70]. The two methods of forming multiple independent beams are to apply multiple receiver hardware configurations and use a separate hardware set for each beam, or to use a single set of

hardware and form multiple beams through DSP. Also, it is possible to integrate the two methods to form multiple digital beams for each set of multiple receiver hardware sets [70].

The main advantage of forming multiple beams through hardware is the ability to apply beams in multiple areas of the frequency spectrum simultaneously. As each beam has an independent set of hardware, the RF hardware for each beam can be tuned separately as required. The major disadvantage of applying multiple beams through hardware is the cost, in terms of monetary cost and the size, weight, and power required to implement the required hardware. Adding a beam requires the addition of a complete set of receiver hardware and DSP processing hardware. The main advantage of forming multiple digital beams is the ability to form multiple beams simultaneously in all possible directions allowed by the array. As each beam is implemented in software, adding digital beams requires only an additional computational cost. All beams, however, are required to be in the same frequency range. A hybrid system of multiple hardware receiver configurations, each with the ability to form multiple digital beams, would still have the costs associated with implementing multiple receiver hardware sets. The hybrid system would require fewer hardware configurations than the hardware-only multiple beam implementation, as multiple beams within the same frequency range could be handled by applying multiple digital beams.

One example environment that an ES receiver is expected to operate in is pictured in Figure 2. The scenario demonstrates both how multiple beams are required for a ES signal collection receiver and how interference sources complicate the tasks of detecting and estimating the signal of interest. In this scenario the ES receiver is tasked with collecting the signal transmitted from the global system for mobile (GSM) communication cellphone of a high value target (HVT). In the scenario the

HVT is not the only user of the GSM network. In addition to the GSM users there are interference signals in the environment from appliances such as microwave ovens, radio and television broadcasts from terrestrial and satellite sources, along with other possible noise sources. The ES receiver is on an airborne platform observing the terrestrial scene. The ES receiver must isolate and collect the GSM signal from the HVT. While techniques for RF device fingerprinting can distinguish between different cellular devices [49, 84], these techniques require the signature of the HVT cell phone to be known *a priori*. If the assumption is made that all GSM users are indistinguishable by the receiver, each GSM signal must be considered a SOI and a separate beam formed toward each GSM user.

The inability to distinguish between different GSM users requires that a separate beam is required to isolate each GSM signal for further processing. Furthermore, because of the complex interference environment adaptive DBF is required to effectively estimate the GSM signals. This is true regardless of how the multiple beams are implemented; if multiple receiver hardware sets are used, then an adaptive DBF algorithm is applied to the output of each hardware set. For a single hardware set, multiple adaptive DBF algorithms are applied to the same receiver hardware output.

Before any adaptive DBF algorithm is applied by the ES receiver tasked with collecting the phone call from the HVT, two main questions need to be answered. In what spatial and temporal (spectral)[2] directions is the adaptive beamformer applied? What adaptive DBF algorithm should be used? The first question is partially answered when the ES receiver is tasked. In the current scenario the ES receiver knows what type of signal to collect (GSM), and therefore knows the spectral region in which to apply the adaptive DBF algorithm. The spatial direction and what adaptive DBF algorithm to implement are not as easily determined.

---

[2]The spectral direction of a signal refers to the region in frequency space occupied by the signal.
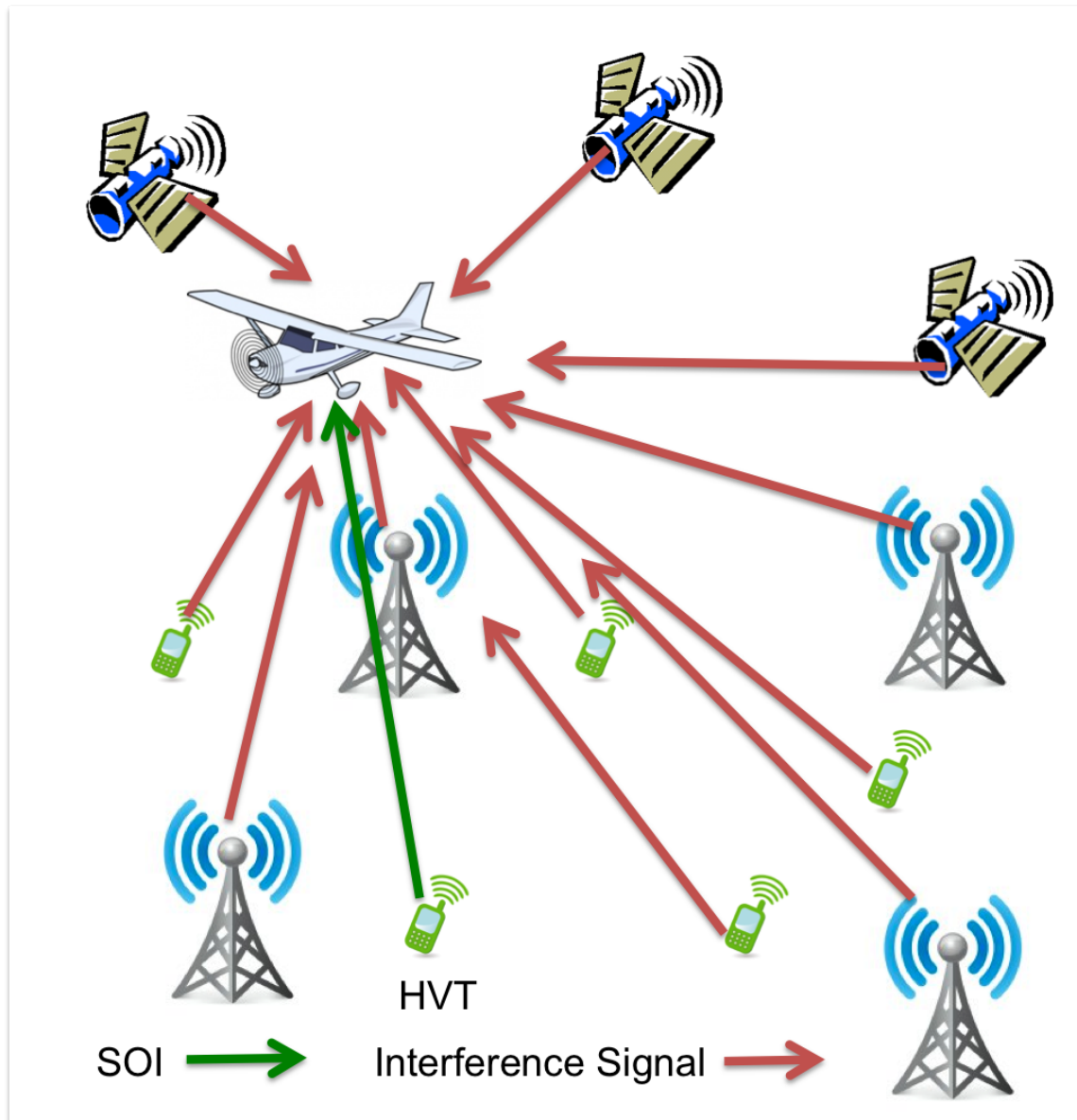
Figure 2. ES receiver notional operation and application.

The ES receiver has no *a priori* knowledge about the directions-of-arrival (DOAs) of the GSM signals, nor the interference signals. The ES receiver must estimate the DOA of the GSM signals and the interference signals. This is similar to the RWR operation in that the RWR determines the direction of threat emitters and notifies the pilot of their location. The RWR receiver also must differentiate between "friend" and "foe" emitters as the ES collection receiver must differentiate between GSM signals and interference signals. The difficulty for the collection receiver arises in that the SOIs often have much less signal power than the interference signals. Whereas, for the RWR all signals are considered to be high power signals. For the scenario depicted in Figure 2, the interference signals can be terrestrial television and radio signals which have the potential of being much higher power than a GSM signal. In either case the ES receiver must use the available data from the environment to determine the angles of arrival of all signals in the environment as well as to differentiate the signals of interest from the interference signals.

The proposed receiver framework separates the SOIs from the interference sources using spatial and spectral filtering operations. Once the SOIs are separated from the interference signals the ES receiver is required to decode the GSM signal. While digital communication techniques are designed to be robust against noise and interference [96], the GSM scenario is just an example and ES receivers are required to decode information from other signal types such as analog communication signals where the decoder requires a signal as close to the transmitted signal as possible. Beamformers are designed to mitigate the effects of interference and noise on a received signal and can be thought of as estimators of the transmitted signal. Beamformers mitigate directional interference sources by placing a directional beam towards a SOI and placing nulls toward all interference signals [70]. Applying an adaptive beamformer estimates the desired SOI by placing a spatial beam, spatial nulls, and removing

noise [33, 70]. The ES receiver task is complete once each SOI is estimated. All of the processing for detecting all SOIs, separating the SOI and interference sources, forming the adaptive filter weights, and estimating each SOI must be completed in enough time to allow the process to repeat quickly enough to track any changes in the EM environment.

1.3 Assumptions

The proposed receiver framework is intended to be applicable to digital receivers that use digitized data for each channel of a multi-element array antenna. The formulations presented throughout this dissertation are based upon an uniform linear array implementation; use of other types of arrays requires utilizing the correct forms of the adaptive DBF algorithms as well as correct forms of the environment parameter estimation algorithms [70, 114]. To ensure that the receiver framework is able to beamform on all SOIs it is assumed that the total number of signals in the environment is less than the degrees of freedom of the implemented array.

Algorithm discussion does not assume any particular computation hardware architecture or software environment. All computations and simulations are performed using Mathworks MATLAB R2012b. MATLAB is chosen due to its ease of implementing matrix equations along with its availability. Because MATLAB is an interpreted language, no direct measurements of computation time are performed and all complexities are given in "big O" notation to be platform agnostic.

1.4 Document Overview

The organization of the rest of the dissertation follows. Chapter Two is a review of literature describing each of the adaptive DBF algorithms applied in the RM. The literature review also covers the spectral estimation and direction of arrival algorithms

used to implement the RM. Literature on cognitive radio (CR) is discussed with respect to the similarities of CR spectral hole detection and signal detection in the RM. An overview of literature with concepts similar to the receiver framework and adaptive algorithm selection concludes the chapter.

Chapter Three provides a detailed development of the proposed receiver framework. The presentation includes a description of how the RM chooses an appropriate adaptive DBF algorithm and provides the algorithm for implementation by the ES receiver. Each functional block of the RM is discussed including the choice of environment estimation and signal of interest detection algorithms. The chapter describes how the electromagnetic environment is parameterized and how the RM handles environments with multiple signals of interest. The chapter also describes the computational efficiency of the RM algorithm including the computational complexities of each functional block of the RM.

Chapter Four contains descriptions of the five adaptive DBF algorithms chosen to demonstrate the receiver framework. The algorithm description section discusses each algorithm and the rationale for choosing the set of algorithms. After the mathematical description of each algorithm, the chapter provides a sensitivity analysis of the algorithms with respect to different environment parameters. The sensitivity analysis is used in developing scenarios to generate the look-up-table of adaptive DBF algorithms chosen by the RM algorithm based upon the sensed environment. All scenarios are listed as well as each algorithm's performance when applied to the given scenario. The performance of each algorithm is presented in terms of the SINR improvement ratio and the computational complexity of the adaptive DBF algorithm. The complexities of each adaptive DBF algorithm are provided with their respective mathematical description. The chapter concludes with the final listing of the LUT for use by the RM algorithm.

Chapter Five provides a validation of the RM. The validation is presented as application of the RM to four data scenarios. The first three scenarios are simulated environments. Each simulated environment is designed to show the RM performance in a specific type of environment. The first scenario contains only wideband interference signals, the second scenario contains only narrowband interference signals, the third scenario contains a mixture of wideband and narrowband interference signals. The final two scenarios are composed of data collected from the Air Force Research Laboratory (AFRL) McWESS and MUD-WASP adaptive array testbeds. Application of the RM against McWESS and MUD-WASP data validates the performance against measured data showing that its applicability is not just theoretical.

Chapter Six provides concluding remarks on how the receiver framework is able to determine the environment and apply an appropriate adaptive DBF algorithm across a wide variety of interference environments. The chapter also provides future areas of research. These future areas of research are continuations of the research presented in this dissertation along with possible research into the application of the receiver framework in an operational receiver system.

II. Literature Review

Adaptive digital beamforming (DBF) algorithms are designed to mitigate the effects of interference and noise incident upon the array of a receiver. Application of an adaptive DBF algorithm is a preprocessing step for electronic support (ES) receivers. An ES receiver is designed to detect and characterize signals-of-interest (SOIs). In an ideal situation there would be neither interference nor noise present in the radio frequency (RF) environment, and the ES receiver would perform whatever characterization algorithms are necessary. Receivers, however, do not operate in ideal conditions, and the RF environment incident upon the receiver's array contains noise and often multiple interference sources. The preprocessing step of beamforming is applied to remove the noise and interference as much as possible and feed a "cleaned up" signal to the post processing algorithms. In this manner, an adaptive DBF algorithm is an estimation algorithm that provides at its output an estimate of the unknown transmitted signal where the estimate is of the desired transmitted signal waveform.

The proposed receiver framework is designed to adaptively choose the *best* adaptive DBF algorithm, based upon the parameterized RF environment, from a set of adaptive DBF algorithms made available to the framework. The criteria of what makes an algorithm the *best* is determined by the framework implementor. For demonstration purposes, this work bases algorithm selection upon signal-to-interference-plus-noise ratio (SINR) improvement and algorithm computational complexity. The SINR improvement is a measure of adaptive DBF algorithm output SINR of a desired signal over the input SINR of the signal with respect to all interference and noise signals in the environment. Algorithm computational complexity is analytically determined for each algorithm chosen for the framework demonstration.

When implementing the receiver framework the implementor must choose a set

of adaptive DBF algorithms for possible selection. The resource manager (RM) of the framework estimates the RF environment parameters and picks the *best* adaptive DBF for an RF environment characterized by the estimated parameters. The five adaptive DBF algorithms chosen for demonstration purposes in this work are the wideband, linearly constrained minimum variance (LCMV) called Frost's algorithm [21], a generalized discrete Fourier transform (GDFT) implementation [65], a time reversal method (TRM) implementation [56, 57], a least squares space-time beamformer (LSSB) implementation [134, 135], and a narrowband LCMV implementation [21].

All the selected adaptive DBF algorithms, estimation algorithms, and detection algorithms used throughout this work are described in terms of a common signal and data model. This chapter first describes the signal and data models. The initial section on the data model also includes the assumptions and notation associated with the model and algorithm descriptions. This chapter then provides a detailed description of the five adaptive DBF algorithms chosen for the framework implementation used as discussion throughout this work. This chapter also provides background on the direction-of-arrival (DOA) estimation algorithms, spectral estimation algorithms, and signal detection algorithms used in the design of the RM portion of the framework. The techniques used for both SOI and interference signal detection are borrowed from the cognitive radio (CR) literature and the background on the multi-taper method (MTM) spectral estimator and generalized likelihood ratio test (GLRT) are presented in terms of their CR usage. The usage of the detector and MTM in CR translate directly to their usage in the RM function of the proposed receiver framework.

2.1 EW Environment Model

The electromagnetic (EM) environment has three main components: the signal of interest, interference signals, and receiver noise. To construct the model first consider the SOI. Define the SOI as a deterministic time function given by

$$s(t) = u(t) e^{-j2\pi f_o t + \psi(t)} , \tag{1}$$

where $u(t)$ is the baseband complex signal representation, f_o is the center frequency, and $\psi(t)$ is a time dependent phase. The complex baseband signal is in general a wideband signal. While there are numerous definitions of what a wideband signal is, [55, 97, 106, 107], for the purposes of this research a wideband signal is one where the instantaneous bandwidth, B, of the baseband signal is greater than 10% of the center frequency, f_o. The SOI is considered to be located in the far field of the receiver and incident upon the receiver at an azimuth angle of ϕ_s, and an elevation angle of θ_s with respect to the look direction of the receiver. Figure 3 provides a graphical representation of scenario geometry.

An interference signal is defined as any signal that is not $s(t)$. DBF algorithms are designed to suppress interference from the measured RF environment. In doing so the DBF algorithms are only concerned with the power and DOA of the interference signals [112]. This allows the interference signals to be modeled as stochastic signals defined by a power spectral density (PSD) and a DOA. Representing each of the $\daleth$ interference signals similar to $s(t)$, the model for each interference signal I_ς is given by

$$I_\varsigma(t) = \varrho_\varsigma(t) e^{-j2\pi f_\varsigma t + \psi_\varsigma(t)}, \quad \varsigma = 1, 2, \cdots, \daleth \tag{2}$$

where $\varrho_\varsigma(t)$ is the complex stochastic envelope of $I_\varsigma(t)$; f_ς and $\psi_\varsigma(t)$ are the center frequency and phase, respectively, for interference signal I_ς. The PSD for $I_\varsigma(t)$ is a
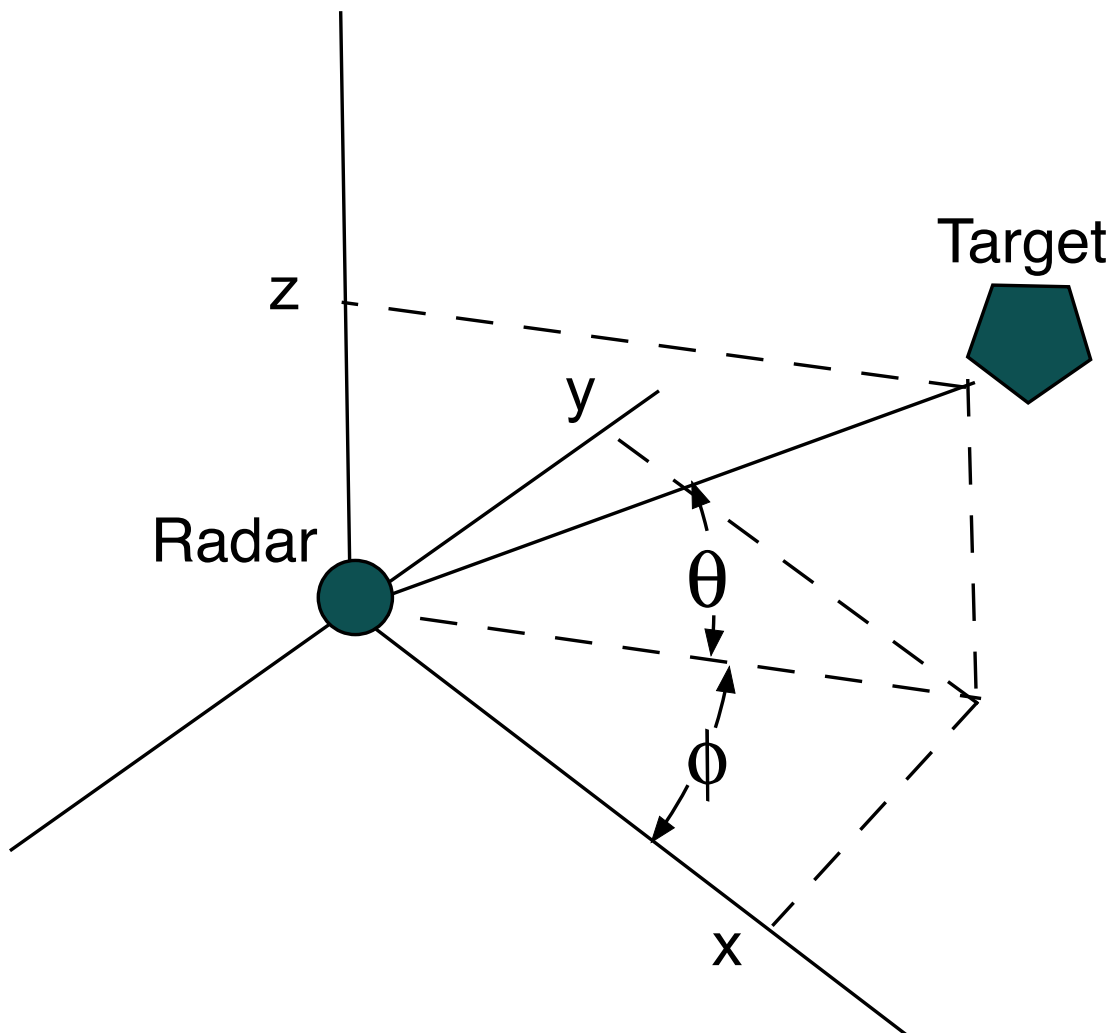
Figure 3. Antenna coordinate frame showing the azimuth ϕ and elevation θ with regard to the beam direction indicated by the target position.

frequency shifted version of the PSD of $\varrho_\varsigma(t)$. Each interference signal is also considered to be wideband and in the far field of the receiver, with azimuth and elevation angles of ϕ_{I_ς} and θ_{I_ς} respective to the receiver look direction. The interference signal power for interferer I_ς is given by: $\gamma^2 = E\left[\varrho_\varsigma(t)\,\varrho_\varsigma(t)^*\right]$, where $E\left[\cdot\right]$ is the expectation operator and $(\cdot)^*$ is complex conjugation.

Thermal noise is modeled as a zero-mean complex white Gaussian stochastic process $n(t)$, with power $\sigma^2_{noise} = E\left[n(t)\,n(t)^*\right]$. The EM environment model is then the superposition of the SOI, interference signals, and noise given by

$$x(t) = s(t) + \left(\sum_{\varsigma=1}^{\daleth} I_\varsigma(t)\right) + n(t). \tag{3}$$

The signal model of (3) is a general model that can incorporate any number of interference sources. The interference sources, as well as the SOI, can be either narrowband or wideband.

2.2 Data Model

All algorithms used in this dissertation are digital and operate on digitized samples of the environment. To keep the data model platform agnostic, the environment as modeled in Section 2.1 is assumed to be sampled and digitized such that Nyquist criteria are met and the bit depth is sufficient to meet all calculation accuracy requirements for the chosen processing system.

To fully develop the data model, consider a system with M channels and K time samples per channel. For channel $m \in \{0, \cdots, M-1\}$, the environment of (3) is sampled as

$$\mathbf{x}_m = [x_m[0], \cdots, x_m[K-1]], \tag{4}$$

17

where each $x_m(k)$ is

$$x_m(k) = s(t - kT - \tau_m) + \left(\sum_{\varsigma=1} I_p(t - kT - \tau_m) \right) + n(t - kT - \tau_m), \quad (5)$$

given T is the system sampling period and τ_m is the delay the signal experiences in traversing from a reference array element to element m. For this work, the reference element is considered to be the leftmost array element and $\tau_0 = 0$. When K samples from the M channels are considered the data can be arranged in matrix form as

$$\mathbf{X} = \begin{bmatrix} \mathbf{x}_0 \\ \mathbf{x}_1 \\ \vdots \\ \mathbf{x}_{M-1} \end{bmatrix}, \quad (6)$$

where the number of data samples can range from one to 16,000 for each of the 64 channels of the MUD-WASP system.

One further restriction to the data model is that the elevation pattern of the simulated array is considered isotropic. This assumption is made to partially model the MUD-WASP system which has a fixed elevation pattern. This limitation simplifies the required steering vectors to only require azimuth specification. Throughout the document all incidence angles are therefore referring only to the azimuthal incidence angle.

2.3 Notation and Terminology

- Scalars are denoted by Roman font lower case (e.g. t)

- Vectors are denoted by Roman bold face, lower case (e.g. $\mathbf{x}$)

- Matrices are denoted by Roman bold face, upper case (e.g. $\mathbf{R}$)

- Estimated quantities are denoted with a hat character (e.g. $\hat{\theta}$)

- Complex conjugation of an object with a superscripted $*$

- Vector or matrix transpose operation is denoted by superscripted T

- Complex conjugate transpose, i.e. the Hermitian transpose vector or matrix, is denoted with superscripted H

- $\| \cdot \|$ denotes the Euclidean norm of a vector

- the propagation speed of RF waves is denoted by c, i.e. the speed of light

Throughout the document the terms *electromagnetic environment* and *interference environment* are used interchangeably. Both terms refer to the combination of directional interference signals and noise as discussed in Section 2.1. In both cases the environment also contains all signals of interest. The RM is broken into different functions referred to as *functional blocks*. Each block contains multiple algorithms used for estimating parameters of the environment from the data matrix. The term *spatial estimate* refers to the estimate of the signals' direction of arrival. Likewise, *spatial beams* refer to angular regions in physical space that are created by applying delay-and-sum beamformers toward a given direction.

2.4 Beamforming

2.4.1 Beamforming Overview.

Beamforming in this work is considered a data time series estimator. The adaptive DBF algorithms operate on sampled array channel data and output an estimate of the desired transmitted signal. Adaptive DBF algorithms operate either on a time sample-by-time sample basis or on a block of time data. For a given time sample the

data from the array is a column vector $\tilde{\mathbf{x}}[k]$ corresponding to the kth column of (6). If a block of data is used the data is represented by an $M \times K'$ sub matrix of (6), where M again corresponds to the number of array channels in the receiver, and K' is the number of samples included in the data block. If a single time sample is used for beamforming the output for time k is found by

$$y[k] = \mathbf{w}^H \tilde{\mathbf{x}}[k] \tag{7}$$

where $\mathbf{w}$ is a column vector of complex filter weights. If the beamformer is a data block implementation the output has a similar form

$$y[k] = \sum_{i,j} \{\mathbf{W}^* \odot \tilde{\mathbf{X}}'[k]\}_{i,j} \tag{8}$$

where $\mathbf{W}$ is an $M \times K'$ block of filter weights, $\tilde{\mathbf{X}}'$ is an $M \times K'$ data block, $\odot$ is the Hadamard product, and the summation is performed for all elements of a $K' \times K'$ matrix of weighted .

The format of the beamformer in (8) is referred to as the delay-and-sum beamformer as it operates by summing over multiple weighted data samples that are separated in time by a known delay. All delay-and-sum beamformers can be written in the form of (7). First stack the columns of both $\mathbf{W}$ and $\mathbf{X}'$ into length MK' column vectors as

$$\mathbf{w}' = \begin{bmatrix} \mathbf{w}_1 \\ \mathbf{w}_2 \\ \vdots \\ \mathbf{w}_{K'} \end{bmatrix} \tag{9}$$

where $\mathbf{w}'_k$ is the k'^{th} column of $\mathbf{W}$. Similarly, create an length MK' column vector

from the data sub matrix $\mathbf{X}'$ as

$$\tilde{\mathbf{x}}' = \begin{bmatrix} \tilde{\mathbf{x}}_1 \\ \tilde{\mathbf{x}}_2 \\ \vdots \\ \tilde{\mathbf{x}}_{K'} \end{bmatrix} \tag{10}$$

where $\tilde{\mathbf{x}}'_k$ is the k'^{th} column of $\mathbf{X}'$. With these two definitions the output of the delay-and-sum beamformer is written as

$$y[k] = \mathbf{w}'^{H} \tilde{\mathbf{x}}'[k] \tag{11}$$

where the k refers to the output at time sample k and $\tilde{\mathbf{x}}'[k]$ represents the data sub matrix from time k to time $k + K'$.

Narrowband beamformers typically apply the form given in (7) and wideband beamformers apply the forms of (8) or (11). The difference is because narrowband beamformers apply a single filter weight to each channel per time sample, while wideband beamformers apply a finite impulse response (FIR) filter to the output of each array channel. The FIR applied to the output of each channel allows the adaptive DBF algorithm to control the beamformer response across multiple angles and frequencies [114], where a single filter weight vector applied at one time sample provides beam pattern control at a single frequency [70, 114]. The weight matrix $\mathbf{W}$ for a wideband beamformer is then a matrix consisting of a length K' row vector of FIR filter weights for each of the M array channels.

The forms of (7), (8), and (11) appear simple but hide the complexity of forming the actual beamforming weights for a given adaptive DBF implementation. The next section provides background on the development of adaptive beamformers in recent history. After the brief history, each of the five adaptive DBF algorithms used in this

21

work are described in detail.

2.4.2 Early Beamforming Practices.

Initial works presenting beamforming in its present sense of adaptive arrays appeared in the 1960s [22–24, 129, 130]. Due to the immaturity of RF sources and modulation techniques, the majority of the research in the 1960s and throughout the 1970s was narrowband focused. The techniques presented in these papers, using analog phase shifters to form complex filter weights and tapped delay lines, are also applicable to wideband adaptive beamforming. Wideband beamforming was introduced first in the context of acoustic direction finding, where the bandwidths of the sources predicated wideband beamforming techniques [6, 15, 44, 93]. The earliest wideband beamforming was used for acoustic direction finding in both air and water.

While analog adaptive array processing advances such as the Rotman lens [88] proved quite capable, the systems could be bulky and sensitive to factors such as temperature and humidity [97]. Gains in adaptive array processing made in recent times are a result of the proliferation of digital computers. Using digital computers allows adaptive techniques such as Weiner and Kalman filtering [33, 70]. These adaptive digital techniques greatly improve the signal-to-noise-ratio (SNR) of modern receivers [70, 77]. Many algorithms such as minimum variance distortionless response (MVDR) and linearly constrained minimum variance (LCMV) are reformulations of the Weiner filter [114]. One powerful algorithm available from digital processing is the least squares derived beamformer that can adaptively place space-time nulls to cancel the effects of numerous interference sources [134, 136, 137]. The problem with the LCMV, MVDR, and least squares techniques is their computational complexities. Computer hardware in the 1970s and into the 1980s was slow, bulky, and costly to implement. The computational capability for the best algorithms was too great for

implementation. Furthermore, to satisfy the Nyquist criteria wideband processing systems such as radar warning receiver (RWR) with bandwidths of 500 MHz [112] required sampling rates greater than 1 GHz. Such analog to digital converters (ADCs) were not available until the 1990s [105, 117]. Given these limitations the earliest digital algorithms were also narrowband in nature.

With modern hardware able to provide the required ADC and processing to realize adaptive wideband DBF algorithm implementation, there is a resurgence of wideband adaptive DBF research. This section covers the recent advances in adaptive wideband array processing applied in the proposed receiver framework. Section 2.4.3 details the development of wideband versions of narrowband adaptive DBF techniques, Section 2.4.4 details modern space-time adaptive techniques for wideband beamforming, Section 2.4.5 details a new beamforming technique based on true time delay beamforming in the digital domain, and Section 2.4.6 details sub-space beamforming methods.

2.4.3 Adaptive Wideband Beamforming.

Narrowband adaptive beamforming continues to be an active research area. Many of the adaptive DBF algorithms developed for narrowband application are simplifications of wideband algorithms. This section details the development in the literature of wideband adaptive beamforming algorithms based on narrowband techniques.

The first mention of adaptive arrays was in a technical report by Applebaum for the Syracuse Research Laboratory [2]. Applebaum derived "control loops" for adapting array channel weights to null out the effects of a jammer in the sidelobe of an array [2]. The method was applicable to narrowband arrays and updated the

array channel weights as

$$\mathbf{w} = \mathbf{w}_q - \left(\frac{p_j}{p_n + M p_j} \right) G\left(\beta_j\right) \mathbf{v}_j^* \tag{12}$$

where $\mathbf{w}_q$ is the quiescent[1] weight for a noise only array, p_j and p_n are the jammer power and noise power, respectively, G is the quiescent beam pattern function, M is the number of array channels, d is array interlement spacing, λ is the wavelength of the transmitted signal,

$$\beta_j = \frac{2\pi d}{\lambda} \sin \phi_j, \tag{13}$$

and

$$\mathbf{v}_j = \left[1, e^{j\beta_j}, \ldots, e^{j(M-1)\beta_j} \right]^T \tag{14}$$

is the jammer steering vector, with ϕ_j ithe jammer incidence angle. The Applebaum beamformer was implemented in analog hardware and provided an effective means for nulling jammers within the sidelobes of the array [2]. If the jammer was in the main lobe of the array, however, the method provided poor performance.

Modern adaptive beamforming algorithms, while having roots with Applebaum, are more directly linked to the work of Widrow, *et al.* [129]. Widrow was the first to apply adaptive filters to the output of antenna arrays [129] and adapted filter weights by choosing the weighs that minimized the mean-squared error of the filter output with respect to the desired signal, leading to development of the least mean squares (LMS) algorithm. If the weight vector $\mathbf{w}$ is considered to be applied at time sample k the LMS update equation for the filter weights at time $k+1$ is given by

$$\mathbf{w}\left(k+1\right) = \mathbf{w}\left(k\right) + k_s \nabla \sigma_y\left(k\right), \tag{15}$$

---

[1]The quiescent weight vector is the vector that would be applied in a noise only environment.

where k_s is a weighting factor and ∇ is the gradient operator. The error between the desired signal d_{sig} at time k and the filter estimate of d provided by applying the filter weights at time sample k is given as

$$\epsilon = d_{sig}(k) - \mathbf{w}^H \mathbf{x}(k). \tag{16}$$

The LMS algorithm requires knowledge of the second order statistics of the desired signal. In situations where this information is available, the LMS algorithm is effective and is referenced in many adaptive antenna and adaptive algorithm books, such as [33, 70]. The algorithms of Widrow are equally applicable to wideband and narrowband signals.

Griffiths reformulated the LMS problem for cases when *a priori* knowledge of the second order statistics [26,27] is not available. Frost made further developments in the area of beamforming by proposing a different constrained least squares beamformer that only requires knowledge of the DOA of the desired signal [21]. Frost solved the beamfomer problem by minimizing the output power of the beamformer while placing a hard constraint in the direction of the main beam. Furthermore, Frost demonstrated that the LMS beamfomer of Griffiths was the same as the Frost beamformer, where soft quadratic constraints were imposed as opposed to the hard constraints of Frost [21]. In addition to imposing hard constraints in the beamforming problem, Frost's iterative algorithm was numerically stable, where the algorithm of Griffiths becomes numerically unstable for long data runs on fixed-precision machines.

The beamformer first published by Frost, is known today as either the MVDR or LCMV beamformer, depending upon whether or not the SOI is present in the training data used to formulate the beamformer weights. The formulation of Frost continues to be an active area of research. Modern research on Frost-type beamformers concentrates on improving the robustness of the algorithm against steering vector

mismatches. One simple method for improving robustness, at the cost of reduced sensitivity, mentioned in most textbooks on the subject, is to diagonally load the covariance matrix of the received data [58, 70, 113]. The works of [1, 20, 108] attempt to improve the algorithms through changing the constraints imposed upon the least squares (LS) problem.

The works of Widrow and Frost [21, 129] while implemented for narrowband receivers at first, are equally applicable to wideband receivers. The transition to wideband receivers in both algorithms requires using the block data approach with a FIR filter used in each array channel. Early work using FIR filters with fewer than ten filter taps per channel showed improved wideband performance over the narrowband beamformer implementations [54, 67, 89, 116]. Rodgers and Compton demonstrated a wideband version of the LMS algorithm employing FIR filters at each channel [86]. The wideband performance of Frost was demonstrated using FIR filters at each array channel in [119, 121].

2.4.3.1 LCMV Beamformer.

The LCMV was first described by Frost [21] as a way to adaptively update filter weights to beamform on a signal in noise. Frost's algorithm was known as the MVDR algorithm. The MVDR was a minimization of the array output variance with a constraint that the beamformer response in a given direction be unaltered. Frost's early beamformer required signal-free training data to form the covariance matrix estimate used in the computation of the filter weights. As in the current context, when training data containing the SOI is unavoidable, the same minimization technique is applied leading to the LCMV beamformer. The following development of the LCMV filter weights follow that of [114].

To fully understand the mathematical description of the LCMV beamformer, first

consider that a beamformer provides an estimate of the SOI time series. The receiver array provides measurements of the electromagnetic environment in the form of sampled array channel data. The array data is written in matrix form of (6). The beamformer is asked to provide an estimate of the desired signal using this set of measured data. As the name would imply, the LCMV provides the DBF weights that minimize the variance of the signal estimate. A signal estimate is given by

$$y[k] = \mathbf{w}^H[k]\tilde{\mathbf{x}}[k], \tag{17}$$

where

$$\mathbf{w} = [w_0, w_1, \cdots, w_{M-1}]^T \tag{18}$$

is the vector of adaptive filter weights at time kT_s for sample time T_s, and $\tilde{\mathbf{x}}[k]$ is the kth column of the data matrix $\mathbf{X}$ from (6) representing a vector of data for all M channels at a single time k.

Each of the measurements $\tilde{\mathbf{x}}[k]$ is a random vector and so the estimate $y[k]$, which is a function of a random vector, is a random variable. The variance of the estimate is then

$$\sigma_y^2 = E\left[(y[k] - \bar{y}[k])(y[k] - \bar{y}[k])^*\right], \tag{19}$$

where $\bar{y}[k]$ is the mean of $y[k]$, $E[\cdot]$ is the expectation operator. Then by substituting equation (17) into (19) the variance of the estimate can be written as

$$\sigma_y^2 = E\left[\left(\mathbf{w}^H[k]\tilde{\mathbf{x}}[k] - \bar{y}[k]\right)\left(\mathbf{w}^H[k]\tilde{\mathbf{x}}[k] - \bar{y}[k]\right)^*\right], \tag{20}$$

where all variables are as defined above. At this point in the literature it is typically assumed that all signals, including the SOI are zero-mean signals. The zero-mean assumption is valid for modulated radio frequency signals that oscillate about zero

volts tending the mean toward zero. The thermal noise is also assumed to be zero-mean noise due to the fact that it occurs from thermal excitation of electrons in the receiver hardware. The assumption of statistically independent signals, interference sources, and noise is also invoked. Under these assumptions the variance (20) becomes

$$
\begin{aligned}
\sigma_y^2 &= E\left[\mathbf{w}^H\left[k\right]\tilde{\mathbf{x}}\left[k\right]\tilde{\mathbf{x}}\left[k\right]^H\mathbf{w}\left[k\right]\right] \\
&= \mathbf{w}^H\left[k\right]E\left[\tilde{\mathbf{x}}\left[k\right]\tilde{\mathbf{x}}\left[k\right]^H\right]\mathbf{w}\left[k\right] \\
&= \mathbf{w}^H\left[k\right]\mathbf{R}_{\tilde{x}\tilde{x}}\mathbf{w}\left[k\right],
\end{aligned}
\tag{21}
$$

where $\mathbf{R}_{\tilde{x}\tilde{x}}$ is the correlation matrix is for the measured data vector $\tilde{\mathbf{x}}$.

Finding the filter weights $\mathbf{w}\left[k\right]$ that minimize (21) creates a filter that minimizes the power output of the DBF. This DBF would tend to eliminate the SOI from the filter output in addition to minimizing the interference and noise contributions to the output. To prevent SOI degradation, the LCMV minimizes (21) subject to the constraint that the signal received from the DOA of the SOI is not distorted. This constraint can be written as

$$
\mathbf{w}^H\left[k\right]\mathbf{v}\left(\phi_s\right) = 1,
\tag{22}
$$

where $\mathbf{v}\left(\phi_s\right)$ is the steering vector toward the SOI defined by

$$
\mathbf{v}\left(\phi_s\right) = \left[1, e^{j2\pi f\frac{d\sin\phi_s}{c}}, e^{j4\pi f\frac{d\sin\phi_s}{c}}, \cdots, e^{j2(M-1)\pi f\frac{d\sin\phi_s}{c}}\right]^T.
\tag{23}
$$

The linearly constrained optimization problem to minimize (21), subject to (22), is solved by the method of Lagrange multipliers [7, 33]. Solution by the method of Lagrange multipliers requires minimization of the Lagrangian cost function

$$
L\left(\mathbf{w}, \lambda\right) = \mathbf{w}^H\left[k\right]\mathbf{R}_{\tilde{x}\tilde{x}}\mathbf{w}\left[k\right] + \mathcal{R}\left[\lambda^*\left(\mathbf{w}^H\left[k\right]\mathbf{v}\left(\phi_s\right) - 1\right)\right],
\tag{24}
$$

where λ is the complex Lagrange multiplier and $\mathcal{R}\left[\cdot\right]$ takes the real part of the enclosed value. To determine the minimum of L in (24) we assume that $\hat{\mathbf{w}}$ is the global minimum. Then a necessary optimality condition is the gradient of L with respect to the filter weights $\mathbf{w}$ is set equal to zero giving

$$\nabla_{\mathbf{w}} L = 2\mathbf{R}_{\tilde{x}\tilde{x}}\mathbf{w} + \lambda \mathbf{v}\left(\phi_s\right) = 0. \tag{25}$$

The solution for the LCMV filter weights is

$$\hat{\mathbf{w}}\left(\lambda\right) = -\frac{\lambda}{2}\mathbf{R}_{\tilde{x}\tilde{x}}^{-1}\mathbf{v}\left(\phi_s\right), \tag{26}$$

where the solution is in terms of the unknown Lagrange multiplier. The Lagrange multiplier is eliminated from (26) by substituting (26) into (22), then solving for the optimal $\hat{\lambda}$ to get

$$\hat{\lambda} = -\frac{2}{\mathbf{v}^H\left(\phi_s\right)\mathbf{R}_{\tilde{x}\tilde{x}}\mathbf{v}\left(\phi_s\right)}. \tag{27}$$

Using (27) in (26), the LCMV filter weights are given as:

$$\mathbf{w}_{LCMV} = \hat{\mathbf{w}}\left(\hat{\lambda}\right) = \frac{\mathbf{R}_{\tilde{x}\tilde{x}}^{-1}\mathbf{v}\left(\phi_s\right)}{\mathbf{v}^H\left(\phi_s\right)\mathbf{R}_{\tilde{x}\tilde{x}}^{-1}\mathbf{v}\left(\phi_s\right)}. \tag{28}$$

The expression for the LCMV filter weights in (28) is correct if the correlation matrix for the measured data and the DOA of the SOI, are known completely. In reality neither of these quantities is known and both must be estimated. Algorithms are available to estimate the DOA of all detectable signals in the environment. The inverse data correlation matrix of $\mathbf{R}_{\tilde{x}\tilde{x}}^{-1}$ can be estimated through the sample matrix inversion (SMI) method [114]. In SMI multiple time samples of the array channel data vector $\tilde{\mathbf{x}}\left[k\right]$ are considered. If K data time samples are available as in (6), then the SMI method first estimates $\mathbf{R}_{\tilde{x}\tilde{x}}$ as the average of the sample correlation matrices

through

$$\hat{\mathbf{R}}_{\tilde{x}\tilde{x}} = \frac{1}{K} \sum_{k=0}^{K-1} \tilde{\mathbf{x}}\left[k\right] \tilde{\mathbf{x}}\left[k\right]^{H}.\tag{29}$$

The inverse of the correlation matrix then entails a standard matrix inversion. Implementation of the LCMV algorithm in (28) is exacted using the given estimates.

A major consideration with algorithms such as the LCMV above is that an inverse computation is required. Matrix inverse algorithms are computational complex and can become numerically unstable when the matrix is poorly conditioned. One method to overcome the instability is to use the Moore-Penrose pseudo inverse [33, 114]. The pseudo inverse is more numerically stable; however, it is still a computationally complex algorithm. To achieve a numerically stable and less complex algorithm, Frost [21] rewrote the LCMV as an iterative algorithm that updates the filter weights based on the current sample of array channel data eliminating the requirement for a covariance matrix inversion. The new method does require a matrix inverse; however the inverse is of a smaller constraint matrix reducing the time required for algorithm computation and increasing computational accuracy.

The following implementation of Frost's algorithm [21] also increases the number of constraints used to determine the LCMV filter weights. By adding constraints beyond (22) the algorithm has greater control over beam pattern at the cost of increased computational complexity. Each new constraint is of the form

$$\mathbf{v}\left(\phi_i\right)^{H}\mathbf{w} = f_i,\tag{30}$$

where ϕ_i is the angle of the new constraint and f_i is the desired beam pattern value in direction ϕ_i. All constraints of the form (30) are written in matrix form as

$$\mathbf{C}^{H}\mathbf{w} = \mathbf{f},\tag{31}$$

where

$$\mathbf{C} = [\mathbf{v}\,(\phi_1)\,,\mathbf{v}\,(\phi_2)\,,\cdots,\mathbf{v}\,(\phi_{N_c})] \tag{32}$$

is a matrix containing the N_c steering vectors for N_c different constraints and

$$\mathbf{f} = [f_1, f_2, \cdots, f_{N_c}]^T\,. \tag{33}$$

The recursive algorithm begins with an initial solution that meets the required constraints

$$\mathbf{w}_0 = \mathbf{C}\left(\mathbf{C}^H\mathbf{C}\right)^{-1}\mathbf{f}. \tag{34}$$

The solution is then updated in the direction of the negative gradient of the LCMV objective equation (24) as

$$\mathbf{w}\,[k+1] = \mathbf{w}\,[k] - \mu\,[\mathbf{R}_{\tilde{x}\tilde{x}}\mathbf{w}\,[k] + \mathbf{C}\lambda\,[k]]\,, \tag{35}$$

where μ is a weighting factor that controls the rate of convergence of $\mathbf{w}\,[k+1]$ and the Lagrange multiplier $\lambda\,[k]$ is found by forcing the solution $\mathbf{w}\,[k+1]$ to meet the LCMV constraints. The weight update equation is then written as [21]

$$\mathbf{w}\,[k+1] = \mathbf{w}\,[k] - \mu\left[\mathbf{I} - \mathbf{C}\left(\mathbf{C}^H\mathbf{C}\right)^{-1}\mathbf{C}^H\right]\mathbf{R}_{\tilde{x}\tilde{x}}\mathbf{w}\,[k] + \mathbf{C}\left(\mathbf{C}^H\mathbf{C}\right)^{-1}\left[\mathbf{f} - \mathbf{C}^H\mathbf{w}\,[k]\right]. \tag{36}$$

Frost used this formulation to emphasize that due to digital computation inaccuracies the term $\mathbf{f} - \mathbf{C}^H\mathbf{w}\,[k]$ is not zero, that is the constraints are not exactly met. This formulation allows for small corrections, required due to numerical inaccuracy, to be made during each iteration to force the new solution to exactly meet the constraints.

For a length M array an M dimensional vector $\boldsymbol{\Xi}$ may be defined as

$$\boldsymbol{\Xi} \triangleq \mathbf{C}\left(\mathbf{C}^{H}\mathbf{C}\right)^{-1}\mathbf{f} \tag{37}$$

and the $M \times M$ matrix

$$\boldsymbol{\beth} \triangleq \mathbf{I} - \mathbf{C}\left(\mathbf{C}^{H}\mathbf{C}\right)^{-1}\mathbf{C}^{H}. \tag{38}$$

The algorithm update may be written as

$$\mathbf{w}\left[k+1\right] = \boldsymbol{\beth}\left[\mathbf{w}\left[k\right] - \mu\mathbf{R}_{\tilde{x}\tilde{x}}\mathbf{w}\left[k\right]\right] + \boldsymbol{\Xi}. \tag{39}$$

Equation (39) is a deterministic constrained gradient descent algorithm requiring knowledge of the input correlation matrix $\mathbf{R}_{\tilde{x}\tilde{x}}$. As stated previously, this matrix is unavailable. Frost's algorithm [21] uses a simple approximation for $\mathbf{R}_{\tilde{x}\tilde{x}}$ available at each iteration. The approximation at each iteration k is simply the outer product of the sampled array channels $\tilde{\mathbf{x}}\left[k\right]$ given as $\tilde{\mathbf{x}}\left[k\right]\tilde{\mathbf{x}}\left[k\right]^{H}$. Substitution of this estimate for $\mathbf{R}_{\tilde{x}\tilde{x}}$ into (39) provides the final format of Frost's adaptive LCMV formulation [21] as

$$\begin{aligned}
\mathbf{w}\left[0\right] &= \boldsymbol{\Xi} \\
\mathbf{w}\left[k+1\right] &= \boldsymbol{\beth}\left[\mathbf{w}\left[k\right] - \mu y\left[k\right]\tilde{\mathbf{x}}\left[k\right]\right] + \boldsymbol{\Xi}.
\end{aligned} \tag{40}$$

Frost's algorithm [21] derivation up to this point has been applicable to narrow-band sources only. This is evidenced in the formation of the data vector $\tilde{\mathbf{x}}$ and steering vector $\mathbf{v}\left(\phi_i\right)$, which is only a function of arrival angle. LCMV algorithms, to include Frost's implementation, naturally extend to the wideband data case by defining a wideband data matrix, a wideband steering vector, and a wideband weight matrix based upon the wideband receiver design.

Receivers designed for wideband data have an FIR filter at the output of each array channel in place of a single adaptable filter weight [35, 70, 114]. The FIR filter implementation allows for beam constraints to be placed at multiple angles during wideband beam pattern design. Narrowband DBF algorithms can use FIR filter taps at each channel; however, for narrowband signals a single filter weight can provide adequate beam control. The addition of the FIR filters adds unnecessary complexity for narrowband signals. How much the beam pattern can be affected over a range of frequencies is dependent upon the number of filter taps in each FIR filter. The number of taps for each channel need not be fixed; for this research effort, however, the number of FIR filter taps is assumed to be constant across all array channels. The format of the wideband data matrix, wideband steering vector, and wideband data matrix depend on the number of filter taps in the receiver.

Because the single filter weight for each array channel is replaced by an FIR filter, wideband adaptive DBF algorithms must derive filter weights for each filter tap of each array channel. For J filter taps per channel, this amounts to $M \times J$ weights per update cycle. The filter weights can be arranged in matrix form, where $\mathbf{W}_{i,j}$ is the weight for the jth filter tap of the ith array channel. To implement the LCMV algorithm, however, a filter weight vector is required. To form a vector, consider the form of the filter weight matrix as

$$\mathbf{W} = [\mathbf{w}_1, \mathbf{w}_2, \cdots, \mathbf{w}_J] \tag{41}$$

with

$$\mathbf{w}_j = [w_{1,i}, w_{2,i}, \cdots, w_{M,i}]^T. \tag{42}$$

By stacking the columns of $\mathbf{W}$ such that

$$\mathbf{w}' = \left[\mathbf{w}_1^T, \mathbf{w}_2^T, \cdots, \mathbf{w}_J^T \right]^T \tag{43}$$

the wideband weights are in a vector form that can be used in the LCMV algorithm.

The data matrix (6) is also reformatted to provide the correct array sample values for algorithm implementation. The new wideband data vector $\mathbf{x}'$ is formed as

$$\mathbf{x}' = \left[\tilde{\mathbf{x}} \left[0 \right]^T, \tilde{\mathbf{x}} \left[1 \right]^T, \cdots, \tilde{\mathbf{x}} \left[J - 1 \right]^T \right]^T. \tag{44}$$

To develop the implementation of the steering vector $\mathbf{v}(\phi_i)$ used in wideband adaptive algorithm consider the narrowband steering vector of (23), where the steering vector is for a single frequency and for a given time sample. Advancing one sample period, the time between filter taps, advances the phase in the exponential by ωT_s where $\omega = 2\pi f$. Wideband steering vectors apply the appropriate phase delay to array data simultaneously at multiple sample times. If the steering vector of (23) is considered the delay for zero delay then the required delay to phase correct for the sample vector at $k = 1$ is

$$\mathbf{v}(\phi_i)_{k=1} = \left[1, e^{j\omega \frac{d \sin \phi_i}{c} + \omega T_s}, e^{j2\omega \frac{d \sin \phi_i}{c} + \omega T_s}, \cdots, e^{j(M-1)\omega \frac{d \sin \phi_i}{c} + \omega T_s} \right]^T. \tag{45}$$

Noting (23) as $\mathbf{v}(\phi_i)_0$ and (45) as $\mathbf{v}(\phi_i)_1$, then extending the development to all J time delays for each tap of the FIR filter applied to each channel

$$\mathbf{v}(\phi_i)_k = \left[1, e^{j\omega \frac{d \sin \phi_i}{c} + \omega k T_s}, e^{j2\omega \frac{d \sin \phi_i}{c} + \omega k T_s}, \cdots, e^{j(M-1)\omega \frac{d \sin \phi_i}{c} + \omega k T_s} \right]^T. \tag{46}$$

the multi-delay steering vector containing the phase shifts for each channel at multiple

sample times is written as:

$$\mathbf{v}\left(\phi_i\right)_{WB} = \left[\mathbf{v}\left(\phi_i\right)_0^T, \mathbf{v}\left(\phi_i\right)_1^T, \cdots, \mathbf{v}\left(\phi_i\right)_{J-1}^T\right]^T, \tag{47}$$

where the steering vector is derived for a single frequency f and a single angle ϕ_i. To implement wideband algorithms a steering vector is created for each frequency of interest and used in the adaptive DBF implementation.

In the wideband implementation of Frost's algorithm [21], the above defined wideband data vector, weight vector, and steering vectors directly replace their narrowband counterparts $\tilde{\mathbf{x}}[k]$, $\mathbf{w}[k]$, and (23) respectively. The final form of Frost's algorithm [21] defined in (40) becomes:

$$\begin{aligned} \mathbf{w}'[k+1] &= \mathbf{J}\left[\mathbf{w}'[k] - \mu y[k]\mathbf{x}'[k]\right] + \mathbf{\Xi}, \\ \mathbf{w}'[0] &= \mathbf{\Xi} \end{aligned} \tag{48}$$

where $y[k] = \mathbf{w}'^H[k]\mathbf{x}'[k]$.

One last implementation issue of the wideband Frost algorithm [21] is the constraint definition. The algorithm now has the ability to place constraints on a beam pattern in both the spatial and temporal domains. This requires an additional constraint for every angle-frequency pair where the weight vector and steering vectors in (30) and (31) are replaced with the appropriate wideband weight and steering vector formats. The wideband steering vectors and weight vector replace the narrowband versions in (30) through (38) and the adaptive DBF algorithm processing proceeds the same as for the narrowband case. This additional control over the beam pattern has a corresponding increase in computational complexity from the increase in vector size and the increased number of constraints forming $\mathbf{C}$.

The computational complexity of the LCMV algorithm is derived from (40) and

the precursor equations (37) and (38). For N_c constraints and an M-element array with J filter taps on each channel, $\boldsymbol{\Xi}$ has a complexity of $O\left(N_c^3 + MJN_c^2 + MJN_c\right)$. The cubic in the complexity is for the matrix inverse, and the remaining terms are from matrix multiplications. Calculation of $\boldsymbol{\beth}$ utilizes some of the computations from $\boldsymbol{\Xi}$ and adds $O\left((MJ)^2 N_c + (MJ)^2\right)$ complexity for additional matrix multiplications and additions. The computation of $\boldsymbol{\Xi}$ and $\boldsymbol{\beth}$ are only required once for the algorithm. Frost's algorithm [21] then iterates towards an optimal solution with a per iteration cost of $O\left((MJ)^2 + MJ\right)$ for additional matrix multiplications and additions. In operation, Frost's algorithm [21] converges quickly, and $\mathbf{w}$ can be considered stable after only a few iterations. This allows the recursive nature of the algorithm to be absorbed into the big-O notation such that the computational complexity of the Frost algorithm [21] can be written as

$$O\left(N_c^3 + MJN_c^2 + (MJ)^2 N_c + (MJ)^2 + MJN_c + MJ\right). \tag{49}$$

Figure 4 shows a representative LCMV beamformer beam pattern for eight different normalized frequencies. The beamformer was created to have a peak at 0° and to null an interference source at -30°. While there is no distinct null at -30° the sidelobe pattern is down over 30 dB at -30°. The null placed by the LCMV algorithm is not clearly visible because of its narrowness; however the LCMV algorithm does place a null in the beampattern where interference sources are located.

2.4.4 Data Independent Space-Time Beamforming.

The data dependent LCMV beamformers use the sampled array data to produce filter weights. The adaptive DBF algorithms form nulls in the direction of interference sources present in the data across the instantaneous bandwidth of the array. It is possible to formulate a space-time beam pattern placing nulls in given directions and
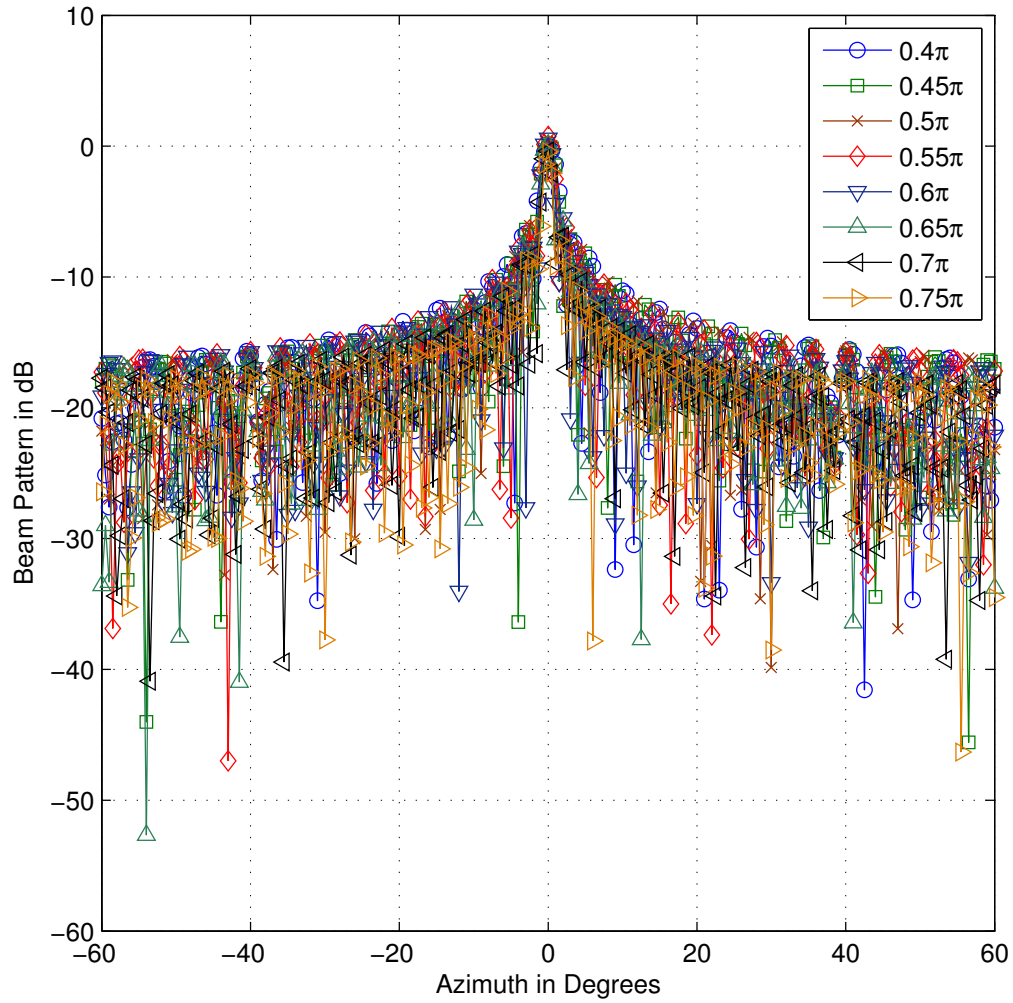
Figure 4. **Multiple beampattern frequency cuts for the linearly constrained minimum variance beamformer with a main beam at 0° and an interference source at -30°. Each frequency cut is for a normalized frequency between 0 and π.**

at given frequencies without using sampled array data. The beamformer weights are formed using the method of least squares to minimize the Euclidean distance between a desired beam pattern and the beam pattern formed by the filter weights. The general problem formulation is written as [72]

$$\min_{\hat{\mathbf{r}},\omega} \|\mathbf{H}_{arr}(\hat{\mathbf{r}},\omega) - \mathbf{H}_{ref}(\hat{\mathbf{r}},\omega)\| \tag{50}$$

where $\mathbf{H}_{arr}(\hat{\mathbf{r}},\omega)$ is the beam pattern due to the calculated filter weights at all points in space $\hat{\mathbf{r}}$ at given frequency ω, and $\mathbf{H}_{ref}(\hat{\mathbf{r}},\omega)$ is the desired, or reference beam pattern at all spatial points for the given frequency; $\|\cdot\|$ is the L_2 norm. Applying the minimization problem of (50) at all frequencies of interest allows for control of the beampattern at all angles and frequencies of interest for the beamformer designer. Solving for a specific beam pattern that varies in frequency for each angle is computationally intractable for a large number of frequencies and angles. In practice beamformer designers place frequency invariant constraints on the problem where the angle response is constrained to be constant across all frequencies of interest [134, 136, 137]. The frequency invariant constrained minimization problem is solvable using least squares as demonstrated in [134, 137]. In a few cases for specific constraints, moving away from frequency invariance allows for solvability using the methods of convex optimization [39, 118, 120]. The computational complexity of the convex methods is usually greater than direct solution of the LMS problem. This research applies a frequency invariant form of the beamformer of (50) denoted as the LSSB.

2.4.4.1 LSSB Algorithm.

The LSSB determines the wideband filter weights by attempting to minimize the Euclidean distance between the designed beam pattern $F(\omega, \phi)$ output and a desired

beam pattern shape $\beth(\omega, \phi)$. LSSB beamformers are not adaptive in the traditional sense as they do not update the filter weights based upon measurements of the environment but place space-time nulls in the wideband beam pattern. Adaptation occurs by placing space-time nulls in the beam pattern at those locations where interference sources are estimated to exist. When the RM senses that the electromagnetic environment has changed, new filter weights are formed to account for the changes and place the required space-time beams.

The following development of the LSSB uses the wideband weight vector (9), data vector (10), and steering vector (47) representations [134, 136, 137]. Beam patterns for all adaptive filters are constructed by applying the derived filter weights to a set of steering vectors that span the range of frequencies and angles over which the beam pattern is designed. Application of the LSSB to a single steering vector is given as $y_b = \mathbf{w}'^H \mathbf{v}_{WB}(\omega, \phi)$, where the steering vector is now considered as a function of space and time consistent with (47). Algorithm weight solution requires the minimization of the Euclidean distance between the beam pattern $F(\omega, \phi)$, comprised of the filter output y_b for all desired frequencies and angles, and a desired beampattern $\beth(\omega, \phi)$. If the minimization is considered over the possible range of frequencies and angles for the array, the LS cost function is

$$J_{LS} = \int_\Omega \int_\Phi \left| \mathbf{w}'^H \mathbf{v}_{WB}(\omega, \phi) - \beth(\omega, \phi) \right|^2 d\omega d\phi, \tag{51}$$

where Ω and Φ represent the frequency range and angle range of interest, respectively.

As with the LCMV algorithm, a distortionless algorithm is desired such that the SOI is passed through unmodified and the interference sources are reduced to a sufficiently low level. This leads again to a constrained optimization problem. The simplest form of the LSSB minimizes (51) and does not form specific space-time nulls but ensures that the response to all signals except the SOI is kept to a low level.

The distortionless constraint requires constraining $\beth(\Omega_s, \phi_s) = 1$ where Ω_s is in the frequency range of the SOI and ϕ_s is the DOA of the signal of interest. The resulting optimization problem is then [134, 136, 137]

$$\min_{\mathbf{w}'} \ J_{LS} \text{ subject to } \beth(\Omega_s, \phi_s) = 1. \tag{52}$$

There is, in general, no closed form solution to (52). The solution is found by first discretizing the field of regard of the array into a uniformly spaced grid of $(\Omega_\eta, \phi_\kappa)$ frequencies and angles [134, 136, 137]. Once the frequency-angle space has been discretized, the cost function can be broken into two cost functions. The first cost function minimizes the Euclidean distance between the algorithm output and the beam pattern shape in the constraint area. The second constraint minimizes the power outside of the constrained frequencies and angles. Using this discretization and split, the LS cost function of (51) becomes [134, 136, 137]

$$J_{LS} = \sum_{\omega \in \Omega_s} \sum_{\phi \in \Phi_s} \left| \mathbf{w}'^H \mathbf{v}_{WB}(\omega, \phi) - 1 \right|^2 + \alpha \sum_{\omega \notin \Omega_s} \sum_{\phi \notin \Phi_s} \left| \mathbf{w}'^H \mathbf{v}_{WB}(\omega, \phi) \right|^2, \tag{53}$$

where α is a control parameter that can be used to tradeoff mainbeam and sidelobe performance. Then , for notational convenience, denote

$$\mathbf{V}(\omega, \phi) = \mathbf{v}_{WB}(\omega, \phi) \mathbf{v}_{WB}^H(\omega, \phi), \tag{54}$$

which allows the definition of

$$\mathbf{Q}_{LS} \triangleq \sum_{\omega \in \Omega_s} \sum_{\phi \in \Phi_s} \mathbf{V}_R(\omega, \phi) + \alpha \sum_{\omega \notin \Omega_s} \sum_{\phi \notin \Phi_s} \mathbf{V}_R(\omega, \phi), \tag{55}$$

where $\mathbf{V}_R(\omega, \phi)$ is the real part of $\mathbf{V}(\omega, \phi)$; also denote

$$\mathbf{a} = \sum_{\omega \in \Omega_s} \sum_{\phi \in \Phi_s} \mathbf{v}_{WB}(\omega, \phi). \tag{56}$$

Finally, let

$$d_{LS} = \sum_{\omega \in \Omega_s} \sum_{\phi \in \Phi_s} 1. \tag{57}$$

Using (54) through (57) allows the rewriting of (53) in quadratic form as

$$J_{LS} = \mathbf{w}'^H \mathbf{Q}_{LS} \mathbf{w}' - 2\mathbf{w}'^H \mathbf{a} + d_{LS}, \tag{58}$$

the solution of which is recognized to be

$$\mathbf{w}'_{LS} = \mathbf{Q}_{LS}^{-1} \mathbf{a}. \tag{59}$$

Another way to formulate the LSSB algorithm is to apply a frequency invariance constraint to (51) [134, 136, 137]. Consider again a discretization of angles and frequencies (ω, ϕ). The adaptive array beampattern is first constrained to be invariant over the bandwidth of the SOI through the definition of a spatial variation (SV) cost function that replaces (53). The SV cost function is

$$SV = \sum_{\omega \in \Omega_i} \sum_{\phi \in \Phi_{FI}} \left| \mathbf{w}'^H \mathbf{v}(\omega, \phi) - \mathbf{w}'^H \mathbf{v}(\omega_r, \phi) \right|^2, \tag{60}$$

where ω_r is a reference frequency and Φ_{FI} is the spatial angle range over which the frequency invariance is considered. The frequency invariance can be forced over the main beamwidth of the adaptive LS beamformer or over the entire field of regard of the array. For the purposes of this research, the frequency invariance will be kept over the entire spatial field observable by the array.

The adaptive LS beamformer is again constrained to have low sidelobe levels by also considering the secondary cost function [134, 136, 137]

$$J_1 = \sum_{\phi \in \Phi_{sl}} \left| \mathbf{w}'^H \mathbf{v}(\omega_r, \phi) \right|^2, \tag{61}$$

where Φ_{sl} is the set of angles in the spatial sidelobes and ω_r is the same reference frequency as in (60). Because the beamformer is not able to form an arbitrarily narrow main beam, the constraint of minimizing over all angles that are not the DOA of the SOI is relaxed to allow for a more generally defined sidelobe region.

Now that the beamformer has been designed to have a frequency invariance with respect to a reference frequency, a distortionless mainbeam is forced over all frequencies by defining the linear constraint [134, 136, 137]

$$\mathbf{w}'^H \mathbf{v}(\omega_r, \phi_s) = 1, \tag{62}$$

where ω_r is again the reference frequency and ϕ_s is the DOA of the SOI. The two cost functions (60) and (61) and the constraint (62) can now be combined to form the constrained LS problem [134, 136, 137]

$$
\begin{aligned}
J_{CLS} &= \sum_{\eta=0}^{\mathcal{N}-1} \sum_{\kappa=0}^{\mathcal{K}-1} \left| \mathbf{w}'^H \mathbf{v}(\omega_\eta, \phi_\kappa) - \mathbf{w}'^H \mathbf{v}(\omega_r, \phi_\kappa) \right|^2 + \beta \sum_{\phi_\kappa \in \Phi_{sl}} \left| \mathbf{w}'^H \mathbf{v}(\omega_r, \phi_\kappa) \right|^2 \\
&\text{subject to } \mathbf{w}'^H \mathbf{v}(\omega_r, \phi_s) = 1,
\end{aligned}
\tag{63}
$$

where β is a control parameter, and $\mathcal{N}$, $\mathcal{K}$ are the number of discrete frequencies and angles, respectively, considered for frequency invariance. The constrained LS problem of (63) can be solved using Lagrange multipliers, as was done for previous beamformers.

As of yet, the full capability of the LSSB has not been implemented. The LSSB

can apply space-time nulls towards interference sources. Space-time nulls are created by adding constraints similar to (62) to the LS problem of (63). If there exist ℸ interferences, a series of ℸ nulls, up to the degrees-of-freedom of the array, can be formed through the constraint equations

$$\mathbf{w}'^{H}\mathbf{v}\left(\omega_{\eta},\phi_{\varsigma}\right)=\epsilon_{\varsigma},\ \text{for all}\ \omega\in\Omega_{I}, \tag{64}$$

where Ω_{I} is the set of frequencies over which the interference sources are to be minimized and each ϵ_{ς} is a small value to limit the adaptive DBF response in the given direction and frequency band. If a steering vector matrix is defined as

$$\mathbf{C}=\left[\mathbf{v}\left(\omega_{1},\phi_{1}\right),\cdots,\mathbf{v}\left(\omega_{\mathcal{N}},\phi_{1}\right),\mathbf{v}\left(\omega_{1},\phi_{2}\right),\cdots,\mathbf{v}\left(\omega_{\mathcal{N}},\phi_{\daleth}\right)\right], \tag{65}$$

and a constraint vector as

$$\mathbf{f}=\left[1,\epsilon_{1},\cdots,\epsilon_{2},\cdots,\epsilon_{\varsigma},\cdots,\epsilon_{\daleth}\right]^{T}, \tag{66}$$

then the constraints of (62) and (64) can be combined into one constraint equation

$$\mathbf{C}^{H}\mathbf{w}'=\mathbf{f}. \tag{67}$$

Then forming an auxillary matrix similar to (55) as

$$\begin{aligned}\mathbf{Q}_{CLS}\ &\triangleq\ \sum_{\eta=0}^{\mathcal{N}-1}\sum_{\kappa=0}^{\mathcal{K}-1}\left(\mathbf{v}\left(\omega_{\eta},\phi_{\kappa}\right)-\mathbf{v}\left(\omega_{r},\phi_{\kappa}\right)\right)\left(\mathbf{v}\left(\omega_{\eta},\phi_{\kappa}\right)-\mathbf{v}\left(\omega_{r},\phi_{\kappa}\right)\right)^{H}\\ &+\beta\sum_{\phi_{\kappa}\in\Phi_{sl}}\mathbf{V}\left(\omega_{r},\phi_{\kappa}\right),\end{aligned} \tag{68}$$

the LS optimization problem of (63) can be written as a new constrained optimization

problem

$$\min_{\mathbf{w}'} J_{CLS} = \min_{\mathbf{w}'} \mathbf{w}'^H \mathbf{Q}_{CLS} \mathbf{w}' \text{ subject to } \mathbf{C}^H \mathbf{w}' = \mathbf{f}, \qquad (69)$$

where the DBF weights $\mathbf{w}'$ are now designed to place space-time nulls toward interference sources in addition to reducing noise.

The linearly constrained adaptive DBF weights of (69), due to the form of the constraint equation $\mathbf{C}$, can no longer be derived using the Lagrange multiplier method. The problem of (69) is a linearly constrained quadratic problem, which can be solved using semi-definite programming (SDP) [7, 39, 40, 118, 120, 131]. Each SDP solution of (69) creates a joint domain adaptive wideband DBF. As the electromagnetic environment is constantly changing, the problem needs to be resolved periodically. This allows the DBF algorithm to track moving emitters as well as null interferes as they appear and disappear from the electromagnetic environment.

One issue with SDP solvers is they are iterative algorithms, and therefore no set computational complexity is available. Research in SDP solvers has demonstrated complexities of equal or lesser values than Lagrange multiplier algorithms [7]. For implementation in actual ES systems, SDP solvers may allow for complex space-time beams to be formed with low computational complexity. Each implementation would have to be tested individually to determine how the complexity of the SDP solver compares with the complexities of the other possible adaptive DBF algorithms. This research is intended to demonstrate the proposed receiver framework performance and is not meant to be inclusive of all adaptive DBF algorithms. Thus, only the Lagrange mulitplier defined LSSB [134, 136, 137] is considered for inclusion in the look-up-table (LUT); this allows for a closed form solution of the LSSB computational complexity for adaptive DBF algorithm performance comparisons.

The computational complexity of the LSSB is from two main computations. The first is the derivation of $\mathbf{Q}_{LS}$ and $\mathbf{a}$ from (55) and (56) respectively. The number

of computations is dependent upon how the space-time coordinates are discretized. Consider N_Ω frequency points and N_ϕ angular subdivisions. Then, considering the $MJ \times 1$ space time steering vectors $\mathbf{v}(\Omega_\eta, \phi_\kappa)$ the number of computations to determine $\mathbf{Q}_{LS}$ is $O\left(N_\Omega N_\phi (MJ)^2\right)$. To calculate $\mathbf{a}$ requires and additional $O\left(N_\Omega N_\phi MJ\right)$ computations.

The second major computation for the LSSB algorithm is the inverse required in (63). The matrix $\mathbf{Q}_{LS}$ is $MJ \times MJ$ requiring $O\left((MJ)^3\right)$ computations to find the inverse. The final multiplication to find the filter weights $\mathbf{w}_{LS}$ requires an additional $O\left((MJ)^2\right)$ computations. The final computational complexity for the LSSB is then

$$O\left(N_\Omega N_\phi (MJ)^2 + N_\Omega N_\phi MJ + (MJ)^3 + (MJ)^2\right). \tag{70}$$

The dominant terms in the complexity are $N_\Omega N_\phi (MJ)^2$ and $(MJ)^3$. To keep computations low the number of frequency and azimuthal sample points are kept low on the same order of the number of array channels and FIR filter taps allowing the overall complexity of the LSSB to be written as $O\left((MJ)^3\right)$.

Figure 5 shows a representative least squares formed frequency invariant beamformer (FIB). The mainbeam is toward 0° and a null is placed toward -30°. The least squared beamforer is able to place deep nulls of greater than 40 dB down toward interference sources as demonstrated in the beamformer plot.

2.4.4.2 Fourier Transform Based Frequency Invariant Beamformer.

A less computationally complex FIB is formed by applying an inverse fast Fourier transform (FFT) to a frequency angle map of the desired beamformer response [13, 59–62, 65, 74, 92]. In the notation of [63], the less computationally complex algorithm

45
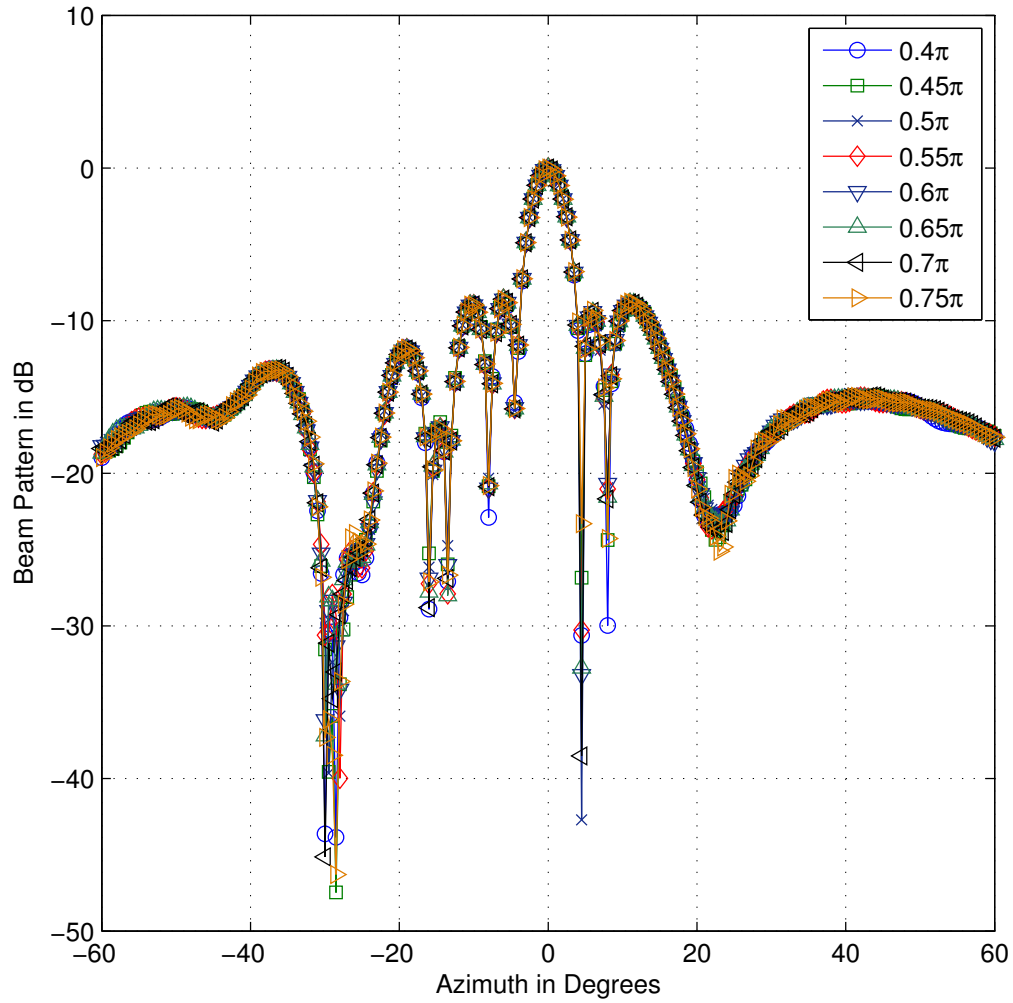
Figure 5. Multiple beampattern frequency cuts for the least squares space-time beamformer (LSSV) with a main beam at 0° and an interference source at -30° where each data set is a normalized frequency cut of the space-time beamformer beam pattern.

first forms a nominal narrowband beam pattern

$$P\left(\omega, \phi\right) = \int_{-\infty}^{\infty} e^{-j\frac{\omega \sin \phi}{c}x} D\left(x, \omega\right) dx, \tag{71}$$

at an arbitrary frequency ω and angle ϕ where

$$D\left(x, \omega\right) = \int_{-\infty}^{\infty} d\left(x, t\right) e^{-j\omega t} dt \tag{72}$$

is the sensor response to frequency ω at position x, and $d\left(x, t\right)$ is the inverse fast Fourier transform (IFFT) of the array response. Combining (71) and (72) gives the narrowband beamformer response as:

$$P\left(\omega, \phi\right) = \int_{-\infty}^{\infty} \int_{-\infty}^{\infty} d\left(x, t\right) e^{-j\frac{\omega \sin \phi}{c}x} e^{-j\omega t} dx dt. \tag{73}$$

The goal of this method is to find the array filter weight matrix $\mathbf{W}$ from discretizing $d\left(x, t\right)$ such that the response of the array at a given angle ϕ is constant for all frequencies. If (73) can be written in terms of two terms containing $e^{-j\omega_i \alpha}$. The filter weights can be found using an IFFT. Forming an FIB then requires forming a desired frequency invariant beam pattern and taking the IFFT. The transformation of (73) is accomplished by making the substitutions $\omega_1 = \frac{\omega \sin \phi}{c}$ and $\omega_2 = \omega$ then rewriting (73) as [61]

$$P\left(\omega_1, \omega_2\right) = \int_{-\infty}^{\infty} \int_{-\infty}^{\infty} d\left(x, t\right) e^{-j\omega_1 x} e^{-j\omega_2 t} dx dt. \tag{74}$$

The response of the beamformer is now a two-dimensional FFT of the array weights $d\left(x, t\right)$ which are found by taking the IFFT of the desired array response $P\left(\omega_1, \omega_2\right)$. When creating the desired beam response in $\left(\omega_1, \omega_2\right)$ space the conditions allowing for frequency invariance, namely $\omega_1 = \frac{\omega \sin \phi}{c}$ and $\omega_2 = \omega$, must be considered. The sine function can only have values between -1 and 1. Therefore, the desired beam

47

pattern $P(\omega_1, \omega_2)$ only exists when $-\omega_2/c \leq \omega_1 \leq \omega_2/c$. When this constraint is not met all values of $P(\omega_1, \omega_2)$ are set to zero.

Formulation of the FIB beam patterns for the disambiguation algorithm filter bank follows that of [61]. An arbitrary frequency dependent beam pattern is written as

$$P(\omega, \phi) = \sum_{m=-\infty}^{\infty} \sum_{n=-\infty}^{\infty} \mathbf{d}[m,n] e^{-jm(\omega \sin \phi/c)d} e^{-jn\omega T} \tag{75}$$

where $\mathbf{d}$, the discrete version of $d(x,t)$ from (72), is an infinite matrix of Fourier weights, ω is radial frequency, d is inter-element spacing, and T is the sample period. The beam pattern is approximated by truncating $\mathbf{d}$ to a $M \times J$ matrix of M length J FIR filters $\mathbf{d}[m,n]$, with $m \in M$ and $n \in J$, used as a wideband beamformer. Assuming alias-free sampling and an inter-element spacing of $\lambda_{max}/c/2$ where λ_{max} is the wavelength corresponding to a signal at one half the sampling frequency, the frequency is normalized as

$$\Omega = \frac{d\omega}{c} = \omega T. \tag{76}$$

The frequency dependent beam pattern (75) is now written as

$$P(\Omega, \phi) = \sum_{m,n=-\infty}^{\infty} d[m,n] e^{-jm\Omega \sin \phi} e^{-jn\Omega}. \tag{77}$$

Analysis of (77) allows for the substitutions $\Omega_1 = \Omega \sin \phi$ and $\Omega_2 = \Omega$ and the rewriting of (77) as a two-dimensional DFT of the weighting matrix $d[m,n]$ given by

$$P(\Omega_1, \Omega_2) = \sum_{m,n=-\infty}^{\infty} d[m,n] e^{-jm\Omega_1} e^{-jn\Omega_2}. \tag{78}$$

From (78) the array weights for any beam pattern $P(\Omega_1, \Omega_2)$ are found using an IFFT. The beam pattern, however, is still frequency dependent. A frequency independent beamformer is only a function of ϕ, the pointing direction of the beam,

or $\sin \phi$ in sine space. A frequency invariant beam pattern requires that when $\Omega_1 = \Omega \sin \phi$ and $\Omega_2 = \Omega$ are substituted back into (78), the pattern can be written as a frequency independent beam pattern $P(\sin \phi)$. This requires that the beam pattern involve Ω_1 and Ω_2 such that

$$P(\Omega_1, \Omega_2) = P\left(\frac{\Omega_1}{\Omega_2}\right) = P(\sin \phi). \tag{79}$$

The design procedure for a FIB based upon (78) requires the specification of a desired beam pattern $F(\sin \phi)$. The two-dimensional response is formed by making the substitution $P(\Omega_1, \Omega_2) = F(\Omega_1/\Omega_2)$. An IFFT is taken of $P(\Omega_1, \Omega_2)$ resulting in the filter weight matrix $d[m, n]$. Applying the IFFT requires caution. Recall the substitutions of $\Omega_1 = \Omega \sin \phi$ and $\Omega_2 = \Omega$. Because of this constraint the frequencies Ω_1 and Ω_2 must have the relationship: $-\Omega_2 \leq \Omega_1 \leq \Omega_2$. To account for this dependence of Ω_1 on Ω_2, the two-dimensional beamformer is written as:

$$P(\Omega_1, \Omega_2) = \begin{cases} F\left(\frac{\Omega_1}{\Omega_2}\right), & \text{when } \left|\frac{\Omega_1}{\Omega_2}\right| \leq 1 \ \wedge \ \Omega_2 \neq 0 \\ 0, & \text{otherwise} \end{cases} \tag{80}$$

where the beam pattern is set to zero when undefined because of the constraints.

The final step in finding the filter weight matrix $\mathbf{W} = d[m, n]$ is truncation. In creating $P(\Omega_1, \Omega_2)$, the normalized frequency spectrum where $\Omega \in [-\pi, \pi]$ is discretized. For a smooth beam pattern the discretization would include a large number , say Υ samples. The resulting beamformer, however, has a limited number of channels with a limited number of FIR taps per channel. The initial $\mathbf{d}[m, n]$ found from the IFFT, however contains $\Upsilon \times \Upsilon$ samples. The final FIB requires truncating the resulting matrix to $M \times J$ samples for the proper weight matrix size.

2.4.5 Time Reversal Method.

If a signal is incident upon an array from broadside and no interference signals are present in the RF environment, an estimate of the incident signal is simply the average over the input of all array channels. When the signal is incident from other than broadside there is a delay between the signal arriving at subsequent antenna array elements. Modeling the delay of each channel as a linear system allows a time reversal filter to be specified for each channel [57]. Applying the time reversal filters to each channel of the array is equivalent to wideband beamformers applying an FIR filter to the output of each array channel. For signals arriving off boresight on an array, beamformer weights are formed by finding the time reversal filter weights and then applying the correct coefficients to account for averaging over the M array elements. The resulting beamformer is referred to as the time reversal method (TRM).

The TRM DBF used in this research is a more complex algorithm that applies the TRM as a pre-steering algorithm that "points" the array toward the SOI [57,102,132]. At this point, the SOI is considered to be at array broadside. The term pre-steering is used for the first step of the TRM algorithm, because the first step does not attempt to null any interference sources nor counter the effects of noise. After the pre-steering is applied the TRM DBF algorithm applies a LCMV algorithm to the pre-steered array data. The LCMV algorithm applied when the SOI is known to arrive from broadside uses a simplified constraint matrix equation

$$\mathbf{C} = \begin{bmatrix} \mathbf{1} & \mathbf{0} & \cdots & \mathbf{0} \\ \mathbf{0} & \mathbf{1} & \cdots & \mathbf{0} \\ \vdots & \vdots & \ddots & \vdots \\ \mathbf{0} & \mathbf{0} & \cdots & \mathbf{1} \end{bmatrix} [\mathbf{w}] = \begin{bmatrix} \mathbf{1} \\ \mathbf{1} \\ \vdots \\ \mathbf{1} \end{bmatrix} \tag{81}$$

where $\mathbf{1}$ and $\mathbf{0}$ are $M \times 1$ vectors of ones and zeros respectively. This simplified

constraint equation is more efficiently solved than the general versions of (31) and (32) [70, 114].

The pre-steering step of the TRM algorithm is based on the fact that for a plane wave traveling through a medium, the backward traveling wave solution is found by time reversing and conjugating the forward propagating plane wave solution [56, 57]. If the DBF receiver architecture is treated as a propagation medium, the backward solution of the sampled array channel data can be found and then back-propagated through the receiver to arrive at the signal that was incident upon the array. The backward propagated wave solution is free from any artifacts introduced by the receiver hardware, to include inter-element delay due to the reception of signals off broadside. It should be noted that this method assumes that hardware artifacts are deterministic.

The following derivation follows that of [57]. In order to back-propagate a measured signal through the array, the impulse response of the array is required. The receiver impulse response function can be calculated by measuring the response of a carefully selected probe signal. Consider a probe signal $\rho(t)$ chosen such that

$$\rho^*(-t) * \rho(t) \cong \delta(t),\tag{82}$$

where $\delta(t)$ is the dirac delta function. Also consider from linear systems theory that output of the array $z(t)$ is the probe signal $\rho(t)$ convolved with the array impulse response function $h(t)$ given as

$$z(t) = \rho(t) * h(t).\tag{83}$$

Using both (82) and (83) with linear systems theory the impulse response is calculated

as

$$h\left(t\right) \cong \rho^{*}\left(-t\right) * z\left(t\right).$$ (84)

The formula of (84) is sufficient to calculate the array impulse response when (82) is met exactly. Because of transmission system limitations and the fact that the calculations exhibit numerical inaccuracies due to digital implementation, (82) in practice cannot be met [56, 57]. An estimate of the array response function is formulated by considering the response $\breve{z}\left(t\right)$ of an array to a transmitted signal $z\left(t\right)$ approximately meeting the requirement of (82)

$$\breve{z}\left(t\right) = h\left(t\right) * z\left(t\right).$$ (85)

All values are Fourier transformed to eliminate the convolution integrals giving

$$\breve{Z} = HZ$$ (86)

where the non-bold capital letters represent the Fourier transform of the lower-case equivalent. The impulse response weights are found by first normalizing H in (86) as

$$\breve{Z} = \frac{H^{*}}{H^{*}}HZ = \frac{\left|H\right|^{2}Z}{H^{*}}$$ (87)

and then rearranging the terms of (87) as

$$\frac{H^{*}}{\left|H\right|^{2}} = \frac{\breve{Z}}{Z}.$$ (88)

The final processing step requires recognizing the expression for the impulse response

function and performing the inverse Fourier transform (IFT)

$$\hat{h} = F^{-1} \left[\frac{H^*}{|H|^2} \right] \tag{89}$$

assuming that the IFFT exists. The TRM pre-steering is applied by convolving the pre-steering TRM filter $\hat{h}(t)$ with the measured input signal $z(t)$.

Implementing wideband beamforming through the TRM requires the formation of TRM impulse response functions $\hat{h}_{\omega,\phi}(t)$ over the frequency band Ω and possible DOA angles Φ_κ of the SOI for each array channel. TRM beamforming is performed by convolving the impulse response function $\hat{h}_{\omega,\phi}$ for the estimated DOA and frequency of the SOI, for each array channel, with the sample data $x_m(t)$ from the corresponding array channel data as

$$\breve{x}_m(t) = \hat{h}_{\omega,\phi} * x_m(t). \tag{90}$$

For DBF application the impulse response function and array channel data are discretized so that

$$\breve{x}_m[k] = \hat{h}_{\omega,\phi,m}[k] * x_m[k] \tag{91}$$

where the notation $\hat{h}_{\omega,\phi,m}$ reflects that a different array response function exists for each array channel. The pre-steered $\breve{x}_m[k]$ for each channel can be arranged as a pre-seteerd data matrix

$$\breve{\mathbf{X}} = \begin{bmatrix} \breve{\mathbf{x}}_0 \\ \breve{\mathbf{x}}_1 \\ \vdots \\ \breve{\mathbf{x}}_{M-1} \end{bmatrix}. \tag{92}$$

Complexity of the TRM algorithm, like the GDFT algorithm, includes the complexity from the LCMV implementation. The LCMV implementation for use with

53

the TRM method, however, is a simplified version of the LCMV and has less computational cost. To implement the TRM properly requires applying predetermined filters to each channel of the data similar to the GDFT. The current effort applies the TRM filters in the frequency domain and so requires an FFT of each data channel before filter application and an IFFT after the TRM filters have been applied. The cost of the FFT is again $N \log N$ where N is the number of data points in the FFT. The TRM method requires M such FFT operations for a complexity of $O(MN \log N)$. Application of each filter requires $O(MN)$ for multiplication and an additional $O(MN \log N)$ for the IFFT. The total complexity is then:

$$O\left(MN \log N + MN + \left(N_c^3 + MJN_c^2 + (MJ)^2 N_c + (MJ)^2 + MJN_c + MJ\right)\right),$$

(93)

where the latter part is the complexity added due to the LCMV processing. The dominant term from the FFT and FFT operations given by $O(MN \log N)$.

Figure 6 is a representative beampattern for the combination TRM and LCMV beamformers. The mainbeam is formed toward 0° and an interference source is at -30°. As with the general LCMV beamformer the implementation used in conjunction with the TRM does places a null at -30° that is not clearly visible because of how narrow the null is. The null, however, is at -40 dB, similar in depth to the LSSB placed null.

2.4.6   Sub-Band Methods.

Full space-time processors are computationally complex. The complexity of wideband beamforming is reduced through sub-band processing. Sub-band processing lessens the computational burden of wideband processing by reducing the rank of the array data covariance matrix through reducing the spatial or temporal extent the beamformers are required to cover. Sub-banding can be applied in either the spatial

54
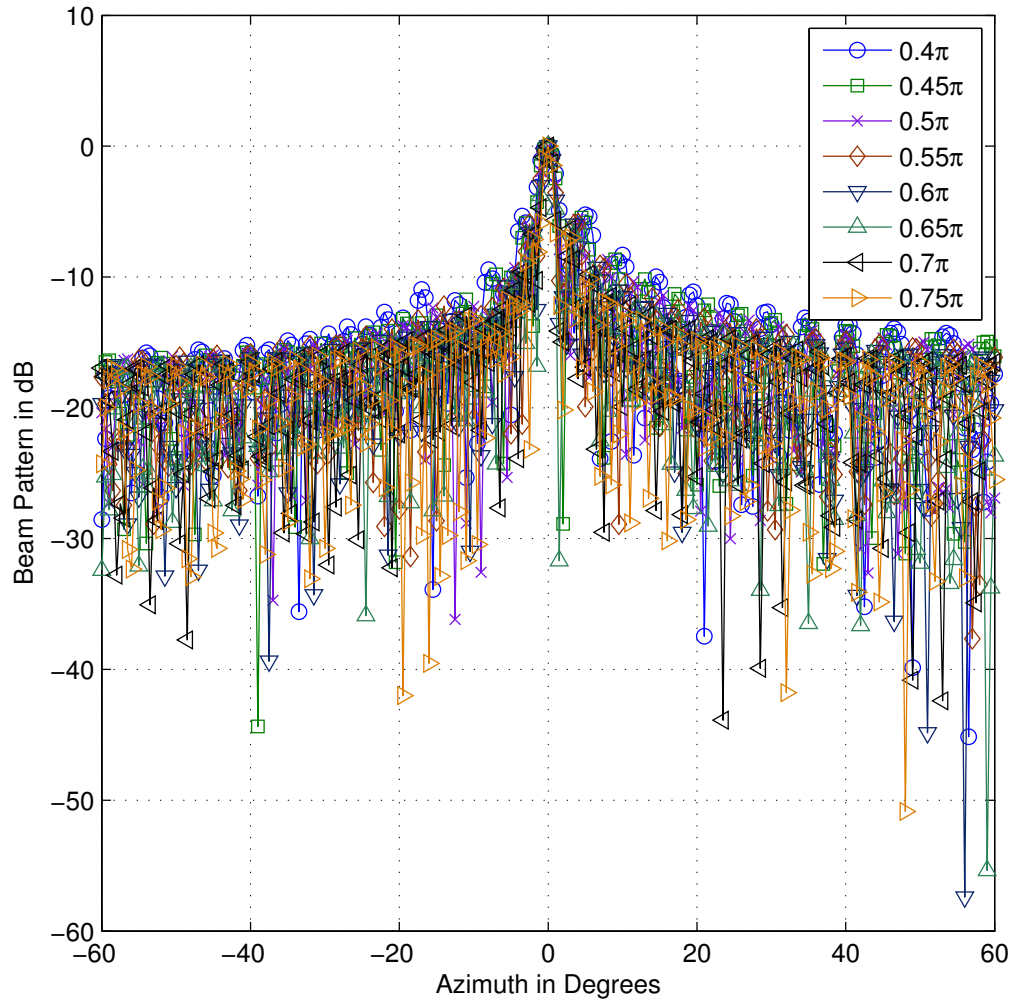
Figure 6. Multiple beampattern frequency cuts for the time reversal method beam-former with a main beam at 0° and an interference source at -30°. Each frequency cut is for a normalized frequency between 0 and π.

or frequency domain.

Spatial sub-band processing is referred to as beamspace processing, because the spatial domain is filtered into spatial sub bands [65, 92, 136]. These papers apply the FFT-based FIB of Section 2.4.4 to form a FIB filter bank to cover the spatial field of interest to the array. Frequency-based adaptive processing is then applied to each beam.

A more common form of sub-banding utilizes frequency sub-bands, where narrowband adaptive DBF algorithms are applied to each frequency sub-band [28–30, 36, 42, 48, 68, 75, 82, 94, 101, 126–128]. Further reductions in processing time are made through use of the GDFT, which in addition to applying adaptive algorithms in sub-bands uses multi-rate processing. Multi-rate processing downsamples, in time, the array data to reduce the amount of processed data allowing for faster algorithm implementation [29, 30, 126, 128]. Removing data through downsampling effectively lowers the sampling rate of the system; however, because the data was sub-banded in frequency the Nyquist constraint is still met and no aliasing occurs. The sub-banding and downconversion are applied simultaneously in multi-rate processing through a modified discrete Fourier transform (DFT) matrix. A separate DBF algorithm is applied to each frequency sub-band of the data. After DBF processing the post DBF signal from each sub-band is upsampled in time and combined using another DFT referred to as the synthesis filter. The final output from the GDFT is an estimate of the desired wideband signal.

2.4.7   GDFT Algorithm.

GDFT is a sub-band adaptive algorithm that attempts to lower the computational complexity of wideband beamforming by applying narrowband adaptive DBF algorithms in frequency sub-bands of the wideband array data. Each channel of wide-

band array data is filtered into sub bands using what are known as analysis filters. Narrowband adaptive DBF algorithms are applied to each sub-band produced by the analysis filters. Each sub-band thus contains an estimate of the the corresponding SOI sub-band. The narrowband estimates are recombined into the final wideband signal estimate using synthesis filters. The GDFT is so named because the sub-band filters are generated from a prototype filter by a generalized DFT operation [64, 126–128]. The analysis filters $h_k[n]$ and GDFT operation is given by

$$\breve{h}_k[n] = e^{j\frac{2\pi}{\breve{K}}(\breve{k}+\breve{k}_0)(n+n_0)} \cdot \varphi[n], \quad \breve{k}, n \in \mathbb{N}, \tag{94}$$

where $\breve{K}$ is the number of sub bands, n is the sample number or discrete time index, and $\varphi[n]$ are the prototype filter coefficients. The operation is a generalized DFT due to the n_0 and $\breve{k}_0$ offsets.

Implementation of the GDFT algorithm does not involve directly solving for the prototype filter coefficients $\varphi[n]$. The analysis filter coefficients $\breve{h}_{\breve{k}}[n]$ and synthesis filter coefficients $g_{\breve{k}}[\breve{k}]$ are found by minimizing the stop-band attenuation of each filter and the distortion error imposed upon the signal when passed through the analysis and synthesis filters [28–30]. To limit distortion in both the analysis and synthesis stages the filters are made to maintain a linear phase by setting $n_0 = \frac{L_p-1}{2}$ and $\breve{k}_0 = \frac{1}{2}$ where L_p is the length of the prototype filter. All synthesis filters $g_{\breve{k}}[n]$ are time reversed complex conjugates of the analysis filters, i.e.

$$g_{\breve{k}}[n] = \breve{h}_{\breve{k}}^*[L_p - n + 1], \tag{95}$$

where L_p is again the length of the prototype filter. The stop-band attenuation is limited by minimizing the attenuation over a grid of selected points [73, 87].

The stop-band attenuation of the GDFT is dependent upon the design of the

prototype filter used for derivation of the analysis and synthesis filter banks. Design of the prototype filter for the GDFT follows that of [28–30] and takes into consideration not only the stop-band attenuation of the filter, but also the resulting error imposed upon a signal when passed through both the analysis and synthesis filters.

Solution of the filter coefficients $h_{\tilde{k}}[n]$ results from labeling the reconstruction error as ξ_1, the stop-band energy as ξ_2 and minimizing their sum given by

$$\xi = \xi_1 + \gamma\xi_2, \tag{96}$$

The factor γ is a positive weight factor to trade off the two criterion. Assuming that in-band aliasing is sufficiently suppressed, the impulse response of the GDFT filter bank is the convolution of the analysis and synthesis filters

$$\iota[n] = \sum_{\check{k}=0}^{\check{K}-1} \check{h}_{\check{k}}[n] * g_{\check{k}}[n]. \tag{97}$$

From [80] the convolution of the $\check{k}^{th}$ filter can be written in matrix notation as

$$\iota_{\check{k}} = \begin{bmatrix} \check{h}_{\check{k}}[0] & 0 & \cdots & 0 \\ \check{h}_{\check{k}}[1] & \check{h}_{\check{k}}[0] & \cdots & 0 \\ \check{h}_{\check{k}}[2] & \check{h}_{\check{k}}[1] & \cdots & 0 \\ \vdots & \vdots & \ddots & \vdots \\ 0 & 0 & \cdots & \check{h}_{\check{k}}[L_p-1] \end{bmatrix} \begin{bmatrix} g_{\check{k}}[0] \\ g_{\check{k}}[1] \\ g_{\check{k}}[2] \\ \vdots \\ g_{\check{k}}[L_p-1] \end{bmatrix} = \mathbf{H}_{\check{k}}\mathbf{g}_{\check{k}}. \tag{98}$$

Summing over each $\iota_{\check{k}}$ from (97) written in the form of (98) allows the rewriting of

58

(97) as

$$\iota = \begin{bmatrix} \mathbf{H}_0 \ \mathbf{H}_1 \ \cdots \ \mathbf{H}_{\check{K}-1} \end{bmatrix} \begin{bmatrix} \mathbf{g}_0 \\ \mathbf{g}_0 \\ \vdots \\ \mathbf{g}_{\check{K}-1} \end{bmatrix} = \mathbf{Hg}. \tag{99}$$

Consider a GDFT that does not apply an adaptive DBF algorithm to the sub-bands. The signal at the output of the GDFT is ideally the input signal delayed by the amount of samples required to apply the analysis and synthesis filters. Any difference between the input signal and the output of this GDFT and the delayed signal out of the GDFT is reconstruction error. The reconstruction error is defined mathematically as the Euclidean distance between the impulse response ι and a perfect delay δ represented by

$$\xi_1 = \|\iota - \delta\|^2 = \|\mathbf{Hg} - \delta\|^2 \tag{100}$$

The stop band attenuation is calculated in [73, 87] by selecting a dense grid of frequency points $[\omega_0, \omega_1, \cdots, \omega_N]$ covering the stop band and then calculating

$$\xi_{2,\check{k}} = \left\| \begin{bmatrix} 1 & \cos(\omega_0(1)) & \cdots & \cos(\omega_0(L_p-1)) \\ 1 & \cos(\omega_1(1)) & \cdots & \cos(\omega_1(L_p-1)) \\ \vdots & \vdots & \ddots & \vdots \\ 1 & \cos(\omega_N(1)) & \cdots & \cos(\omega_N(L_p-1)) \end{bmatrix} \begin{bmatrix} g_{\check{k}}(0) \\ g_{\check{k}}(1) \\ \vdots \\ g_{\check{k}}(L_p-1) \end{bmatrix} \right\|^2$$

$$= \|\check{\mathbf{P}}_{\check{k}} \mathbf{g}_{\check{k}}\|^2 \tag{101}$$

where $\check{\mathbf{P}}_{\check{k}}$ describes the required specification on the $\check{k}^{th}$ analysis filter. Rewriting

(96) using (100) and (101) gives

$$\xi = \left\| \begin{bmatrix} \mathbf{H} \\ \gamma\check{\mathbf{P}} \end{bmatrix} \mathbf{g} - \begin{bmatrix} \delta \\ \mathbf{0} \end{bmatrix} \right\|^2 \tag{102}$$

where $\mathbf{0}$ is a matrix of zeros, $\check{\mathbf{P}}$ is a block diagonal matrix where the sub-matrices on the diagonal are the $\check{\mathbf{P}}_{\check{k}}$ from (101) written as

$$\check{\mathbf{P}} = \mathrm{diag}\left(\check{\mathbf{P}}_0, \check{\mathbf{P}}_1, \cdots, \check{\mathbf{P}}_{\check{K}-1}\right) \tag{103}$$

and

$$\mathbf{g} = \begin{bmatrix} \mathbf{g}_0^T & \mathbf{g}_1^T & \cdots & \mathbf{g}_{\check{K}-1}^T \end{bmatrix}^T. \tag{104}$$

The filter coefficients $h_k[n]$ are derived by minimizing (102) with respect to $\mathbf{g}$ using the iterative least squares design algorithm of [29, 30].

The GDFT algorithm applies the $\mathbf{h}_{\check{k}}$ and $\mathbf{g}_{\check{k}}$ found through minimizing (102) for each $\check{k} \in \check{K}$ to form the analysis and synthesis filter banks. The analysis filter bank is applied to the array channel data forming the $\check{K}$ sub-bands. A narrowband LCMV algorithm is then applied to each sub-band. The synthesis filter bank is applied to each of the $\check{K}$ narrowband signals after application of the LCMV. The output from each of the $\check{K}$ synthesis filters is summed to form the GDFT adaptive DBF output.

Computational complexity of the GDFT algorithm incorporates the complexity of the LCMV algorithm, as a LCMV algorithm is applied to each sub band. Computational savings can occur as each sub band requires fewer FIR filter coefficients per channel and also fewer constraints. In addition to the complexity from the LCMV algorithm, GDFT requires application of a filter bank for data analysis and a second filter bank for synthesis. Because the frequency range of the desired SOI is known *a priori*, the filter coefficients $\check{\mathbf{h}}$ of (94) are determined off-line of algorithm implemen-

tatiom and do not add to the computational complexity. Application of the filters for both analysis and synthesis are applied in the frequency domain and require FFT of the data and IFFT of the post synthesis data filters. The cost of an FFT is $O\left(N \log N\right)$ where N is the number of points in the FFT. To keep implementation fast, N should be set as a power of two. Implementation of each filter then requires $O\left(M\check{K}N\right)$ for N multiplications in each of M channels for K filter banks per channel. The same number of operations is required for synthesis filter bank implementation. Summing up the complexity from the analysis filters, the synthesis filters, and the $\check{K}$ required LCMV algorithms the total complexity is:

$$O\left(\check{K}N \log N + M\check{K}N + \check{K}\left(N_c^3 + MJN_c^2 + (MJ)^2 N_c + (MJ)^2 + MJN_c + MJ\right)\right),$$
(105)

where the latter part of (105) is due to the $\check{K}$ implementations of a LCMV algorithm. The dominant term is from the $\check{K}$ LCMV applications leading to $O\left(\check{K}\left(MJ\right)^2 N_c\right)$.

2.5 Environment Estimation Techniques

2.5.1 DOA Estimation.

Wideband DOA estimation is fundamental to wideband beamforming because adaptive DBF algorithms require knowledge of the DOA of the SOI. The narrowband DOA estimation techniques Capon and multi-signal classification (MUSIC) [10, 91] are based upon the N_{eigs} eigenvectors corresponding to the N_{eigs} highest eigenvalues, of the array data matrix being equal to the steering vectors of the signals present in the measured data. These N_{eigs} eigenvectors form a signal subspace orthogonal to the noise subspace corresponding to the $M - N_{eigs}$ eigenvectors with eigenvalues equal to the noise power σ_{noise}^2. The Capon and MUSIC spectra are found by discretizing the angle space of the array and forming a set of steering vectors corresponding to

each discrete angle. Each steering vector is projected onto the noise subspace; the inverse of the results of the projections are plotted as the spectra. The maxima of the spectrum correspond to those eigenvectors, and thus angles, most nearly orthogonal to the noise subspace and thus signal directions present in the measured data. When the signals impinging upon the array are wideband, however, each signal adds multiple eigenvectors to the covariance matrix and the CAPON and MUSIC methods fail to properly locate the signal's DOA.

As with narrowband DOA estimation, the maximum likelihood estimator (MLE) can be used to locate the arrival directions of wideband signals of interest. The MLE is a consistent estimator, in that as the number of data samples used in the estimate grows large, the variance of the estimate approaches the Cramer-Rao lower bound (CRLB) [81, 124]. The MLE, however, is computationally complex and not suitable for direct implementation [113]. Wideband DOA estimation is, in practice, implemented using the frequency sub-banding approach.

The earliest methods of wideband DOA estimation performed averaging of DOA estimates found in each sub-band [122]. Sub-band averaging DOA estimation methods require high SNR and have large variances [12]. Coherent signal subspace DOA estimation methods were introduced by Kaveh, *et al.* in [122]. Coherent methods apply the DOA estimation to all sub-bands at the same time eliminating any losses due to averaging. Coherent methods are capable of performing wideband DOA estimation with lower SINR and operate on correlated signals. The method of Kaveh is a coherent frequency sub-band method that applies unitary transformation matrices to the covariance matrix estimate of each sub-band such that the eigenvectors of each correlation matrix are "focused" to a desired frequency while not affecting the eigenvector norm. A reduced rank covariance matrix is formed by averaging the focused narrowband covariance matrices. Narrowband DOA estimation methods such

as Capon and MUSIC are applied to the averaged covariance matrix to estimate the DOA of all impinging signals. Further work on Kaveh's method has improved the formulation of the transformation matrices to improve the variance and bias of the resulting DOA estimates [8, 9, 17, 41, 93, 95, 103].

The coherent subspace DOA estimation methodology of Kaveh, while effective, requires initial coarse group angle estimates for the signal DOAs [37, 122]. Group angles are directions about which multiple sources are expected to be grouped in angular space. Environments with large numbers of interference signals would require multiple initial group angle estimates. The focusing matrices were formed using matrices of steering vectors in the direction of the group angle estimates. The initial angle estimates were found using a narrowband DOA estimation algorithm at selected frequencies.

To be effective in blind detection and DOA estimation, an algorithm is desired that requires no *a priori* information about the incoming sigal directions. The requirement for initial DOA estimates is overcome in [37] where focusing matrices are found using global minimization. The focusing matrices sought are those that minimize the Euclidian distance between the true wideband steering vectors and the transformed steering vectors for all angles within an angular region [37]. To mathematically describe this global minimization problem, consider the frequency dependent steering vector $\mathbf{v}(\phi, f)$ from (47) and a region in sine space, where sine space involves the transformation of $\mu = \sin \phi$ for all angles. The new focusing matrices $\mathbf{T}\left(f_{\tilde{j}}\right)$ are found through the minimization of

$$\min_{\mathbf{T}(f_{\tilde{j}})} \int_{\mu_{initial}}^{\mu_{final}} \parallel \mathbf{T}(f_{\tilde{j}})\mathbf{v}(\phi, f_{\tilde{j}}) - \mathbf{v}(\phi, f_c) \parallel^2 d\mu, \text{ for each } \tilde{j} = 1, \ldots, \tilde{J} \qquad (106)$$

for $\tilde{J}$ frequency bands, where f_c is the focusing frequency for the DOA estimator. Note that the integration is performed in sine space. Each steering vector $\mathbf{v}\left(\phi, f_{\tilde{j}}\right)$

can be written in terms of μ. The notation is left in terms of ϕ to keep in mind that the process is designed to estimate the DOA ϕ of all signals in the RF environment. The minimization is further constrained by $\mathbf{T}^H(f_{\tilde{j}})\mathbf{T}(f_{\tilde{j}}) = \mathbf{I}$ resulting in unitary transformation. Applying the unitary constraint to (106) allows the problem to be written as a maximization problem

$$\max_{\mathbf{T}(f_{\tilde{j}})} \int_{\mu_{initial}}^{\mu_{final}} \mathbf{v}^H(\phi, f_{\tilde{j}})\mathbf{T}^H(f_{\tilde{j}})\mathbf{v}(\phi, f_c) + \mathbf{v}^H(\phi, f_{\tilde{j}})\mathbf{T}^H(f_{\tilde{j}})\mathbf{v}(\phi, f_{\tilde{j}})d\mu,$$

$$\text{for each } \tilde{j} = 1, \ldots, \tilde{J}. \tag{107}$$

This can be reduced further to

$$\max_{\mathbf{T}(f_{\tilde{j}})} \mathcal{R}\left[\text{Tr}(\mathbf{R}_{gcn}\mathbf{T}(f_{\tilde{j}}))\right], \quad \text{for each } \tilde{j} = 1, \ldots, \tilde{J}, \tag{108}$$

where $\mathcal{R}[\cdot]$ is the real part of the bracket and $\text{Tr}[\cdot]$ is the trace of the matrix. The matrix $\mathbf{R}_{gcn}$ is the outer product of steering vectors given by

$$\mathbf{R}_{gcn} = \int_{\mu_i}^{\mu_f} \mathbf{v}(\phi, f_c)\mathbf{v}^H(\phi, f_{\tilde{j}})d\mu \tag{109}$$

where the subscripts on the integration limits have been shortened from *initial* to i and from *final* to f. If the DOA estimation search is performed over a symmetric interval (i.e., $\mu_i = -\mu_f$), then the (p, q) element $[\mathbf{R}_{gcn}]_{pq}$ of the $M \times M$ matrix has the simple form of

$$[\mathbf{R}_{gcn}]_{pq} = 2\sin\phi_i\text{sinc}\left\{\frac{d\sin\phi_i}{c}((p-1)\omega_c - (q - 1(\omega_{\tilde{j}})))\right\}, \tag{110}$$

for $p, q \in \{1, 2, \ldots, M\}$ where $c > 0$ is the speed of propagation [37]. Solution of (108) is exacted by performing a singular value decomposition on $\mathbf{R}_{gcn}$, such that

$\mathbf{R}_{gcn} = \mathbf{U}\mathbf{\Sigma}\mathbf{V}^H$, resulting in

$$\max_{\mathbf{T}(f_{\tilde{j}})} \mathcal{R} \left\{ \mathrm{Tr} \left[\mathbf{U}(f_{\tilde{j}}) \mathbf{\Sigma}(f_{\tilde{j}}) \mathbf{V}^H(f_{\tilde{j}}) \mathbf{T}(f_{\tilde{j}}) \right] \right\}, \ \tilde{j} = 1, \ldots, \tilde{J}. \tag{111}$$

The solution of (111) is, as shown in [41], $\mathbf{T}^\dagger \left(f_{\tilde{j}} \right) = \mathbf{U}(f_{\tilde{j}}) \mathbf{V}^H(f_{\tilde{j}})$ where $[\cdot]^\dagger$ refers to the optimal solution providing the maximum value of the trace.

To solve for the angles of arrival, a single covariance matrix is formed from the $\tilde{J}$ narrowband matrices as

$$\mathbf{R}_{foc} = \sum_{\tilde{j}=1}^{\tilde{J}} \mathbf{T}(f_{\tilde{j}}) \mathbf{R}_{\mathbf{x}}(f_{\tilde{j}}) \mathbf{T}^H(f_{\tilde{j}}), \tag{112}$$

where $\mathbf{R}_{\mathbf{x}} \left(f_{\tilde{j}} \right)$ is the spectral covariance matrix of the array data matrix $\mathbf{X}$ at frequency $f_{\tilde{j}}$. The final step is to apply the narrowband MUSIC DOA estimation algorithm to $\mathbf{R}_{foc}$. A description of the MUSIC algorithm is provided in Appendix A.

2.5.2 Model Order Selection.

The problem of determining the number of signals in an environment is written as the minimization of the Akaike information criteria (AIC) [19, 125] over the possible number of sources. The possible number of sources is limited to one less than the number of array elements used in the sensing array. The AIC as a function of sources is [19, 125]

$$AIC\left(\varsigma\right) = -2\log \left[\left(\frac{\prod_{i=\varsigma+1}^{M} l_i^{\frac{1}{(M-\varsigma)}}}{\frac{1}{M-\varsigma} \sum_{i=\varsigma+1}^{M} l_i} \right)^{(M-\varsigma)\check{N}} \right] + 2\varsigma\left(2M - \varsigma\right), \tag{113}$$

where ς is the number of interference signals, l_i is the ith eigenvalue of the estimated covariance matrix from (112), M is the number of sensors in the array, and $\breve{N}$ is the number of data points used to estimate $\mathbf{R}_{foc}$. As $\mathbf{R}_{foc}$ is determined using frequency domain processing, $\breve{N}$ is the number of frequency samples used in the construction of $\mathbf{R}_{foc}$. Also, the method assumes the eigenvalues of $\mathbf{R}_{foc}$ are arranged such that $l_1 \geq l_2 \geq \cdots \geq l_p$.

2.5.3 Cognitive Radio.

The cognitive radio (CR) literature provides insight into blind environment estimation. Current CR technology is designed to transmit communication signals in underused portions of the spectrum to better use the existing spectrum. This is important as the available spectrum is becoming increasingly crowded with competition for every spectral region [31, 34, 35]. CRs search for spectral "holes" in which the radio can transmit without affecting the primary user of the spectrum [31].

In contrast to spectral holes, the RM of the proposed receiver framework looks for filled regions of the spectrum. CR receivers search for holes either by using edge detection or through the use of a GLRT detecting where signals are present and declaring a hole where there is no signal. Edge detection in the same way determines the filled portions of the spectrum as a GLRT is designed to detect signals in a spectrum. Thus, no modification to the CR spectral detection algorithms is required for application to the proposed receiver framework.

Methods for detecting spectral holes require a spectral estimate of the electromagnetic environment [3,11,31,32,43,56,90,111,123,133]. Spectral estimates for spectrum utilization must be unbiased with low variance for small sample sizes for efficient operation. The estimator used throughout the CR literature is the multi-taper method (MTM) spectral estimator [31,32]. The MTM method was first described by Thom-

son in [109]. The MTM is a multiple window spectral estimation [110], where multiple windowed periodograms are averaged to form a final spectral estimate. MTM estimates are designed using the discrete prolate spheroidal sequence (DPSS) derived by Slepian in a series of papers for Bell laboratories [52,53,98–100]. The DPSS are used because, for a given sequence length, the DPSS are the sequences out of all possible sequences whose spectrum provides the greatest concentration of power over a given bandwidth [99,109].

2.5.3.1   MTM Spectral Estimation.

Bandwidth determination and signal detection require estimating the spectrum of the environment. The spectrum is estimated using the MTM [109] of spectral estimation. Classical estimation methods such as the Periodogram [47] and Bartlett [47] estimators suffer from biased estimates due to spectral leakage from the choice of windows used in the estimation. The MTM spectral estimator, however, through the use of DPSS has low spectral leakage [31,109]; for this reason the MTM estimator is chosen for the RM algorithm. The MTM works similar to the method of Bartlett; however, MTM uses specially chosen weighting sequences (windows) for each direct spectrum estimate to minimize spectral leakage. Using multiple windowed direct estimates reduces the variance of the overall MTM spectral estimate. Thomson *et al.* [109], developed the MTM estimator based on the work of Slepian with DPSS [99].

Slepian considered doubly infinite sequences $\tilde{h}_n$, $-\infty \leq n \leq \infty$ where

$$\tilde{H}(f) = \sum_{n=-\infty}^{\infty} \tilde{h}_n e^{-j2\pi fn} \tag{114}$$

represents the Fourier transform of the sequence. Slepian [99] then solved the problem of what length N subsequence of $\tilde{h}_n$, with normalized bandwidth $|B| \leq \frac{1}{2}$, maximizes

the ratio

$$\tilde{\lambda} = \frac{\sum_{N_o}^{N_o+N-1} |\tilde{h}_n|^2}{\sum_{-\infty}^{\infty} |\tilde{h}_n|^2}. \tag{115}$$

That is, what such sequences have the most spectral content in bandwidth B? The summations in (115) are performed over any N-length data sequence, where the starting point is given as N_o. The answer from Slepian is the zeroth-order DPSS denoted by $\nu_{n-N_o}^{(0)}(N, B)$. The sequence orthogonal to $\nu_{n-N_o}^{(0)}(N, B)$ possessing the second most spectral content in B is $\nu_{n-N_o}^{(1)}(N, B)$. The orthogonalization process can be generalized to the N sequences with the most spectral content in given bandwidth B. The DPSS $\nu_{n-N_o}^{(k)}(N, W)$ and their corresponding eigenvalues $\tilde{\lambda}_\varpi(N, B)$ are found from the solution of

$$\sum_{\bar{m}=0}^{N-1} \frac{\sin 2\pi B(n-\bar{m})}{\pi(n-\bar{m})} \nu_{\bar{m}}^{\varpi}(N, B) = \tilde{\lambda}_\varpi(N, B) \nu_n^{(\varpi)}(N, B) \quad n = 0, \pm 1, \pm 2, \ldots, \tag{116}$$

normalized so that

$$\sum_{j=0}^{N-1} \nu_j^{(\varpi)}(N, B)^2 = 1, \tag{117}$$

$$\sum_{j=0}^{N-1} \nu_j^{(\varpi)}(N, B) \geq 0, \tag{118}$$

$$\sum_{j=0}^{N-1} (N-1-2j) \nu_j^{(\varpi)}(N, B) \geq 0. \tag{119}$$

The idea of Thomson [109] was to apply the DPSS as defined above to a multi-taper spectral estimate. Thomson's multi-taper spectral estimate is formed by averaging Δ direct spectral estimates as

$$\hat{S}^{(mt)}(f) \triangleq \frac{1}{\Delta} \sum_{\varpi=0}^{\Delta-1} \hat{S}_\varpi^{(mt)}(f) \tag{120}$$

68

where

$$\hat{S}_{\varpi}^{(mt)}(f) \triangleq \Delta \left| \sum_{t=1}^{N} \tilde{h}_{t,\varpi} X_t e^{-i2\pi ft\Delta} \right|^2, \tag{121}$$

and $\tilde{h}_{t,\varpi}$ is the ϖth DPSS used as the data taper (window) for the ϖth direct spectral estimate $\hat{S}_{\varpi}^{(mt)}$ function, and X_t are realizations of the stationary process to which the estimator is applied. The DPSS above were chosen by Thomson, because Slepian showed they provided the least leakage for any taper of length N. The MTM spectral estimators used in practice are regularized versions of the standard MTM estimate provided in (120). The regularized MTM estimates are defined as [79]

$$\bar{S}^{(mt)}(f) \triangleq \frac{\sum_{\varpi=0}^{\Delta-1} \lambda_{\varpi} \hat{S}_{\varpi}^{(mt)}(f)}{\sum_{\varpi=0}^{\Delta-1} \lambda_{\varpi}}, \tag{122}$$

where λ_{ϖ} is the eigenvalue associated with the ϖth DPSS. CR systems determine if a signal is present by applying a GLRT [45] to the MTM spectral estimate [11,31,43,56]. The GLRT can be applied to a single frequency sub-band as in [56], or over a range of sub-bands to detect wideband signals as in [11,43]. A GLRT is applied instead of a standard Bayesian likelihood ratio test (LRT), because the measurements for the detector are the MTM estimates of the spectrum for which the second order statistics are not known.

2.5.3.2 GLRT Implementation.

According to [79] each sample of the spectral estimate $\bar{S}^{(mt)}(f_n)$ is distributed as a scaled Chi-squared random variable $\frac{S(f_n)}{2\Delta}\chi_{(2\Delta)}^2$ with 2Δ degrees of freedom, where $S(f_n)$ denotes the actual sampled PSD of the time series, and Δ is the number of DPSS data windows used in the MTM spectral estimate. Because of the low leakage properties of the DPSS, each $\bar{S}^{(mt)}(f_n)$ is statistically independent [109]. Assume a

vector of independent and identically distributed (i.i.d) spectral estimate samples

$$\bar{S}^{(mt)}(\mathbf{f}) = \left[\bar{S}^{(mt)}(f_0), \bar{S}^{(mt)}(f_1), \ldots, \bar{S}^{(mt)}(f_{N-1})\right] \tag{123}$$

where N is the number of frequency samples in the spectral estimate. The joint probability distribution of (123) is then given by [79]

$$\prod_{\eta=0}^{N-1} \left[\frac{1}{2^\Delta \Gamma(\Delta)}\right] \left[\frac{1}{D'}\right] \left[\frac{\bar{S}^{(mt)}(f_\eta)}{D'}\right]^{\Delta-1} e^{-\frac{1}{2D'}\bar{S}^{(mt)}(f_\eta)}, \tag{124}$$

where $\bar{S}^{(mt)}(f_\eta) \geq 0$, $D' = \frac{S(f_\eta)}{2\Delta}$ and the Gamma function $\Gamma(x) = \int_0^\infty t^{x-1}e^{-t}dt$. The two hypotheses considered for the GLRT are $\mathcal{H}_0 \to$ spectral hole; $\mathcal{H}_1 \to$ signal present. The GLRT formed as $\frac{p(\bar{S})^{(mt);\mathcal{H}_1}}{p(\bar{S})^{(mt);\mathcal{H}_0}}$ is

$$\frac{\prod_{\eta=0}^{N-1} \left[\frac{1}{2^\Delta \Gamma(\Delta)}\right] \left[\frac{1}{D_1}\right] \left[\bar{S}_{Rx}^{(mt)}(f_\eta)\right]^{\Delta-1} e^{-\frac{1}{2D_1}\bar{S}_{Rx}^{(mt)}(f_\eta)}}{\prod_{\eta=0}^{N-1} \left[\frac{1}{2^\Delta \Gamma(\Delta)}\right] \left[\frac{1}{D_0}\right] \left[\bar{S}_n^{(mt)}(f_\eta)\right]^{\Delta-1} e^{-\frac{1}{2D_0}\bar{S}_n^{(mt)}(f_\eta)}} \underset{\mathcal{H}_0}{\overset{\mathcal{H}_1}{\gtrless}} \xi \tag{125}$$

where ξ is a threshold value, $D_1 = \frac{S_{Rx}(f_\eta)}{2K}$, and $D_0 = \frac{S_n(f_\eta)}{2\Delta}$. The subscript Rx refers to the spectral estimate when a signal and noise is present; the subscript n refers to the spectral estimate when only noise are present.

To write the above ratio test in a more compact manner and eliminate the requirement for knowing $S_{Rx}(f_\eta)$ the ratio is written as a log ratio

$$(\Delta - 1) \sum_{\eta=0}^{N-1} \ln\left[\frac{\bar{S}_{Rx}^{(mt)}(f_\eta)}{\bar{S}_n^{(mt)}(f_\eta)}\right] \tag{126}$$

$$-\frac{1}{2}\left\{\left[2\Delta \sum_{\eta=0}^{N-1} \frac{\bar{S}_{Rx}^{(mt)}(f_\eta)}{S_{Rx}(f_\eta)}\right] - \left[2\Delta \sum_{\eta=0}^{N-1} \frac{\bar{S}_n^{(mt)}(f_\eta)}{S_n(f_\eta)}\right]\right\}$$

$$\overset{\mathcal{H}_1}{\underset{\mathcal{H}_0}{\gtrless}} \ln(\xi) - N\Delta \ln\left(\frac{D_1}{D_0}\right) = \xi'.$$

70

Because of the properties of the MTM spectral estimator, the assumption $\bar{S}_{Rx}^{(mt)}(f_\eta) \approx S_{Rx}(f_\eta)$ is made; also the assumption $\bar{S}_n^{(mt)}(f_\eta) \approx \sigma_n^2$ is made due to the constant PSD of white Gaussian noise. Applying these two assumptions to (126) gives

$$(\Delta - 1) \sum_{\eta=0}^{N-1} \ln \left[\bar{S}_{Rx}^{(mt)}(f_\eta) \right] \underset{\mathcal{H}_0}{\overset{\mathcal{H}_1}{\gtrless}} \xi' + (N-1)\,N \ln \left[\sigma_n^2 \right] = \xi''. \tag{127}$$

The final form of the GLRT is

$$T_{LRT}\left(\bar{\mathbf{S}}^{(\mathbf{mt})}\left(\mathbf{f}\right)\right) = (\Delta - 1) \sum_{\eta=0}^{N-1} \ln \left[\bar{S}^{(mt)}\left(f_\eta\right) \right] \underset{\mathcal{H}_0}{\overset{\mathcal{H}_1}{\gtrless}} \xi'' \tag{128}$$

with T_{LRT} as the test statistic and ξ'' as the threshold value for spectrum sensing.

2.6   Resource Management

The proposed receiver architecture applies the *best* adaptive DBF algorithm with respect to beamformer performance criteria established by the receiver framework implementer. A chosen algorithm is the *best* adaptive DBF algorithm of those chosen for implementation, with respect to the performance criteria, for application to a RF environment type. The RF environments are differentiated based upon estimated environment parameters. Adaptive DBF choice is made by a RM. The RM estimates the environment parameters and picks the *best* adaptive DBF algorithm from a LUT of adaptive DBF algorithms. The LUT is derived before receiver implementation based upon the chosen algorithm performance metrics for each algorithm applied to multiple RF scenarios. The receiver implementer develops the LUT based upon the type of RF environments the receiver is expected to operate against, the adaptive DBF algorithms chosen by the implementer, and the desired algorithm performance

criteria.

The term resource manager is used because the choice of adaptive DBF algorithm impacts the loading of the receiver's computational hardware. Using the proposed framework most efficiently uses available computational resources.

Selecting the most appropriate adaptive DBF algorithm is a more precise statement of the algorithm selection problem (ASP) first introduced by Rice in [85]. Rice proposed a mapping from problem space to algorithm space and selected the algorithm as solution, that provided the best algorithm, with regard to finding the most accurate solutions over a variety of optimization problems, out of all algorithms in a given portfolio of algorithms. The ASP is an important problem receiving considerable attention in the field of computer science [51]. In a survey paper Kotthoff states that [51]:

> Researchers have long ago recognised that a single algorithm will not give
> the best performance across all problems one may want to solve and that
> selecting the most appropriate method is likely to improve the overall
> performance. Empirical evaluations have provided compelling evidence
> for this.

Transposed to the problem of adaptive beamforming, the rationale for solving the ASP is the rationale for proposing the new receiver architecture. Selecting separate adaptive DBF algorithms for each electromagnetic environment encountered is "likely" to improve the overall performance.

Even though the ASP has been studied in computer science since the 1970s, little has been done to apply the problem to improving beamforming system performance. Where work has been done is with respect to multiple-input multiple-output (MIMO) communications systems. The works of [16, 38, 78, 115] adaptively select a subset of spatial transmit beams from a randomly generated set of transmit beams that provide for the highest channel capacity. The receivers determine the SINR of all transmit-receive links in the MIMO system and only select the subset of transmitted

beams providing the highest SINR. The beam selection requires a feedback link from the receivers to the transmitters. The four papers [16, 38, 78, 115] present different methodologies for formulating the transmit beams and selecting the most optimal beams.

One other ASP-like problem is defined in [69], where the MIMO system selects an appropriate coding of the transmitted signal based upon the SINR of the signal measured at the receiver. As with the other MIMO systems studied, the communication system requires feedback between the receivers and transmitters.

The available literature to this point does not contain any studies or receiver architectures that extend the ASP to adaptive beamforming beyond the few MIMO systems. The receiver framework is thus beneficial not only for its potential to increase the performance of electronic support receivers, but also to open up a new research thread for adaptive DBF.

2.7   Chapter Review

The adaptive DBF algorithms presented in this chapter are those selected from the available adaptive DBF algorithms for inclusion in the LUT for demonstrating the proposed receiver framework. The choices form a representative set of the different types of adaptive DBF algorithms available and are not meant to be an exhaustive listing of adaptive algorithms. The choice of adaptive DBF algorithms for inclusion in any instantiation of the proposed framework is left to the receiver designer. When choosing algorithms for inclusion in the receiver implementation the designer should consider the types of SOIs as well as the types of environments the receiver will encounter.

Environment and signal detection algorithms presented are selected because of their applicability to CR. Use in the proposed receiver framework is analogous to use

in CR, making their implementation straightforward. The method of Kaveh [122] is used to estimate the DOAs of all signals in the RF environment, because it is able to work in both narrowband and wideband environments. Design of the RM for the receiver framework employs the described signal detection algorithms, DOA estimation algorithms, and the AIC model order selection algorithm. The output of the detection and estimation algorithms is used to decide which of the five adaptive DBF algorithms to use for a given adaptive beam.

III. Resource Manager Framework and Algorithms

Current state of the art electronic support (ES) receivers apply digital signal processing (DSP) to detect signals-of-interest (SOIs) and interference signals in the electromagnetic (EM) environment, formulate adaptive filter weights, and estimate the desired SOIs. The choice of adaptive digital beamforming (DBF) algorithm used to formulate the filter weights is determined traditionally during receiver design. Intelligent receivers, i.e. receivers that operate within Haykin's *perception-action cycle* [31], apply DSP not only for standard ES receiver processing but also to also select the adaptive DBF algorithm used in the processing. This dissertation develops a new receiver framework that *perceives* the EM environment and then performs the *action* of selecting an adaptive DBF algorithm based upon the perceived environment. No initial weighting of the array data is performed upon reception. The raw intermediate frequency (IF) array channel measurements are digitized and used by the receiver. The adaptive DBF weighting is applied after the *best* adaptive DBF algorithm is chosen by the resource manager (RM).

The receiver's perception and action are shown in the diagram of the proposed receiver architecture of Figure 1. The first processing performed by the receiver is perceiving the environment using the functions of the RM. Action is taken when an adaptive DBF algorithm is chosen from a look-up-table (LUT) of adaptive DBF algorithms. The final portion of the receiver is using the chosen adaptive DBF algorithm to estimate the SOIs using the measured array data.

This chapter details the RM that is responsible for perceiving the EM environment. In the case of the proposed receiver framework, perception involves estimating a set of environment parameters that can be used to classify the environment as belonging to one of a set of predetermined environment classes. The RM portion of the receiver framework is designed to be useable for all instantiations of the framework. The LUT

is comprised of adaptive DBF algorithms that are considered the *best* algorithms, from a chosen set, with respect to user-defined algorithm performance criteria. For demonstration purposes this research chooses signal-to-interference-plus-noise ratio (SINR) improvement and computational complexity as the desired algorithm performance criteria. By determining the environment class the RM determines the *best* adaptive DBF to chose from the LUT. An adaptive DBF algorithm must be chosen from the LUT for each SOI detected in the radio frequency (RF) environment. This requires the RM, in addition to classifying the RF interference environment, detect and disambiguate all SOIs in the environment. Detection of the SOI is accomplished through a three-of-three detection process and aided by the Akaike information criteria (AIC) model order selection algorithm. The AIC is used to determine the number of interference signals and the number of SOIs to ensure all signals are accounted for.

One last requirement levied upon the RM is the estimation of all required environment and SOI parameters for adaptive DBF algorithm implementation. As will become clear when the functional blocks of the RM, as depicted in Figure 1, are discussed, the parameters required for adaptive DBF algorithm implementation are estimated for adaptive DBF algorithm selection and SOI detection. It should also be noted that the RM assumes the type of SOI is known to include the spectral region where the SOI exists. The RM requires knowledge of the SOI spectral region to operate. No other *a priori* signal knowledge is assumed.

3.1 Resource Manager Look-Up-Table Interdependence

Design of the resource management algorithm is interdependent with design of the adaptive DBF LUT. The parameters estimated by the resource manager must be sufficient to differentiate between electromagnetic interference environment classes. The different interference environments must likewise allow for differentiation be-

tween adaptive DBF algorithms in the LUT. Because of this interdependence, a brief discussion of how the LUT is developed is required before the resource management algorithm is fully described.

The electromagnetic environment estimates must be parameterized so that performances of adaptive DBF algorithms are sensitive to the parameter changes. Measurable environment parameters include the number of interference signals, bandwidth of interference signals, directions of arrival of interference signals, and power of interference signals. However, power estimates rely on signal knowledge greater than what is known *a priori*, or estimable, by the electromagnetic signal receiver. Simulation experiments in Section 4.2 show the number of interference signals and interference signal bandwidth have the most effect on adaptive DBF performance. For interference signals of similar power, the spatial distribution is shown to have little effect; likewise, the spectral distribution of the interference signals is also shown to have little effect. The one caveat is when the interference signal is within one half beamwidth, with regard to the beamformer applied, in which case the error greatly increases. In such instances data-dependent beamformers are able to differentiate between signal and interference only when there is either spatial or spectral differentiation between the signal and interference sources. When the interference signals are co-located with the signal of interest both spectrally and spatially, no adaptive DBF algorithms are able to separate the signal from the interference.

Of the observable electromagnetic environment parameters, only the number of interference signals present and the relative bandwidths of the interference signals provide for differentiation between the different adaptive DBF algorithms under consideration. The LUT is therefore designed by varying these two parameters to create multiple interference environments against which the chosen adaptive DBF algorithms are tested.

77

The exact number and composition of the electromagnetic environments generated for LUT generation is also determined by the adaptive DBF algorithm sensitivity analyses in Section 4.2. The adaptive DBF algorithms used in the sensitivity analysis demonstrate natural break points with regard to the number of signals and bandwidths of the signals in the interference environments. For the current research a total of eight interference environments were simulated for LUT generation. The parameters for each are listed in Table 1.

Table 1. Listing of scenario environment parameters for LUT generation

Scenario	# of Interference Signals	Bandwidth of Signals
One	1	Wideband
Two	2	Wideband
Three	5	Wideband
Four	10	Wideband
Five	1	Narrowband
Six	2	Wideband and Narrowband
Seven	2	Wideband and Narrowband
Eight	5	Wideband and Narrowband

The selection of adaptive DBF algorithms for the LUT is based upon user defined selection criteria. The framework instantiation used throughout this work for demonstration purposes is designed to accurately estimate an SOI using the most computationally efficient DBF algorithmin available to the receiver. Adaptive DBF algorithms are usually compared with regard to their ability to remove the effect of interference and noise on a signal of interest. One logical measure for consideration in the current instantiation is thus the SINR improvement, which measures an algorithm's ability to reduce the influence of interference and noise on the SOI [70, 113]; for this reason, SINR improvement is the first performance criteria[1] where

$$\text{SINR Improvement} = \frac{\text{SINR out}}{\text{SINR in}} \tag{129}$$

---

[1]Appendix B contains a discussion on the use of SINR and SINR improvement as an adaptive DBF algorithm performance metric.

and

$$\text{SINR} = \frac{p_{sig}}{p_{noise} + p_{interference}}. \tag{130}$$

The sensitivity studies performed to determine the effects of changing environment parameters on receiver performance were achieved using the SINR improvement performance measure.

The current receiver framework instantiation is also designed to increase the efficiency of ES receivers, in addition to providing the best SINR improvement across a large number of interference environments. Algorithm efficiency is measured in terms of computational complexity. LUT entries are those adaptive DBF algorithms not only with high SINR improvement, but those that also have low computational complexity. As a result computational complexity is chosen as the second performance criteria for implementation. Further discussion on receiver efficiency is provided in Section 3.3.

Knowledge of the performance, with respect to the receiver framework implementor's performance criteria, is not sufficient to populate the LUT. The receiver framework implementor must also provide a rule to determine how the algorithm performance is used to determine the *best* adaptive DBF algorithm for each RF environment tested. For the current demonstration framework instantiation the designer is concerned with minimizing the computational complexity of the receiver while meeting a required SINR improvement threshold. The SINR improvement threshold is based upon the post processing performed on the signal estimate. Algorithms for decoding communication signals and creating pulse descriptor words (PDWs) have a known required SINR. The threshold also requires knowledge of the "worst case" SINR environment. The minimum required SINR improvement is then

$$\text{required SINR improvement} = \frac{\text{SINR}_{\text{required out}}}{\text{SINR}_{\text{worst case}}}. \tag{131}$$

The demonstration decision rule is then to find the subset of adaptive DBF algorithms, from the user determined set of adaptive DBF algorithms, that provide the required SINR improvement. Given the subset of adaptive DBF algorithms that most likely meet the SINR improvement threshold, the decision rule chooses the algorithm that has the lowest computational complexity from the set.

3.2   Resource Manager Structure

The structure of the RM is shown in Figure 7. There are two functional blocks that run in parallel. The first block is labeled environment determination, and it provides estimates of the number of signals in the environment, the direction-of-arrival (DOA) of all signals in the environment, and the relative bandwidth of those signals in the environment. The relative bandwidth of the environment refers to whether there are narrowband signals, wideband signals, or a mixture of wideband and narrowband signals in the environment. The environment determination block provides estimates of the environment parameters to the selection algorithm that chooses the *best* adaptive DBF algorithm from the LUT.

The SOI detection block disambiguates the RF environment by separating the SOIs from the interference sources. Upon completion, the SOI detection block provides the number of SOIs in the environment and their respective DOA for creation of adaptive DBF weights. Multiple beams are created when multiple SOIs are detected, and a separate set of adaptive filter weights is created to estimate each SOI.

Processing the two functional blocks uses a single spectral estimate (multi-taper method (MTM) estimation) and then three parallel paths. Path one determines the number of detected signals in the environment using the AIC model order selection algorithm and estimates the DOA of all detected signals in the environment. . Path two determines the relative bandwidths of the signals in the RF environment. Path

three separates the signals from the interference sources and provide the number of interference signals and the DOA of each SOI.
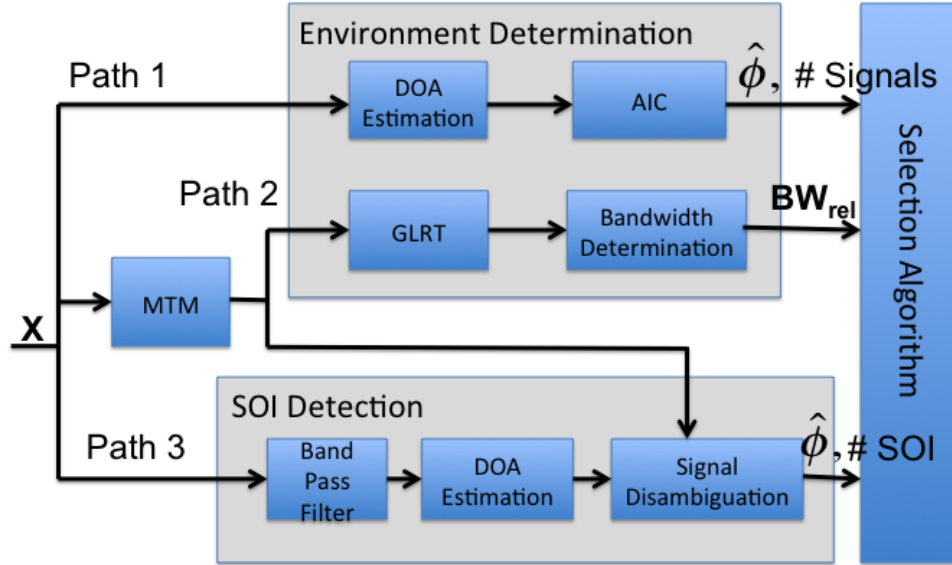
Figure 7. A diagram of resource manager functionality showing the parameter vectors ϕ and BW provided by the environment estimation and SOI detection functional blocks to the selection algorithm.

While the provided RM architecture, to include the AIC, MTM, and generalized likelihood ratio test (GLRT) algorithms can be used without further modification. The framework, however, is flexible and allows for different model order selection algorithms, different spectral estimation algorithms, and different detection algorithms. The choice is based upon the desires of the receiver implementor. Applying the framework with different estimation algorithm requires substituting the new algorithms directly in the framework where the original algorithm was applied. Processing then proceeds as if the original algorithms were in place.

3.2.1 Environment Determination.

The RM classifies EM interference environments based on the number of signals, the relative bandwidths of the signals, and the SOI of the signals; therefore the interference estimation algorithm must determine these two parameters. The interference estimation algorithm must also determine any parameters required for the adaptive DBF filter weights solution. Because the receiver is performing blind sensing, i.e. having no *a priori* knowledge of the interference sources, the adaptive DBF algorithms are chosen to require as few parameters as possible. The adaptive DBF algorithms implemented in this study only require the DOAs of the SOI and interference sources to be known. The interference estimation algorithm must then determine the number of interference signals, the bandwidths of the interference signals, and the DOA of each interference signal.

Referring again to Figure 7, the environment estimation algorithm operates along two parallel paths. Path 1 determines the number of signals as well as the DOA for each signal while Path 2 determines the bandwidths of the interference signals. The algorithm does not associate a bandwidth with each signal and DOA. The LUT is referenced only by the relative[2] bandwidths of the interference signals, i.e., whether there are wideband signals, narrowband signals, or a mixture of wideband and narrowband signals in the RF environment. The RM does not require knowledge of the bandwidth of each interference signal to adaptively select the adaptive DBF algorithm.

3.2.1.1 Signal Detection and Bandwidth Estimation.

Bandwidth determination and signal detection require estimating the spectrum of the environment. The spectrum is estimated using the MTM [109] of spectral

---

[2]Throughout the rest of the document determining whether there are widband signals, narrowband signals, or both wideband and narrowband signals present in the environment is referred to as relative bandwidth determination.

estimation. Classical estimation methods such as the Periodogram [47] and Bartlett [47] estimators suffer from biased estimates due to spectral leakage from the choice of windows used in the estimation. The MTM spectral estimator, however, through the use of discrete prolate spheroidal sequence (DPSS) has low spectral leakage [31, 109]; for this reason the MTM estimator is chosen for the RM algorithm.

Detection and bandwidth estimation of interference signals are implemented by applying a GLRT to the spectral estimate $\bar{S}^{(mt)}(f)$. The GLRT, which is fully developed in Section 2.5.3.2, is applied in spectral sub-bands and returns hypothesis $\mathcal{H}_1$ when a signal is present in the given sub-band, and returns hypothesis $\mathcal{H}_0$ when no signal is determined to be present. The relative bandwidth of the signals is determined using the GLRT output. Determining the relative bandwidth requires that the sub-band size is made sufficiently small such that narrowband signals are expected to mostly fill a sub-band. Signals that span multiple sub-bands are declared to be wideband signals; signals that encompass a only a single sub-band are declared narrowband signals. Using the methodology it is possible that two narrowband signals are present such that when the GLRT is applied the combined output of the two signals is declared to be a wideband signal. Also, it is possible that narrowband signals are hidden in wideband signals. These errors could lead to the mis-characterization of the RF environment.

Consider how the RF environment may be mis-characterized. In both cases narrowband signals are confused for wideband signals. If no other narrowband signals are determined present in the environment the environment is declared to only have wideband signals present. This error leads to beamformers being chosen that are *best* for wideband environments. As will be demonstrated for the receiver framework instantiation used for demonstration in this work when the LUT is fully developed, wideband DBF algorithms always produce a higher SINR improvement than narrow-

band algorithms. In all cases when narrowband signals are confused for wideband signals the resulting adaptive DBF algorithm is capable of providing the required SINR improvement. It is possible, however, that a more efficient adaptive DBF algorithm would be chosen if the correct relative bandwidth was declared. The effect of the error for other instantiations is dependent upon the types of adaptive DBF algorithms implemented and the decision rules used to determine the *best* algorithm. In all cases, however, wideband algorithms are able to beamform in scenarios with narrowband interference signals and the resulting receiver system is capable of meeting the mission requirements regardless of how often the error occurs.

A GLRT is chosen over other detection techniques because it satisfies the Neyman-Pearson criteria of maximizing the probability of detection for a given probability of false alarm given the available data. A standard likelihood ratio test that also satisfies Neyman-Pearson criteria [45] is not applicable, because the test statistics for the environment estimation algorithm are formed from estimated data, and so the exact probability density functions of the data samples are not known.

3.2.1.2 DOA Estimation.

The directions of arrival of the interference signals are found through standard wideband direction of arrival estimation algorithms. As with the spectral estimation, a consistent estimator of the directions of arrival is desired. It is also desired that the estimator operate on multiple signals simultaneously. The method of Kaveh [122] is capable of locating the direction of arrival of multiple sources each to within 1° when applied to a uniform linear array (ULA) and when the number of interference signals does not exceed the degrees of freedom of the array. Furthermore, the method is able to differentiate the DOA of correlated sources. These desirable properties make the method of Kaveh a good choice of DOA estimator for the RM algorithm.

.

3.2.2   Signal Of Interest Detection.

The third parallel path of the resource manager is the signal of interest detection. The signal of interest detector, as did the environment estimator for detection of interference signals, utilizes a MTM spectral estimator and the GLRT detector to determine if a signal of interest is present in the environment. The GLRT is able to search over portions of the spectral estimate. Because the type of signal of interest is known *a priori*, the spectral region of the SOI is known. The MTM estimated samples for this region are used as input into the GLRT to determine if a SOI is present.

Detection of SOI proceeds by first spectrally filtering the array channel data to include only those frequencies where the SOI is known to exist. Second, a DOA estimation algorithm is applied to the spectrally filtered data. If only a single DOA is returned, then a single SOI is assumed to exist and the detection block exits, providing the DOA of the single SOI to the RM. If multiple DOAs are returned, the spectrally filtered array channel data is used in a signal disambiguation algorithm that applies a three-of-three detection algorithm to the signal represented by each returned DOA. The three-of-three detection algorithm separates interference signals from the SOIs. The signal disambiguation algorithm returns the number of SOIs and a DOA for each.

3.2.2.1   Signal of Interest Disambiguation.

SOI disambiguation is required, because SOI detection is based upon a signal having spectral content in a desired spectral region. The DOA estimation algorithm is applied to the data filtered to contain only this spectral region. It is possible

85

interference signals also have spectral content in this same region. Such interference signals provide a DOA when the estimation is performed. If an adaptive algorithm was applied in the direction of each estimated DOAs, beamformers would be applied to estimate interference signals wasting receiver resources. Signal disambiguation separates the SOI from any interference signals with overlapping spectral content.

Operation of the disambiguation algorithm is diagrammed in Figure 8. Data used in the disambiguation algorithm has been spectrally filtered to coincide with the desired frequency range of the SOI. The processing first applies a filter bank of frequency invariant spatial beamformers, where only the directions collocated with an estimated direction of arrival are implemented. At this point there are three possibilities for each spatial beam. The first case is only a signal of interest is present in the beam. The second case is both a signal of interest and an interference signal with frequencies overlapping that of the signal of interest are located in the spatial beam. The third case is only interference signals with frequencies similar to the SOI are present in the spatial beam. The output of the RM and the overall computational complexity are dependent upon which case is selected. The RM only selects an adaptive DBF algorithm for cases one and two. No adaptive DBF algorithm is selected for case three as no SOI is present in the environment.

After application of the frequency invariant beamformer (FIB) filter bank, a MTM spectral estimator is applied to each beamspace output of the filter bank. The spectral estimate is used in a three-of-three (TOT) detection algorithm. The TOT algorithm is an inherently space-time procedure. The spatial domain is set by using a single FIB beam. The spectral domain is previously set by applying a frequency filter to only cover the spectral region of interest. For each spatial beam, the SOI spectral region of the MTM spectral estimate is divided into thirds, and a GLRT detection algorithm applied to each third. If a SOI is present in the environment, all three
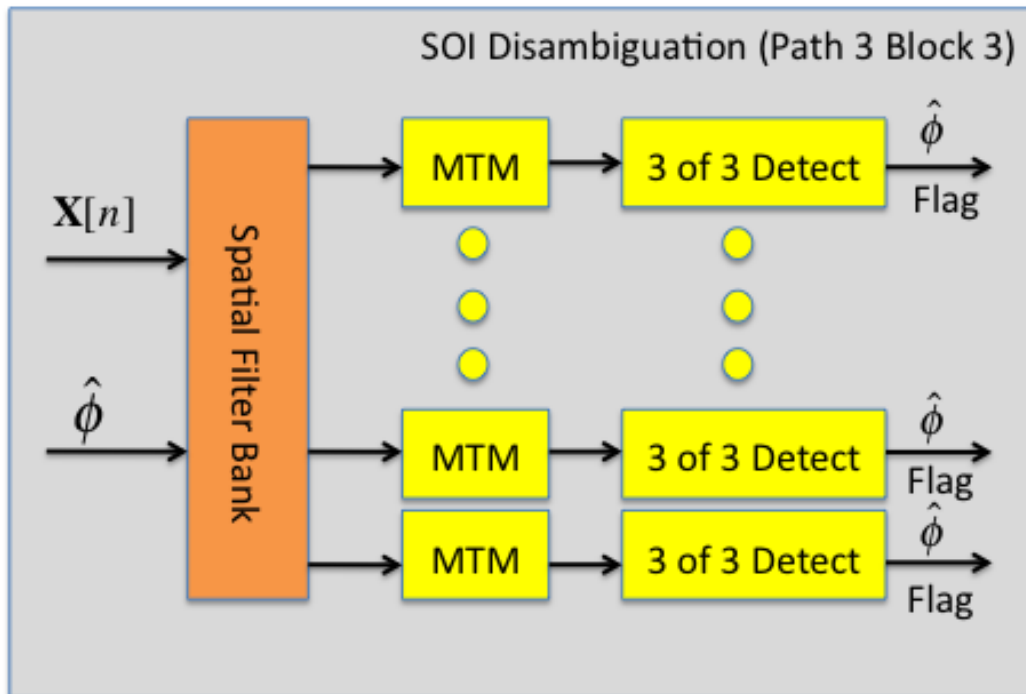
86

Figure 8. Diagram of the signal of interest disambiguation functional block showing the three-of-three algorithm for each spatial sub-band formed toward each DOA estimated by the DOA estimator of the SOI detection functional block. The Flag is set to one when a SOI is present and zero when no SOI is present.

sub-band GLRTs should return $\mathcal{H}_1$. If only noise and interference sources are present in the environment, at least one of the three sub-band GLRT is likely to return $\mathcal{H}_0$ indicating no signal present. The TOT detection algorithm is designed to only return that a SOI is present if all three sub-band GLRT return $\mathcal{H}_1$.

It is possible that a spatial beam containing only noise and interference is returned as a false positive; this is unavoidable if the interference source overlaps more than 66% of the SOI frequency band. In this case the receiver would mistake an interference signal as an SOI, select an adaptive DBF algorithm from the LUT, and apply the adaptive DBF algorithm to attempt to estimate the false signal. It would be up to the data processing of the receiver to determine if the received data contained an actual signal or interference. If more than three sub-bands were used in the detection algorithm, the probability of false alarm could be reduced further, with a corresponding increase in complexity for the additional GLRT. Three sub-bands are chosen as they decrease the probability of false alarm over only using a single GLRT in the desired frequency range while not adding intolerable computational burden. An area of future research would be to determine the optimal number of sub-bands for signal disambiguation which may depend on SOI.

The three-of-three detection algorithm completes the signal disambiguation. Prior to application of the three-of-three detection algorithm the RM considers all signals that have any spectral overlap with the known SOI spectrum as SOI. Thus DOA for all such signals are passed to the three-of-three detection algorithm. The disambiguation algorithm chooses which DOA correspond to actual SOI. With the number of SOIs and their respective DOA determined, the RM has knowledge of both the interference environment and all SOIs present in the environment. This information is used to select the proper adaptive DBF algorithm from the LUT for implementation by the receiver.

3.3 Receiver Efficacy

The proposed receiver framework is designed to have better performance across a wider variety of electromagnetic environments, in terms of SINR improvement than a standard ES receiver, while also increasing the efficiency of algorithm employment. Using an RM the proposed framework selects the most efficient, in terms of computational complexity, adaptive DBF algorithm capable of meeting a required SINR improvement level. Selecting the most efficient algorithm, however, requires additional computational complexity to estimate the number of interference signals and the bandwidths of the interference signals in the electromagnetic environment. In order for the proposed receiver framework to have improved efficiency over standard receivers, the added complexity cannot add significantly to the receiver processing timeline.

It is assumed that all multi-beam receivers must perform some amount of SOI disambiguation to properly form multiple simultaneous beams. The proposed receiver framework, within the context of the RM, performs the newly required environment parameter estimation tasks at the same time as the SOI detection. The processing is split between computational resources using parallel processing.

Parallel processing involves breaking the processing required for an algorithm into different threads, which are all run independently at the same time [14, 50]. Some overhead processing is required to first parse the required data for the parallel paths and to reconstruct the data after the completion of the parallel paths; however, the complexity improvement over processing threads in series far outweighs the extra processing required for parallel processing overhead [14, 50].

Thus, by performing the environment parameter estimation and SOI detection in parallel, the run time of receiver processing is not increased by an amount equivalent with the computational complexity of the "extra" processing. In fact, if the

computational complexity of the environment parameter estimation is less than the computational complexity of the SOI detection process there is no increase in timeline over that of a standard receiver for the proposed receiver framework. Conversely, if the environment parameter estimation process took more time than the SOI detection process there would be an increase in overall receiver processing timeline. Processing that does not increase the run time of a receiver employing the proposed receiver framework when compared to a standard receiver is predicated upon the standard receiver being capable of forming multiple digital beams. While the exact complexity of the detection processing required for multiple beams differs between receiver implementations, some level of effort and amount of complexity must be required to perform the processing. The framework is designed to use efficient algorithms to determine the RF environment so any complexity difference between the SOI detection and the RF environment detection is minimized.

3.3.1 Resource Manager Computational Complexity.

The overall computational complexity of the resource manager is the maximum complexity of either parallel branch. The first parallel branch is the electromagnetic environment determination. The first step in this determination is a MTM spectral estimate. The MTM estimate first solves for the DPSS sequences. An $N \times N$ matrix is formed where the ith, j^{th} element is given as

$$\mathbf{A}_{i,j} = \frac{\sin\left(2\pi B \left(i - j\right)\right)}{\pi \left(i - j\right)} \tag{132}$$

and B is the bandwidth of the spectral estimate. Considering that each computation of the sine function requires constant time for computation, the complexity of this matrix calculation is N^2. The DPSS values are the first Δ eigenvectors of matrix $\mathbf{A}$, where Δ is the number of DPSS sequences used in the MTM estimate. Each eigenvec-

tor and its corresponding eigenvalue are found using EISPACK[3] in N^3 operations [4]. The total complexity for the DPSS is then ΔN^3. The total number of DPSS used during experimentation in Chapter 5, is always calculated as less than 10; the total complexity of the DPSS computation is therefore $O\left(N^3\right)$.

Each DPSS is then applied to a periodogram estimate of the spectrum, and a weighted average, using the eigenvalues as weights, is computed. The cost of each periodogram is $N \log N$ where log is logarithm base 2. The total cost of the weighted average is then $O\left(N \log N\right)$. This complexity is an order of N less that that required to solve for the DPSS, thus the overall complexity of the MTM spectral estimator is $O\left(N^3\right)$ where N is the number of data points used for the estimate.

The second operation required for environment determination is the GLRT, which is applied to the MTM estimate. Multiple instances of the GLRT must be applied to determine if a signal is present over each sub band. If P sub bands are used then P instances of the GLRT need to be applied. Each GLRT is a comparison test. The test statistic can be computed in constant time, and the comparison is done in constant time so each GLRT adds little to the complexity. In the worst case scenario a GLRT will be taken for each sample in the MTM and thus the complexity of the GLRT would be $O\left(N\right)$.

The third component of the environment estimation is the direction of arrival estimation. Using the designator P to denote sub bands again, the method of Kaveh [122] forms P focusing matrices to focus the wideband multi-rank covariance matrices to rank one matrices. Each of the P transformation matrices requires an $N \times N$ matrix computed as

$$\mathbf{R}_{j,k} = 2\mu_i \operatorname{sinc}\left[\left(d\frac{\mu_i}{c}\right)\left[(j-1)\left(2\pi f_c\right) - (k-1)\left(2\pi\mathbf{f}\right)\right]\right] \qquad (133)$$

---

[3]The computational complexity is dependent upon the actual algorithms used in receiver implementation; this dissertation implements algorithms using MATLAB, which in turn uses EISPACK.

where μ_i is the angle extent over which the search is to occur. This angle is dependent upon the spatial surveillance area of the array. The focused frequency is f_c and $\mathbf{f}(p)$ is the center frequency of the pth sub band being focused. The complexity of forming matrix $\mathbf{R}_{j,k}$ is $O(N^2)$. A singular value decomposition is applied to the matrix at a cost of $O(N^3)$. The sensor data is also placed through a band pass filter and the sample matrix inversion technique used to determine the frequency domain covariance matrix for each frequency band. Each band requires $O(N^3)$ calculations for the covariance matrix. The total cost for the focussed matrix is then $O(PN^3)$. The MUSIC method is then applied to the focused covariance matrix at a cost of $O(N^3)$. The total computational complexity for the Kaveh method of DOA estimation is then $O(PN^3)$. If further revisions are required for improved accuracy, each revision requires $O(N^3)$ computations. This increases the multiplication constant in the big O notation, but the overall complexity remains the same.

The environment estimation requires a single MTM estimate, followed by multiple GLRT implementations as well as a DOA estimate. Each of the algorithms has a complexity of at least $O(N^3)$ with the most complex requiring a multiplication factor of P. Thus the total complexity for the environmental estimator is $O(PN^3)$.

The complexity of the signal detection functional block is dependent upon whether there is a single SOI or multiple SOIs. A complexity analysis deals with the worst case scenario the analysis will be done as if there are multiple SOIs present. The algorithm starts with N complex multiplications to apply the bandpass filter followed by a a PN^3 DOA estimate. Now consider that K signals are present in the environment. The next processing is application of K spatial filters for a total complexity of $O(KN)$. The signal disambiguation algorithm applies K spectral estimates for $O(KN^3)$ complexity. The three-of-three detector applies three constant time GLRT algorithms to each estimate adding only $O(N)$. The complexity is now $O(KN^3 + PN^3)$. For

a given receiver, the number of possible detectable signals is limited by the number of array channels. Contrast this with the number of sub-bands used in the DOA estimation. The number of sub-bands is on the order of an fast Fourier transform (FFT) computation using greater than 512 samples [122]. While large arrays exits this research assumes that the array will have less than 512 elements and so $P > K$. The number of signals of interest is absorbed in the hidden multiplication factor of the Big-O notation making the total complexity of the signal detection algorithm $O\left(PN^3\right)$, which is the same as for the environment estimation algorithm.

When equating computational complexities using big-O notation the hidden multiplication factors may differ between the compared complexities. For the case of the environment determination algorithm and the signal detection algorithm, however, the resulting complexities are due to an equivalent number of MTM spectral estimates and GLRT applications. As the operations performed are the same the resulting multiplication factors are also the same. This analysis demonstrates that if parallel processing is used, there is no heavy penalty to pay for implementing a receiver architecture that intelligently senses the environment. Thus any processing gain achieved from selection of the most optimal algorithm can be used to form additional independent spatial beams as is desired.

At first glance it might seem as if the complexity analysis would be incorrect when there is only one signal of interest and the disambiguation algorithm does not need to be run. In this case the complexity is reduced by a factor of K. However, there are a limited number of signals of interest present in any environment. Even when a global system for mobile (GSM) system is considered, because a cell can only handle a given number of users, and only a portion of the cell is under surveillance, the number of possible users will be several factors below that of the number of data points used. Even if only 1024 samples are used at any one time, 50 users would

still be two factors below the size N. Furthermore, consider that if many parallel processors were available, such as on a graphics processing unit (GPU), then each of the K calculations are done simultaneously and there would be no inherent reduction in complexity from only having a single SOI present.

3.3.2 Receiver Complexity Considerations.

As stated above the computational complexities of both functional blocks in the RM are equivalent. Because both parallel paths have an equivalent complexity, the new receiver architecture does not have any added timeline over a receiver employing a single adaptive DBF algorithm in multiple independent beams for multiple SOI meeting the increased efficiency requirement of the proposed receiver framework.

It should be noted that while both algorithms have the same "Big O" complexity, the actual run times of each algorithm will not be exactly the same. Omitted from the notation is a multiplication factor on the PN^3 which could be large or small. The notation assumes that the multiplication factors are less than N and so the differences between the complexities of the two algorithms are roughly equivalent. Further, depending upon the receiver hardware being used for algorithm implementation, the $O\left(PN^3\right)$ complexity may or may not be "fast" enough for real time operation. That determination needs to be made on a system-by-system basis. This research assumes that hardware exists such that real time requirements are able to be met with the $O\left(PN^3\right)$ complexity.

3.4 Resource Manager Review

The addition of intelligence to an ES receiver requires that *perception* beget *action* based upon the *perception*. The RM provides the *perception* and *action* by classifying the EM environment represented by the sampled array channel data and using

the EM environment classification to select an adaptive DBF algorithm from an *a priori* determined LUT of adaptive DBF algorithms. The addition of intelligent action through an RM is a major contribution of this dissertation and has not been demonstrated prior to tis research.

This chapter described the main two portions of the RM. The third portion of the RM is the selection of the *best* adaptive DBF algorithm from the LUT. From the perspective of the RM, once the RF environment parameters are estimated, the type of adaptive DBF to apply only requires a reference to a table. The adaptive DBF algorithms are implemented by the receiver outside of the RM. Therefore, from the perspective of the RM the LUT is considered *a priori* knowledge, determined before receiver operation. For this reason the full description and development of the LUT are afforded their own discussion, provided next in Chapter IV.

IV. Look Up Table Development

The resource manager (RM) of the proposed receiver architecture operates on samples of the electromagnetic environment received by an array. By applying digital signal processing (DSP) the RM is able to parameterize the electromagnetic environment according to the number of interference signals in the environment and their respective bandwidths. The RM also determines the number of signals-of-interest (SOIs) present in the environment and their respective directions-of-arrival (DOAs). Using the estimated parameters, the RM selects the most optimal adaptive digital beamforming (DBF) algorithm on a per SOI basis, from a predetermined look-up-table (LUT) of adaptive DBF algorithms. Selection of the *best* adaptive DBF algorithm is based upon selection criteria determined by the receiver designer[1]. The RM then supplies the optimal algorithm and any parameters required for adaptive DBF implementation to the electronic support (ES) receiver where the ES receiver implements the chosen adaptive DBF algorithms.

Choice of adaptive DBF algorithm optimality criteria is based upon the aims of the proposed receiver framework designer. The current framework under study is designed to improve both beamforming performance and receiver efficiency over standard ES receivers. Receiver efficiency is gauged in terms of adaptive DBF computational complexity. Many adaptive DBF algorithms are capable of estimating the SOI waveform but if the algorithms are overtly complex the receiver system is inefficient. Beamforming performance is usually measured in SINR improvement [70,113]. SINR improvement is a measure of the increase in SINR due to adaptive DBF algorithm implementation. Greater SINR improvement corresponds to greater beamformer performance. Section 4.5 describes how the performance measures of SINR improvement

---

[1]This research uses signal-to-interference-plus-noise ratio (SINR) improvement and computational complexity as the selection criteria for a representative receiver implementation.

and computational complexity are used to select the adaptive DBF algorithms for the LUT.

There are myriad environmental parameters that can be estimated and used to select the optimal adaptive DBF algorithm from the LUT. The larger the number of parameters required to access a solution in the LUT the more complex the environment estimation algorithms must be. Furthermore, the performance of the adaptive DBF algorithms is not sensitive to changes in all parameters. Developing the LUT requires knowledge of what minimal set of environment parameters suffices to differentiate the adaptive DBF algorithm's performance against different electromagnetic environments. Knowledge of the minimal set of environment parameters is generated empirically by performing a sensitivity study of signal bandwidth, number of interference signals in the environment, and the directions of arrival of the interference signals. These three parameters are chosen because they are easily estimated using known DSP techniques. Other environment parameters such as interference signal power could also be estimated. Signal power estimation, however, requires greater signal processing and increases the system complexity. Because the goal of the proposed receiver framework implementation is to estimate the SOI as efficiently as possible, parameters whose estimation increases the computational complexity of the environment estimation are not considered further.

To create the LUT based upon the number of interference signals, the interference signals' bandwidths, and their respective DOAs, a number of interference environments are simulated, varying one or more of the parameters for each successive simulated scenario. The performance of a set of adaptive DBF algorithms, in terms of SINR improvement and computational complexity when applied to each simulated scenario are compared. The decision rule for the receiver framework instantiation presented in this research forms a subset of considered DBF algorithms that provide

97

the required SINR improvement and selects the adaptive DBF from the subset that has the lowest computational complexity.

Each adaptive DBF algorithm chosen for listing in the LUT is referenced by the environment parameters associated with the simulated scenario for which the algorithm was determined to be *best*. Operationally, the RM estimates the environment parameters required to select an adaptive DBF algorithm from the LUT. The RM also estimates the DOA of the SOI and of each interference signal. The RM then chooses the *best* adaptive DBF algorithm from the LUT using the estimated environment parameters. The chosen adaptive DBF algorithm is *best* not only for the canonical radio frequency (RF) environment used to develop the LUT but for any RF environment similar to the canonical environment with respect to the estimated environment parameters. The selected *best* adaptive DBF algorithm wight he number of SOIs and DOA for each SOI are then used to form multiple independent beams and provide estimates of the sought after SOIs waveform.

The remainder of this chapter details creation of the LUT. First is a listing of the five adaptive DBF algorithms considered for inclusion in the LUT. Second, each of the eight simulated interference scenarios are described to include the number, bandwidth, and DOA of all interference signals and the SOI. Third, the results of each of the five adaptive DBF algorithms when used to estimate the SOI in each of the eight interference scenarios are listed. This same section also discusses how the results are interpreted to form the LUT. The chapter concludes with the LUT listing.

4.1 Adaptive DBF Algorithms

As with parameters able to characterize an electromagnetic environment, there are a panoply of different adaptive DBF algorithms that can be applied to estimate an SOI. In any receiver implementation, even receivers capable of applying multiple

adaptive DBF algorithms, a choice must be made of which algorithms to implement. The receiver designer may choose a set of algorithms based upon the desired outcome of the receiver implementation and the decision rules used to select the *best* algorithms for inclusion in the LUT. The receiver designer should consider selecting a set of adaptive DBF algorithms that are known to be effective against the RF scenarios the receiver framework is expected to operate against. The effectiveness of the adaptive DBF algorithms should be in terms of the LUT decision rule criteria which are in terms of desired receiver framework outcomes. Greater variability in the algorithm considered *best* requires multiple decision criteria when selecting algorithms for the LUT.

Returning again to the purpose of this research effort, that is developing and demonstrating the applicability of a new receiver framework, the algorithms chosen for the current framework implementation need not be state-of-the-art. The chosen algorithms must meet the stated receiver desires of providing a required SINR improvement with low computational complexity. Furthermore, the chosen algorithms should span the range of adaptive DBF algorithms with respect to computational complexity and SINR improvement.

Not all adaptive DBF algorithms discussed in the available literature are applicable to the current receiver framework implementation. Algorithms such as least mean squares (LMS), minimum mean squared error (MMSE), and the Kalman filter all require knowledge of the SOI [35, 70, 114], which is unavailable in the current receiver framework. The five adaptive DBF algorithms selected for the current effort are thus those adaptive DBF algorithms that are proven effective in the literature while at the same time do not require signal knowledge unavailable to the receiver.

Based on the above qualifications, a set of five adaptive DBF algorithms commonly found in the adaptive DBF literature are used. The algorithms include the

linearly constrained minimum variance (LCMV) beamformer [21], the generalized discrete Fourier transform (GDFT) beamformer [65], the time reversal method (TRM) beamformer [56, 57], and the least squares space-time beamformer (LSSB) beamformer [134, 135]. The fifth and final algorithm is a narrowband implementation of the LCMV algorithm [21]. As previously stated, this set of beamformers is not intended to be all inclusive or to be applicable in all possible ES receiver implementations but chosen to be representative for demonstrating the possibility of processing gain from applying the new receiver framework.

4.2   LUT Parameters

Parameterization of the electromagnetic environment is based on a subset of the possible RM estimable environment parameters. An initial limitation of the parameter set is based upon what parameters are readily estimated from array data without a high computational burden. Three such parameters are the number of signals in the environment, the bandwidths of the signals in the environment, and the spatial separation of each signal in the environment with respect to the SOI. Algorithms exist in the literature for each of these parameters and are readily implemented. The question then is: are all three parameters required, or is there a subset of these three parameters that is adequate? Any parameter set must be such that changing one or more of the parameters affects the performance of the available adaptive DBF algorithms in a measurable way. A sensitivity analysis of each of the three parameters determines which parameters have the most impact on adaptive DBF algorithm performance. The sensitivity analysis is performed by simulating scenarios, each containing a single SOI, where two of the three parameters are held constant while the third parameter is varied. The mean-squared error for each of the five adaptive DBF algorithms is plotted with respect to the varying parameter. For each beamformer

the mean-squared error is defined by

$$\epsilon_{MSE} = \| x_s(t) - y(t) \|^2 \qquad (134)$$

where $x_s(t)$ is the SOI and $y(t)$ is the beamformer output signal. In practice the mean-squared error is found by element-wise squaring the difference between the output vector given by

$$\mathbf{y} = [y[1], y[2], \cdots, y[8000]] \qquad (135)$$

which is the difference between the simulated input signal and output signal for all 8000 points. The mean square error (MSE) is the average of (135) squared over the 8000 data points

$$\epsilon_{MSE} = \frac{\mathbf{y}^2}{8000}. \qquad (136)$$

The MSE values are normalized by first creating a vector of errors for each adaptive DBF algorithm where the elements are the MSE for each sensitivity analysis scenario. This normalized error is found by element-wise dividing the error vector by the max error value of that vector given by

$$\epsilon_{norm} = \left[\frac{\epsilon_{MSE}[1]}{\max \epsilon_{MSE}}, \frac{\epsilon_{MSE}[2]}{\max \epsilon_{MSE}}, \cdots, \frac{\epsilon_{MSE}[\# \text{ of scenarios}]}{\max \epsilon_{MSE}} \right]. \qquad (137)$$

Algorithm performance is also presented as a percentage change in error. The percentage change in error is constructed by finding the difference in error, for a given DBF algorithm, between each sensitivity analysis scenario and the error for the scenario with the least error. The difference for each scenario is then divided by the

least error used to determine the difference as

$$PEC = \left[\frac{\epsilon_{MSE}\left[1\right] - \min \epsilon_{MSE}}{\min \epsilon_{MSE}}, \frac{\epsilon_{MSE}\left[2\right] - \min \epsilon_{MSE}}{\min \epsilon_{MSE}}, \cdots, \right.$$
$$\left. \frac{\epsilon_{MSE}\left[\# \text{ of scenarios}\right] - \min \epsilon_{MSE}}{\min \epsilon_{MSE}} \right]. \tag{138}$$

The parameters with the greatest sensitivity are indicated by large changes in error of the estimate as the parameter changes. It is possible that a combination of two or more of the parameters causes a greater sensitivity when changed in tandem than when a single parameter is changed. Such sensitivities are important to consider when implementing an operational system. For the current effort, however, as only the applicability of the proposed receiver framework is being considered, sensitivity due to combinations of parameters with respect to adaptive DBF sensitivity is not tracked. This would be an area of further study.

All sensitivity analyses are done simulating a 64-element array with array spacing of 0.2 meters. The array spacing is based on $d = \lambda/2$ spacing where $\lambda = 0.4$ meters for a maximum frequency of 750 MHz. Each of the array channels has a 20-tap finite impulse response (FIR) filter, where the time delay between taps is equal to the sample time of the array: $T_s = 1.5$ Gsamp/sec. The sensitivity analyses are empirical studies, where each of the five adaptive DBF algorithms are applied to each generated data set used to form the sensitivity analysis. Results are given in plots of normalized error power for the array output plotted against the parameter being tested for algorithm performance sensitivity. The error normalization is applied for each adaptive DBF algorithm separately so the error results for all beamformers range between zero and one.

In the sensitivity analyses that follow, the figures are formed by applying each of the five adaptive DBF algorithms to a number of RF environments. A single data point is the squared error for a beamformer applied to a single RF environment

averaged over 8000 time samples. The input signal to each beamformer is a stochastic signal from (3). All sources in the stochastic signal are zero-mean Gaussian sources; therefore, the input signal is ergodic in the mean [46]. Also, the adaptive DBF algorithms are linear filters, so the output signal $y(t)$ is also ergodic in the mean [46]. Given that both the input signal and the output signal are ergodic signals, the error is also an ergodic signal. The ergodicity of the signals means that averaging across 8000 time samples is equivalent to averaging across multiple realizations; therefore the plot of a single realization is equivalent to plotting the outcomes of a Monte-Carlo simulation. All data plots for the sensitivity analyses are then statistically equivalent to plots performed using a Monte-Carlo analysis.

The first parameter studied is interference signal spatial separation from the SOI. To test the effect of interference spatial separation, an environment with a wideband SOI at 0 degrees (broadside) and a single wideband interference signal is created. All signals have equivalent power. Each interference signal has 200 MHz instantaneous bandwidth and the SOI has 300 MHz instantaneous bandwidth. The direction of arrival of the interference signal is varied from -60 degrees to -5 degrees in 5 degree increments with a final 2.5 degree increment to the minimum DOA of -2.5 degrees. Positive angles are not tested as the array is a uniform linear array, and by symmetry the performance of the beamformer with signals separated in the positive direction is identical to performance from negative separation. The minimum difference of 2.5 degrees was set because at that point the interference signal was within the approximately 2.6 degree half-power main beamwidth [5] of a 64-element array. Furthermore, this angular separation was proven to be adequate based upon the simulation results.

The interference signal spatial separation sensitivity analysis results are given in Figure 9. The figure plots the normalized mean-squared error from each adaptive DBF algorithm for spatial separations equal to the interference signal DOA. The plots

in Figure 9 demonstrate the error trends for the beamformers across all sensitivity analysis scenarios and no comparison of adaptive DBF performance is possible from the figure. Figure 9 demonstrates that none of the five adaptive DBF algorithms are sensitive to changes in interference source spatial separation from the SOI until the DOA of the interference signal is within the half power beamwdith of the array. The percentage change in error of the beamformers, with respect to the minimum error of each beamformer, plotted again as a function of angular separation between the SOI and interference signal in Figure 10, reinforces the observation of the error plots in that the percentage increase in error is minimal until the interference signal is within the half power beamwidth of the array for the wideband beamformers. The narrowband beamformer exhibits increasing error for interference signals within ten degrees of the SOI. While the reasons for the greater error of the narrowband beamformer with respect to spatial separation is not specifically considered in this research, it is most likely due to the wideband nature of the SOI causing a spread in the eigenvectors of the covariance matrix used in the narrowband beamformer.

The result from the spatial separation sensitivity analysis is beneficial in that it simplifies the design of the following sensitivity analyses. As there is no effect on beamformer performance from changing the DOA of interference signals, the signals used in the bandwidth and number of interference signal sensitivity analysis are placed at arbitrarily generated angles. As long as the interference signals are not placed within one half-power beamwidth of the array design, the spatial location of the interference signal with respect to the spatial location of the SOI is inconsequential to adaptive beamformer performance.

The number of interference signals an array can handle is dependent upon the number of degrees of freedom of the array. For a simple linear array the number of degrees of freedom is the number of array elements. The sensitivity analysis utilizes a
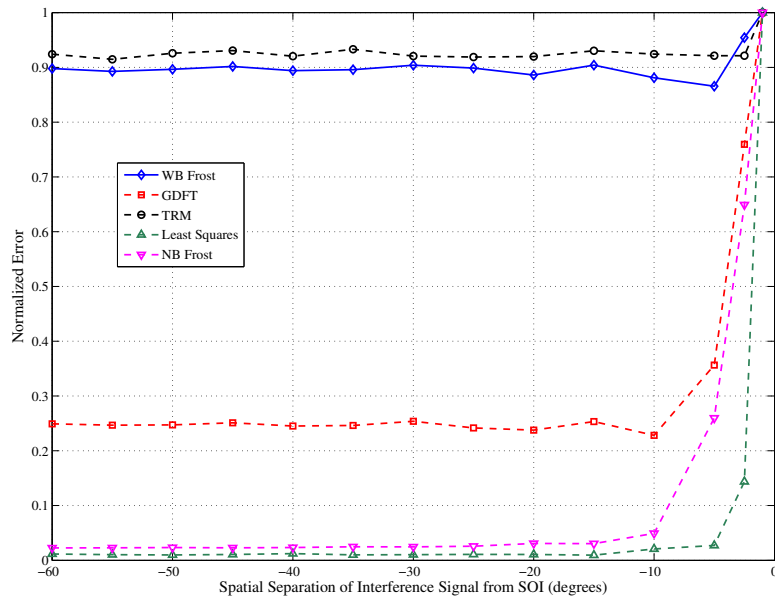
Figure 9. Mean-squared error of adaptive beamformers plotted as a function of angle of arrival with respect to the direction of arrival of the signal of interest. The plot demonstrates algorithm error trends and is not meant for beamformer comparison.
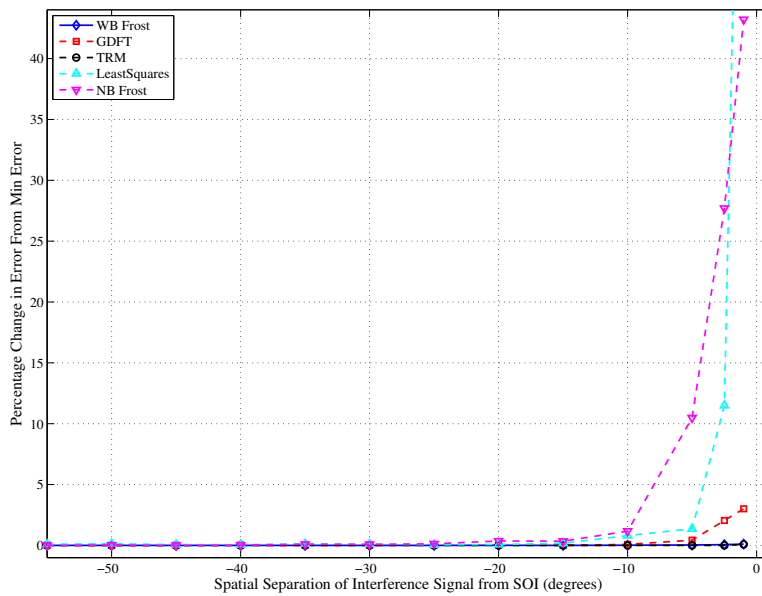

Figure 10. Percentage change of mean-squared error of adaptive beamformers plotted as function of angle of arrival with respect to the direction of arrival of the signal of interest.

105

64-element array and theoretically can cancel 63 interference sources. The purpose of this study is not to determine the maximum number of interference sources the array can cancel, regardless of interference source bandwidth or source spatial distribution, so the number of sources used in the study is less than 63. Figure 11 shows two inflection points in the error profile of the narrowband LCMV algorithm and the TRM algorithm, with respect to the number of SOIs. The first inflection point is at five interference signals and the second break point is at ten signals of interest. Also present in the figure is an inflection point at ten interference sources for the GDFT and wideband LCMV beamformers. Figure 12 plots the percentage change in error, with respect to the minimum error encountered at one interference signal, of the beamformers with respect to the number of interference signals. The two inflection points at five and ten signals of interest are again present in the data for the respective beamformers, reinforcing the sensitivity of three of the beamformers to changing the number of SOIs. While there are inflection points for all but the LSSB algorithm the change in error is much greater than for the other beamformers. However, the RM will select the best adaptive DBF algorithm for each scenario and even a slight change in performance could change the selected beamformer, especially when the computational complexity is taken into account. For this reason LUT table scenarios are created with less than five interference signals, between five and ten interference signals and greater than ten interference signals. Varying the number of signals to encompass all three regions should illuminate how the *best* adaptive DBF algorithm varies with respect to the number of interference sources.

The bandwidth sensitivity analysis uses a broadside, wideband SOI and a single interference source incident from -30 degrees. The instantaneous bandwidth of the array under test is 750 MHz. To keep within the instantaneous bandwidth of the array the bandwidth of the interference source is capped at 650 MHz. The interference
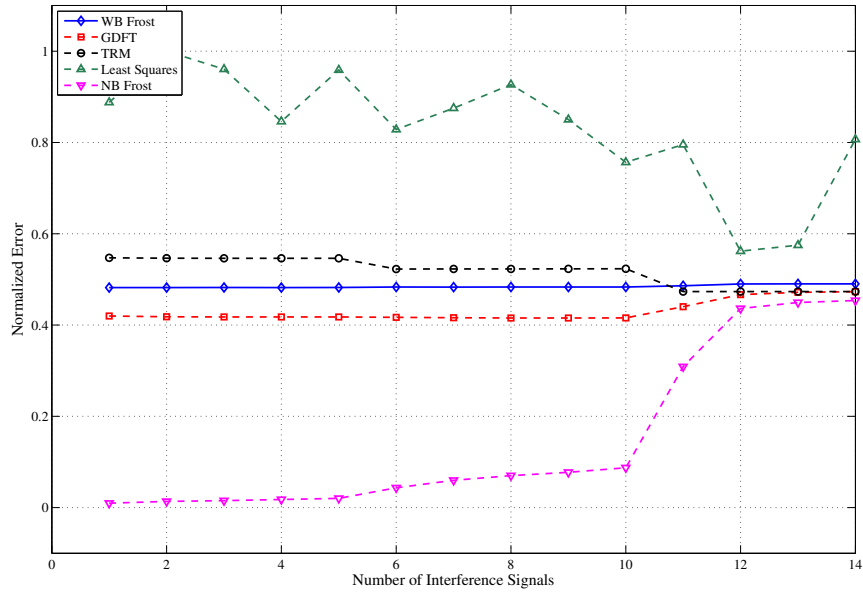
106

Figure 11. Mean-squared error of adaptive beamformers plotted as a function of the number of interference signals in the electromagnetic environment.
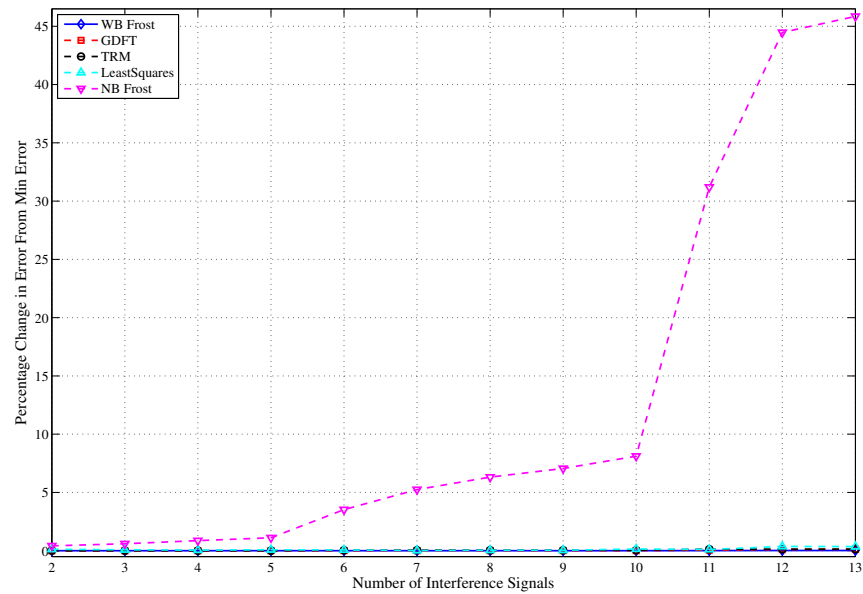

Figure 12. Percentage change in mean-squared error of adaptive beamformers as a function of the number of interference signals in the environment.

107

source bandwidth starts at 10 MHz, then 25 MHz, then 50 MHz, and is further varied from 50 MHz to 650 MHz in 50 MHz increments. The bandwidth sensitivity analysis results are given in Figure 13. The results indicate that wideband adaptive DBF algorithms are insensitive to the bandwidth of the interference sources. As would be expected, however, the narrowband adaptive DBF algorithm has rapidly decreasing performance of signals with bandwidths of greater that 50 MHz. Figure 14, a plot of percent error change for each algorithm, corroborates both the insensitivity of the wideband adaptive DBF algorithms with respect to interference signal bandwidth, and the increasing error of the narrowband adaptive DBF algorithm with increasing interference signal bandwidth. Because of the large difference between the performance of narrowband and wideband adaptive DBF algorithms for signals of increasing bandwidth, the LUT contains electromagnetic environments with interference signals that are narrowband and wideband. It should be noted that the absolute bandwidth of the interference sources is immaterial. The RM algorithm only needs to determine if the interference signals are narrowband or wideband.

4.3 Interference Power Considerations

While the powers of the interference signals in the electromagnetic (EM) environment are not considered for LUT algorithm selection parameters, interference power does affect adaptive DBF performance. The adaptive DBF algorithms implemented in this research are standard algorithms from the literature and are only able to mitigate the effects of interference sources below a given power level. When the interference-to-signal-ratio (ISR) becomes too large, no adaptive DBF algorithm can accurately estimate the SOI present in the environment. Figure 15 shows the MSE for the four implemented wideband adaptive DBF algorithms as a function of ISR. Above an ISR value of 35 dB, all algorithms errors increase by over 40 percent and in simulation no
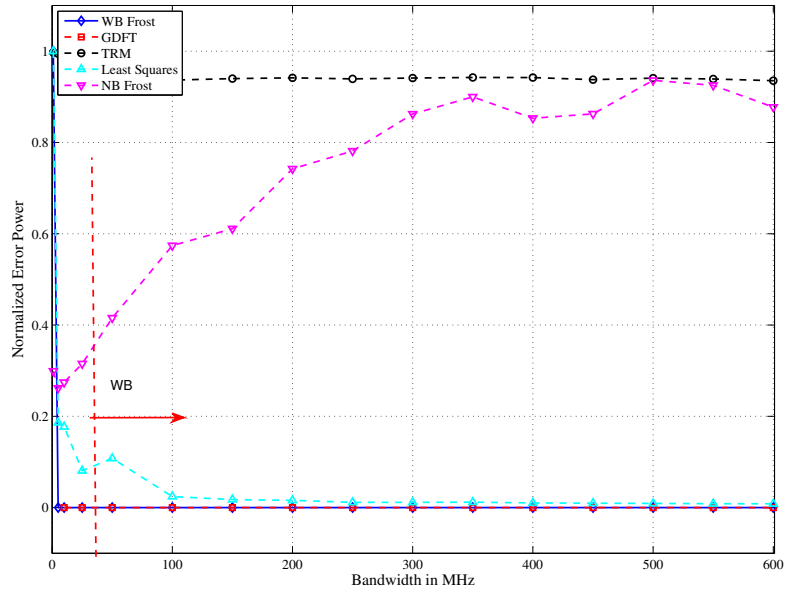
Figure 13. Mean-squared error of adaptive beamformers as a function of the bandwidth of a single interference signal.
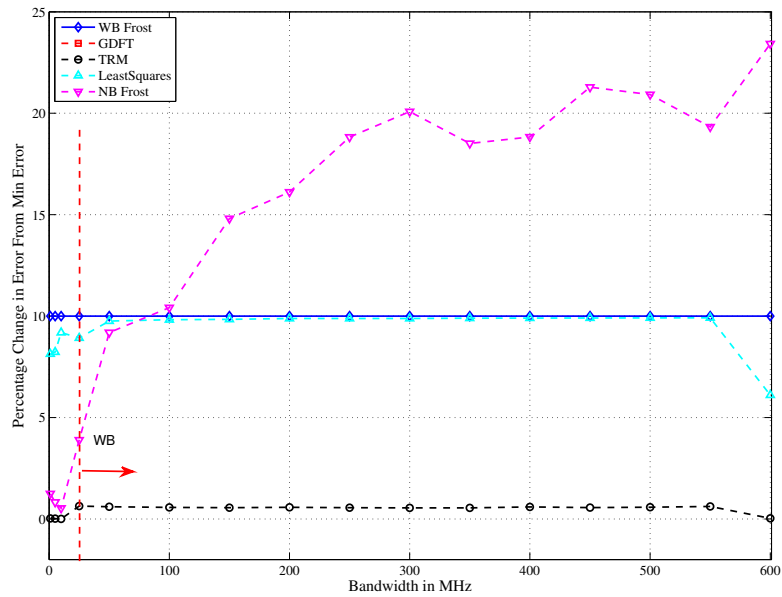

Figure 14. Percentage change in mean-squared error of adaptive beamformers as a function of the bandwidth of a single interference signal.
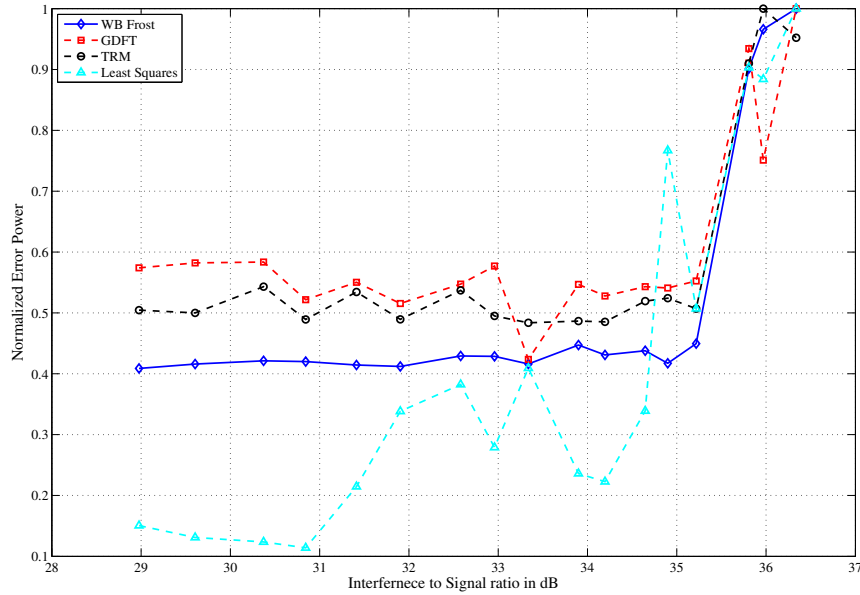
109

accurate estimate of the SOI is possible.

Figure 15. The mean-squared error of four adaptive DBF algorithms as a function of ISR showing a breakdown in algorithm performance for high interference power levels.

4.4   LUT Development Scenarios

The interference environments are developed based upon the results of the environment parameter sensitivity analysis presented above. Scenarios are developed where the number of signals and bandwidths of the signals are varied between scenarios. Because narrowband algorithms perform poorly with wideband interference sources, scenarios consisting of strictly narrowband interference signals are created. Likewise scenarios of strictly wideband interference sources are created. A third type of scenario, containing both narrowband and wideband interference sources was not directly accounted for in the sensitivity analysis. However, to provide an analysis of wider applicability such scenarios are included in the LUT development.

For LUT development, the five adaptive DBF algorithms are applied to eight dif-

ferent simulated electromagnetic environments. All environments contained a single wideband SOI incident from broadside (0 degrees). The SOI is a linear frequency modulated signal with a 300 MHz up-chirp from 300 MHz to 600 MHz. Additive complex white Gaussian noise with a power 10 dB below the SOI signal power of 1 Watt is included in each scenario. The signal of interest is 1 Watt to simplify ISR calculations. The ISR is defined as:

$$\text{ISR} = \frac{\text{Interference Power}}{\text{Signal of Interest Power}}. \tag{139}$$

A description of the interference sources present in each of the eight scenarios is presented in Table 2. For each scenario the table provides the interference number, bandwidth of the interference source, center frequency f_c of the interference source, DOA of the interference source, and interference-to-noise-ratio (INR) of the interference source.

For all scenarios the interference sources DOAs angles are chosen to span a -70° to 70° field-of-view (FOV) for the array. The field of view of the array is chosen to be representative of the Air Force Research Laboratory (AFRL) MUD-WASP testbed that has a FOV from -60° to 60°. The center frequencies are chosen to ensure that all interference signals are in the frequency range of 100 MHz to 700 MHz. This frequency range is desired to keep the signals within the instantaneous bandwidth of the array without taxing the array to operate at its frequency limits.

4.5   Algorithm Performance and LUT Listing

The LUT is developed by ranking the adaptive DBF algorithms based upon a decision rule applied to the algorithm performance. The algorithm performance is measured with respect to the receiver framework implementor's choice of performance

Table 2. Interference Scenario listing for LUT development

Interference #	Bandwidth	f_c	DOA	INR	Relative Bandwidth
		Scenario 1			
1	200 MHz	300 MHz	-60°	20 dB	wideband
		Scenario 2			
1	200 MHz	300 MHz	-60°	20 dB	wideband
2	200 MHz	500 MHz	20°	20 dB	wideband
		Scenario 3			
1	200 MHz	250 MHz	-60°	5 dB	wideband
2	200 MHz	300 MHz	-45°	5 dB	wideband
3	200 MHz	400 MHz	-30°	5 dB	wideband
4	200 MHz	500 MHz	20°	5 dB	wideband
5	200 MHz	600 MHz	50°	5 dB	wideband
		Scenario 4			
1	200 MHz	250 MHz	-65°	5 dB	wideband
2	200 MHz	300 MHz	-55°	5 dB	wideband
3	200 MHz	400 MHz	-45°	5 dB	wideband
4	200 MHz	500 MHz	-35°	5 dB	wideband
5	200 MHz	600 MHz	-25°	5 dB	wideband
6	200 MHz	350 MHz	20°	5 dB	wideband
7	200 MHz	450 MHz	30°	5 dB	wideband
8	200 MHz	550 MHz	40°	5 dB	wideband
9	200 MHz	500 MHz	50°	5 dB	wideband
10	200 MHz	625 MHz	60°	5 dB	wideband
		Scenario 5			
1	10 MHz	400 MHz	-60°	20 dB	narrowband
		Scenario 6			
1	10 MHz	400 MHz	-60°	20 dB	narrowband
2	200 MHz	600 MHz	45°	20 dB	wideband
		Scenario 7			
1	10 MHz	400 MHz	-20°	20 dB	narrowband
2	200 MHz	600 MHz	45°	20 dB	wideband
		Scenario 8			
1	10 MHz	250 MHz	-60°	5 dB	narrowband
2	200 MHz	300 MHz	-45°	5 dB	wideband
3	10 MHz	450 MHz	-30°	5 dB	narrowband
4	200 MHz	500 MHz	20°	5 dB	wideband
5	10 MHz	650 MHz	50°	5 dB	narrowband

measures. The chosen adaptive DBF algorithms are ranked for each interference scenario chosen by the framework implementor. The current demonstration instantiation of the framework uses eight interference scenarios. The performance criteria used to rank the adaptive DBF algorithms are SINR improvement and computational complexity. Each algorithm's computational complexity is determined analytically using the big-O notation from Sections 2.4.3.1-2.4.4.1. Computational complexity for each algorithm is based upon the number of channels in the receiver, the number of FIR filter taps per channel, and the number of sub-bands chosen for each algorithm. All of these parameters are held constant across all interference scenarios allowing for the computational complexity to be calculated once for each adaptive DBF algorithm and used for all algorithm comparisons. Each algorithm's SINR improvement, however, varies for each interference scenario and is calculated empirically for each scenario. An empirical study is applied to allow for greater variations in interference scenario type without the burden of completely determining the second-order statistics of each interference scenario that would be required for an analytical analysis.

The adaptive ES receiver estimates the SOI for all time samples collected by the receiver. Each adaptive DBF algorithm is implemented using a block of data, used to estimate a block of data, then recalculated for the next incoming block of data. To ensure that the algorithm chosen is optimal for all time, the SINR is formed by integrating the SINR across all data samples in a given block. The exact formulation is derived by writing the covariance matrix of the sampled array channel data as a superposition of the signal, interference, and noise covariance matrices

$$\mathbf{R}_{data} = \mathbf{R}_{signal} + \mathbf{R}_{interference} + \mathbf{R}_{noise}. \tag{140}$$

Beamformer implementation is handled separately from beamformer filter weight generation in the receiver framework. As mentioned in Section 2.2 the filter weights are

113

determined using a block of receiver data. Once the filter weights are determined they are applied to the next incoming block of array data, while the receiver framework determines the next "best" set of adaptive DBF filter weights. The output signal of the beamformer for a given block of data is given by $\mathbf{y} = \mathbf{w}^H \mathbf{X}$, where $\mathbf{X}$ is from (6). Using the form of output from the beamformer the output power from the beamformer is given as

$$p_{out} = \mathbf{w}^H \mathbf{R}_{data} \mathbf{w}. \tag{141}$$

By substituting (140) into (141) and then separating the signal power from the interference and noise powers the SINR output from a given adaptive DBF is given by

$$\mathrm{SINR} = \frac{\mathbf{w}^H \mathbf{R}_{signal} \mathbf{w}}{\mathbf{w}^H \left(\mathbf{R}_{interference} + \mathbf{R}_{noise} \right) \mathbf{w}}. \tag{142}$$

The input SINR requires the transmitted signal powers which are computed by substituting $\mathbf{w} = [1, 0, \ldots, 0]$ into (142). This weight vector selects the $\mathbf{R}(0,0)$ term of each covariance matrix corresponding to the power of the SOI, interference signals, and noise.

Based upon discussion in Appendix B, SINR as described in (142) provides a measure of the ability of an adaptive DBF algorithm to estimate the SOI. The current receiver framework instantiation, however, uses SINR improvement as the decision metric. To understand the selection rule used for LUT implementation, recall the purpose of the ES receiver, which is to detect and classify signals of interest in the environment. The adaptive DBF algorithm applied at the array interface is only one part of processing for ES receivers. Typically, receivers are required to "interpret" the received signal waveform such as communication processing for communication reception receivers or pulse descriptor word (PDW) generation for radar warning receiver (RWR) receivers. After the SOI is processed by the adaptive array, it is used

as the input to a second processing algorithm that performs the communication signal decoding or the PDW generation.

Performance of ES receiver processing performed after the initial adaptive DBF algorithm application is dependent upon the SINR of the signal provided by the DBF algorithm. It is incumbent upon the proposed receiver architecture to provide an output signal with adequate SINR. Furthermore, the adaptive DBF algorithm chosen for a given parameter set must provide the required output SINR for all scenarios with similar parameters. As interference signal power is not a measured parameter, the same and similar parameter sets can have vastly different input SINR levels. Each adaptive DBF algorithm chosen for the LUT must be able to provide the required output SINR for all possible combinations of SOI and interference signal power levels that exist for a particular parameter set.

Because the SOI and interference signal power are unknown, choosing the *best* adaptive DBF algorithm requires more problem domain knowledge in the form of a receiver design requirement. The requirement specifies the lowest input SINR the receiver is designed to detect and estimate. The required SINR for beamformer post processing is also known *a priori*. Using these two pieces of data the required SINR improvement for adaptive DBF algorithms chosen for the LUT is

$$\text{required SINR improvement} = \frac{\text{SINR}_{\text{required out}}}{\text{SINR}_{\text{worst case}}}. \tag{143}$$

Any adaptive DBF algorithm chosen for inclusion in the LUT must provide the required SINR improvement. Not all adaptive DBF algorithms considered for LUT inclusion will meet the SINR output requirement, limiting the total number of available adaptive DBF algorithms for possible LUT inclusion. The final choice for LUT inclusion is made based upon the second performance criterion of computational complexity. The adaptive DBF algorithms chosen for inclusion in the LUT are the

115

adaptive DBF algorithms that meet the required SINR improvement level for a given interference environment that have the lowest computational complexity.

Remember this decision rule for algorithm selection is valid only for the particular receiver framework implementation used herein for discussion purposes. The receiver framework implementor must create a decision rule based upon the desired performance outcomes of their receiver implementation. The chosen decision rule may take into consideration more than two performance criteria for better adaptive DBF algorithm differentiation. Exact number and type of performance criteria, along with the accompanying decision rule are provided by the receiver implementor.

Returning to the demonstration receiver instantiation, because the computational complexity of each algorithm, with the exception of a multiplication factor that varies for recursive algorithms, is dependent only upon the array architecture, the LUT entries vary based upon which algorithms have the best SINR improvement for the particular electromagnetic environment considered. It should be noted the adaptive DBF algorithm chosen for a scenario is not necessarily the algorithm that has the best SINR improvement. This is better understood when the second performance criterion, computational complexity is considered. If an algorithm has good SINR improvement but is computationally infeasible, then it is not the *best* algorithm for implementation. The receiver architecture chooses the algorithm that gives a "good enough" SINR improvement while having a manageable computational complexity. The SINR improvement in dB for the five adaptive DBF algorithms, for each of the eight scenarios of Table 2 is provided in Table 3.

The computational complexity of each of the five algorithms for the simulated receiver is given in Table 4. The complexity results are for a 64-element linear array with 20 FIR taps per channel. For the LCMV algorithms, 100 constraints were used. In the GDFT algorithm the spectrum was divided into ten sub bands, and

116

Table 3. SINR improvement in dB for each adaptive DBF algorithm when applied in a given scenario number where the interference environments of the scenarios are described in Table 2. The boldface type indicates those beamformers chosen for inclusion in the look-up-table.

Scenario	1	2	3	4	5	6	7	8
NB LCMV	-0.48	-5.77	-5.81	-10.90	**18.13**	**16.72**	**13.89**	6.84
WB LCMV	**14.83**	9.58	**20.10**	**18.78**	21.41	16.98	14.45	2.21
TRM	30.87	**28.57**	21.84	5.00	53.65	37.88	37.59	**30.28**
GDFT	13.87	6.84	18.10	16.73	-7.05	-7.08	-12.18	-0.54
LSSB	57.60	53.23	60.34	40.81	78.12	49.30	48.26	36.68

LCMV algorithms with two filter taps per sub band were applied. In the LSSB implementation each of the spatial and temporal frequency bands are subdivided into 100 discrete frequency and spatial points respectively. The narrowband LCMV uses two filter taps per channel as was applied in the GDFT algorithm.

Except for the choice of 64-elements, chosen to represent the MUD-WASP receiver hardware, the receiver values are one of an infinite set of possible combinations. The number of filter taps and LCMV constraints are chosen to reduce processing time as would be required in an actual receiver implementation. To understand how varying these receiver characteristics influences the LUT creation consider the following four points. First, increasing the number of filter taps and constraints increases the computational complexity for the wideband LCMV and TRM beamformers while also increasing their accuracy. Second, the number of filter taps for the narrowband LCMV and GDFT algorithms are kept low precisely because they are narrowband. Increasing the number of filter taps would increase the complexity of both algorithms eliminating their design motivation [70,114]. Third, the number of sub-bands is chosen to keep the number of required LCMV beamformers low while ensuring each sub-band is narrowband. Fourth, as the number of array channels is a dominant factor in the computational complexity of all algorithms, changing the array size affects the computational complexity of all the algorithms equally. Based upon the preced-

ing four points changing the array size, number of filter taps per algorithms, and the number of sub-bands for the GDFT algorithm does not affect the resulting LUT formation. Changing the simulation parameters would change the SINR improvement and computational complexity numbers but not the relation of the adaptive DBF algorithms to one another.

Table 4. Computational complexity, constant across all interference environments, of all five adaptive DBF algorithms in units of computational cycles where the constant factor for "big O" notation is ignored.

DBF Algorithm	Computational Complexity
Narrowband LCMV	$O(3.948 \text{x} 10^6)$
Wideband LCMV	$O(1.794 \text{x} 10^8)$
TRM	$O(1.796 \text{x} 10^8)$
GDFT	$O(1.873 \text{x} 10^8)$
LSSB	$O(1.849 \text{x} 10^{10})$

One last design parameter is required before the LUT listing can be completed. As discussed above, the LUT is designed around a receiver specification that lists a required SINR improvement factor. For demonstration purposes this effort will consider an SINR of 10 dB to be sufficient. Applying the chosen algorithm selection criteria, the algorithm that provides at least 10 dB SINR improvement with the lowest complexity is chosen for implementation by the receiver for the given environment, and thus inclusion in the LUT. Remember this decision rule is chosen for demonstration purposes and is not designed to be an optimal decision rule. Algorithms with close complexities such as the TRM and wideband LCMV can vary by as much as 15 dB in terms of SINR improvement. If the computational complexity is close and one algorithm severely outperforms the other in terms of SINR improvement it would make sense to pick the more accurate adaptive DBF algorithm. When the final form of the LUT is discussed the decision rule is changed slightly to better balance the algorithms SINR improvement and computational complexity.

To generate the final form of the LUT table refer again to Table 3. For Scenario

One, the four wideband adaptive DBF algorithms, wideband LCMV, GDFT, TRM, and LSSB provide an adequate SINR improvement. The wideband algorithm with the lowest complexity is the wideband LCMV algorithm and it is the first entry in the LUT. For Scenario Two, only two algorithms provide the required SINR improvement, so the TRM with two orders of magnitude lower complexity than the LSSB algorithm is chosen. In Scenario Three all wideband adaptive DBF algorithms again provide the required SINR and so the wideband LCMV algorithm is chosen. In Scenario Four, a similar situation occurs, except the TRM does not provide adequate SINR improvement; the wideband LCMV algorithm is again chosen. Scenario Five contains only narrowband interference sources. The narrowband LCMV is chosen for the LUT in Scenario Five as it provides adequate SINR improvement against the narrowband interference sources while having a computational complexity two orders of magnitude below that of the other algorithms. Scenarios Six and Seven contain both narrowband and wideband interference sources; however, in both cases the narrowband LCMV algorithm provides adequate SINR improvement with the lowest computational complexity. In all such cases the narrowband LCMV is chosen for inclusion in the LUT. In the final scenario only two algorithms provide the required SINR improvement. The TRM algorithm has the lowest computational complexity of the two and is the final entry into the LUT.

One point to note about the LUT creation is the power levels of the interference sources were varied between a large number of moderate power sources and a few high power sources. Previously the sensitivity analysis demonstrated a sensitivity to the algorithms with regard to the power of the interference. This sensitivity is manifest in the LUT generation data. For instance, the wideband LCMV algorithm was optimal for a single high power source and for multiple moderate power sources, but was not optimal for two high power sources. The TRM algorithm, however, performed well

in all cases with less than five interference sources. For this reason even though the wideband LCMV algorithm had a slightly lower complexity in big-O notation, the LUT will include the TRM for all wideband interference scenarios with less than five interference sources. The LCMV will be used for all cases with greater than five interference sources. This seemingly arbitrary nature of this decision rule change is removed when the nature of the computational complexity performance criteria is considered. The complexity is in big-O notation; therefore the exact complexities are not known. Because of the closeness of their computed values, the computational complexity of the wideband LCMV and the TRM can be considered equal. The decision rule would then default to the algorithm with the highest SINR improvement. Future research needs to consider the power of the interference sources as received at the array and the overall effect of the new required power parameter on receiver operation, to include the additional complexity required of the resource manager. The final results to the LUT are given in tabular form in Table 5.

Table 5. LUT providing the name of the adaptive DBF algorithms chosen for all scenario sets derived from the algorithm sensitivity analysis.

	NB Signals	WB Signals	Mixed BW Signals
Wideband SOI			
< 5 Signals	NB LCMV	TRM	NB LCMV
≥ 5 Signals	NB LCMV	WB LCMV	WB LCMV
Narrowband SOI			
< 5 Signals	NB LCMV	NB LCMV	NB LCMV
≥ 5 Signals	NB LCMV	NB LCMV	NB LCMV

4.6   Chapter Review

This completes the description of both the RM and the LUT generation. The RM portion of the receive framework is intended to be used by all implementors of the framework. The environment and SOIs detection and estimation techniques provide

a way to fully characterize the RF environment in terms of the types of interference signals as well as the number of SOI and their respective DOAs. Each framework implementor, however, is required to perform the analysis provided in the current chapter to design a LUT of adaptive DBF algorithms based upon the performance selection criteria of interest to the receiver implementer. This chapter provided an example LUT development to indicate how the design should proceed.

The next chapter provides a performance analysis of the proposed receiver framework using the LUT developed herein. Application of the RM is first validated through the use of simulated RF environments. After the validation the performance is verified against data collected on two receiver systems at AFRL. Verification ensures that the algorithms performed as designed when used against simulated data, i.e. it determines if the algorithms are mathematically correct. Validation ensures that the receiver framework is viable for its intended mission. In this case validation ensures that the receiver framework correctly detects the SOI and picks the correct adaptive DBF algorithm from the LUT based upon the RF environment.

V. Resource Manager Performance

The proposed receiver architecture intelligently chooses an adaptive digital beam-forming (DBF) algorithm from a look-up-table (LUT) of adaptive DBF algorithms. Algorithm selection is based upon both signal-to-interference-plus-noise ratio (SINR) improvement and computational complexity of the algorithms. As no single adaptive DBF algorithm is optimal for all interference scenarios, intelligent selection of algorithms, *i.e.* choosing algorithms based upon sensing the environment, improves electronic support (ES) receiver performance. ES receivers applying the proposed architecture are able to either apply computationally complex algorithms against a limited number of signals-of-interest (SOIs), obtaining the best possible signal estimate, or apply less computationally complex adaptive DBF algorithms against an increased number of SOI when the interference environment environment is less crowded.

The ability to select the best adaptive DBF algorithm for each scenario is derived from decision rule used for algorithm selection. Neither of the two performance criteria, however, are determined directly by the resource manager (RM). The adaptive DBF algorithm achieving the optimal SINR improvement and computational complexity for each interference scenario is stored in the LUT and referenced based upon the estimated parameters of the environment. Therefore, performance of the proposed receiver framework is predicated on the RM's ability to correctly parameterize the electromagnetic environment. If the environment is correctly parameterized, the algorithm chosen from the LUT developed in Chapter 4 is considered *best* in terms of SINR improvement and computational complexity. Making the assumption that the LUT is properly developed, the receiver architecture's performance is based upon the ability of the RM to correctly parameterize the interference environment and isolate each SOI from all interference sources as well as additional SOIs.

Parameterizing the electromagnetic (EM) environment and disambiguating the

different SOIs through digital signal processing (DSP) allows performance analysis of the RM to focus on the ability of the chosen DSP to affect the desired outcomes. RM operation is verified by creating simulated SOI and interference scenarios and determining if the chosen algorithms correctly parameterized the electromagnetic environment and correctly disambiguated all SOI. The verification stage employs four scenarios with differing SOI bandwidths and interference sources to ensure proper parameterization across a range of scenario types. After the receiver framework is verified to work as designed, the RM is validated against two scenarios formed from measured array data. The validation scenarios are portions of tests run at Air Force Research Laboratory (AFRL) Sensors Directorate on two receiver testbeds. The validation is performed by applying the adaptive environment estimation algorithms of the receiver framework's RM to data collected from the two receiver testbeds. The first validation scenario uses data collected on the AFRL Sensors Directorate McWess array testbed [57]. The second validation scenario uses data from the AFRL MUD-WASP sensor testbed. Proper function of the receiver framework requires a successful completion of both the verification and validation phases.

The verification scenarios consider only a single SOI. Estimation of the number of SOIs and their respective directions-of-arrival (DOAs) is performed through the signal disambiguation algorithm. The single SOI case extends to the multiple SOIs case by considering that the disambiguation process is the same for all spatial sub-bands considered in the disambiguation. When multiple SOIs are present the disambiguation algorithm indicates that multiple signals are present and returns their DOAs. As the processing is the same for each SOI only the method of disambiguation is required to be verified. The second validation scenario does indicate how the processing occurs for multiple SOIs. The validation shows that the disambiguation algorithm considers all the signals to be SOIs and returns their respective DOAs.

5.1 Receiver Framework Verification

The receiver framework is designed to beamform on both narrowband and wideband signals of interest requiring verification scenarios with both wideband and narrowband SOI. Three of the verification scenarios have a wideband SOI and one verification scenario has a narrowband SOI. The first verification scenario has a wideband SOI and all wideband interference sources, the second verification scenario has a wideband SOI and only narrowband interference sources, the third verification scenario has a wideband SOI and both wideband and narrowband sources. The final verification scenario has a narrowband SOI and both wideband and narrowband interference sources. This set of verification scenarios is not exhaustive but provides an indication of RM performance across a variety of scenarios that provide confidence in RM performance against all EM environment types.

The array system being simulated for the verification scenarios has a sample frequency of 1.5 Gsamp/sec and samples at baseband. The sampling frequency gives the system a 750 MHz instantaneous bandwidth. Array inter-element spacing is equivalent to one half wavelength of the maximum allowable frequency, which due to baseband processing is 750 MHz, giving an inter element spacing of $d = 0.1$ meter. A data record of 8000 samples is generated for each channel and used in all algorithms and DSP.

5.1.1 Wideband SOI Scenario Performance.

The first three verification scenarios contain a 300 MHz bandwidth pseudo-noise signal of interest centered at $f_c = 450$ MHz, incident from broadside (direction of arrival of 0 degrees). The wideband interference signals are pseudo-noise signals with an interference-to-signal-ratio (ISR) of 10 dB. Narrowband interference sources are 20 dB ISR continuous wave signals. Each scenario also contains circularly complex white

Gaussian noise. The power of each SOI and interferer provides a signal-to-noise-ratio (SNR) of 10 dB. Table 6 provides the bandwidths, center frequencies, and DOAs for all interference signals.

Table 6. Frequency and DOA listing for the baseband interference signals implemented in the three wideband SOI RM verification scenarios.

Scenario 1	Bandwidth	f_c	DOA	Relative Bandwidth
Signal 1	100 MHz	300 MHz	-45°	wideband
Signal 2	200 MHz	400 MHz	-20°	wideband
Signal 3	200 MHz	500 MHz	15°	wideband
Signal 4	100 MHz	500 MHz	30°	wideband
Scenario 2	Bandwidth	f_c	DOA	Relative Bandwidth
Signal 1	10 MHz	200 MHz	-15°	narrowband
Signal 2	10 MHz	400 MHz	-30°	narrowband
Signal 3	10 MHz	450 MHz	-45°	narrowband
Signal 4	10 MHz	550 MHz	20°	narrowband
Signal 5	10 MHz	650 MHz	50°	narrowband
Scenario 3	Bandwidth	f_c	DOA	Relative Bandwidth
Signal 1	200 MHz	500 MHz	-45°	wideband
Signal 2	10 MHz	550 MHz	-30°	narrowband
Signal 3	10 MHz	450 MHz	20°	narrowband
Signal 4	200 MHz	300 MHz	50°	wideband
Signal 5	10 MHz	650 MHz	-15°	narrowband
SOI	300 MHz	450 MHz	0°	wideband

Presentation of the RM verification follows the functional blocks laid out in the RM block diagram of Figure 7. The environment estimation functional block output is presented first, followed by the signal detection functional block output. Presentation order does not dictate actual ordering in operational use. When implemented as part of the proposed receiver architecture the environment determination and signal of interest detection functional blocks are performed in parallel. The output of the environment estimation and signal detection functional blocks are presented in tabular form. Supporting graphical representations of the data, when available, provide the basis for the table generation.

5.1.1.1   Wideband SOI Environment Estimation.

The environment estimation functional block detects signals in the EM environment and determines their DOA. Signal detection uses an multi-taper method (MTM) spectral estimate of the environment as developed for cognitive radio (CR) [31]. The spectral estimate is used as input data for the generalized likelihood ratio test (GLRT) detection algorithm. The results of the GLRT algorithm are then used to determine the relative bandwidths of all signals in the environment. Direction of arrival estimation algorithms are applied directly to the array channel data and processing is separate from the signal detection algorithm. The DOA estimation algorithm also estimates the number of interference signals in the environment.

Figures 16-18 are the initial MTM spectral estimates for the wideband SOI with wideband interference scenario, narrowband interference scenario, and mixed bandwidth scenario respectively. The spectral content from 200 MHz to 650 MHz in Figure 16 indicates the presence of wideband interference sources as the signal of interest is only present at frequencies greater than 300 MHz. Also, only wideband interference signals are present as no narrowband interference sources are visible in the spectral estimate. Contrast the estimate of Figure 16 with Figure 17 where five narrowband interference signals are present above the wideband SOI present in the expected frequency range. The MTM spectral estimate of the mixed bandwidth interference environment, given in Figure 18 is a mixture of the spectra from Figure 16 and Figure 17, where a wideband interference source is present in spectral data lower than 300 MHz and the narrowband signals are present at various frequencies with spectral power of higher magnitude than the SOI.

The spectral estimates are analyzed by the RM using a GLRT algorithm. Figures 19-21 are graphical representations of the GLRT output for Figures 16-18 respectively. The constant output of Figure 19 indicates the presence of spectral content in
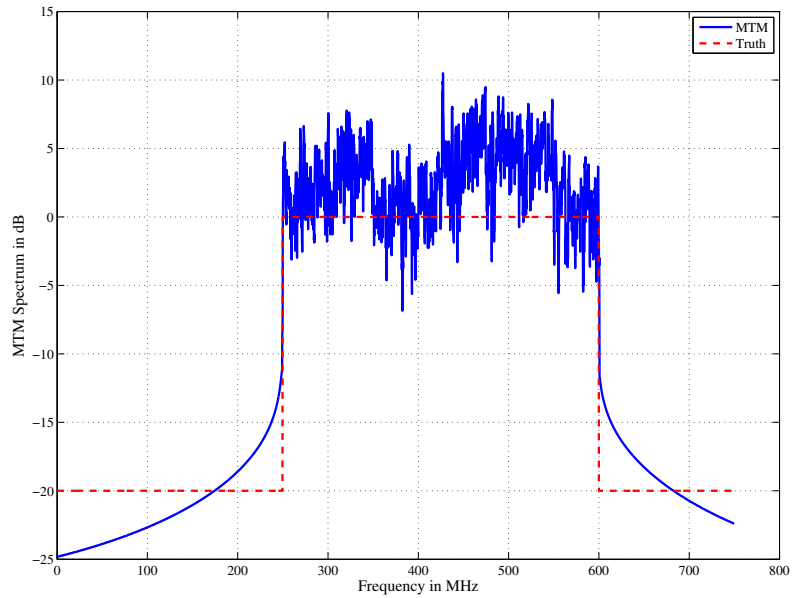
Figure 16. MTM power spectrum estimate of the four wideband interference signals and the wideband SOI in interference scenario 1.
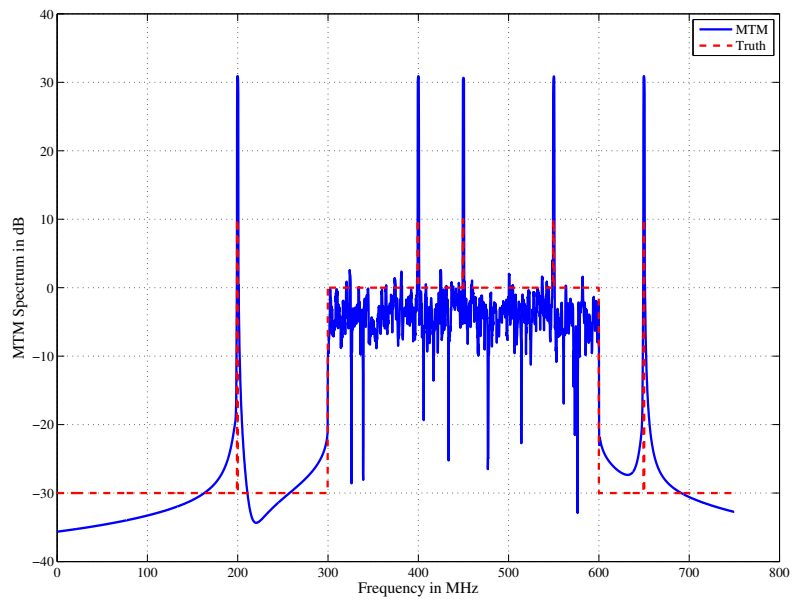

Figure 17. MTM power spectrum estimate of the five narrowband interference signals and the wideband SOI in interference scenario 2.
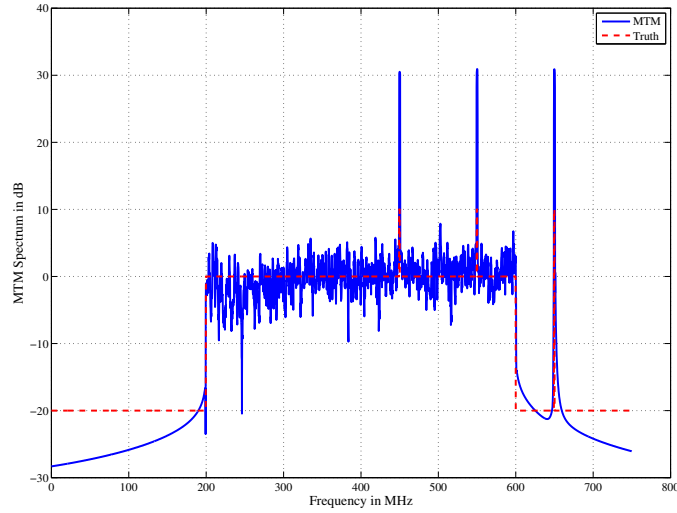
127

Figure 18. MTM power spectral estimate of the two wideband interference sources, three narrowband interference sources, and the wideband SOI in interfernece scenario 3.

all frequency bands from 200 MHz to 650 MHz as shown in Figure 16 above. Figure 20 indicates the presence of two narrowband interference sources in the spectrum. Scenario 2 contains five narrowband interference sources. In this present case three of the sources are hidden in the wideband SOI. The fact that there are narrowband interference sources co-located in frequency with the SOI is resolved by the disambiguation algorithm. Figure 21 incidates that wideband and narrowband signals are present, to include the SOI. The algorithm knows that there are wideband interference signals because there is wideband spectral content from 200 MHz to 300 MHz where the SOI spectral content begins. The narrowband signal present at 650 MHz indicates that the radio frequency (RF) spectrum contains both narrowband and wideband interference signals.

Figures 22-24 plot the multi-signal classification (MUSIC) spectrum from the DOA estimation algorithm for the wideband interference scenario, narrowband interference scenario, and mixed bandwidth scenario respectively. Each MUSIC spectrum is able to locate the DOA of all signals in the environment within one degree of the actual
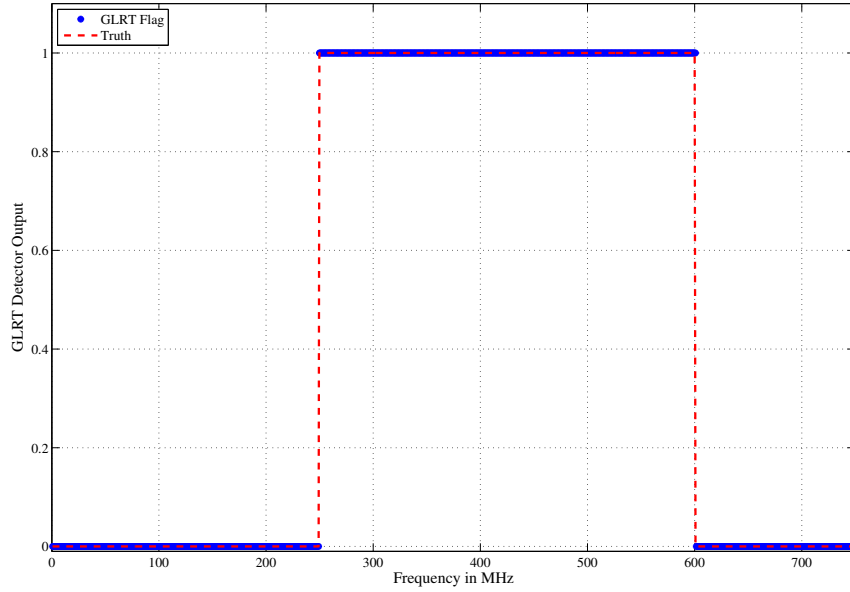
Figure 19. The GLRT output of the RM for interference scenario 1 indicating that there is signal power present in all frequencies from 200 MHz to 600 MHz. A continuous GLRT output of greater than 50 MHz indicates a wideband signal present in the data.
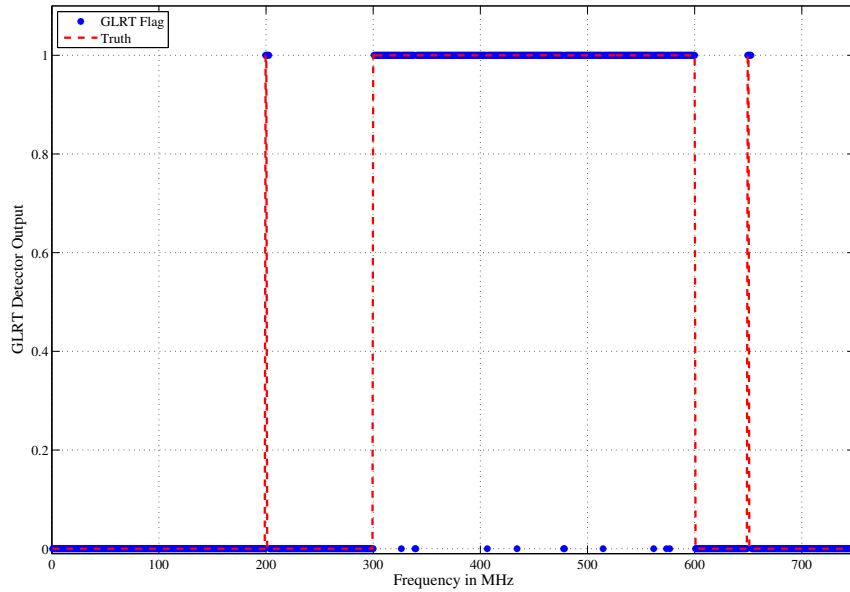

Figure 20. The GLRT output of the RM for interference scenario 2 showing signal energy present across a wideband region and two narrowband regions. The wideband region encompasses the SOI and eclipses three narrowband interference sources.
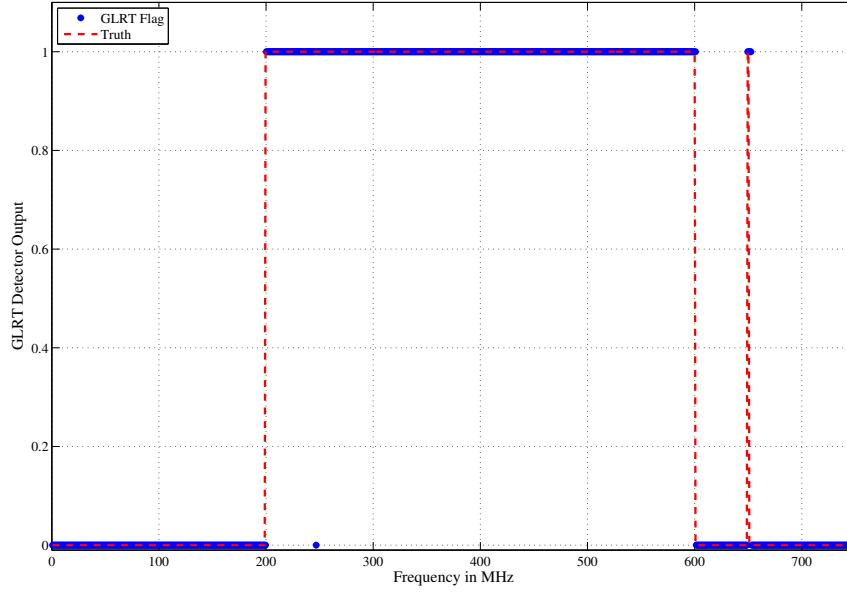
Figure 21. The GLRT output of the RM for interference scenario 3 showing the wideband interference source and SOI from 200 MHz to 600 MHz and a narrowband interference source at 650 MHz. Wideband signals are identified by power existing across contiguous spectral regions of greater than 50 MHz.

transmitted DOA. The Akaike information criteria algorithm is able to correctly estimate the number of signals in each case. Table 7 provides the angles returned by the DOA, the bandwidths of the interference signals detected, and the number of signals detected in the environment, to include the SOI.

Table 7. Output of the environment estimation functional block showing the relative bandwidth of the signals in the environment and the DOA estimates for each signal in the environment to include the SOI and interference signals.

Scenario	Bandwidth	# Signals	DOA
1	WB	5	-45.00^o, -20.03^o, 0°, 14.94^o, 29.72^o
2	NB	6	-45.00^o, -30.06^o, -14.94^o, 0°, 20.03^o, 49.99^o
3	Mixed	6	-44.82^o, -30.06^o, -14.94^o, 0°, 20.03^o, 49.57^o

The data of Table 7 indicates that scenario 1 has five or greater wideband signals. From the LUT the *best*[1] adaptive DBF algorithm for scenario 1 is the wideband

---

[1]The term best is in terms of SINR improvement and computational complexity
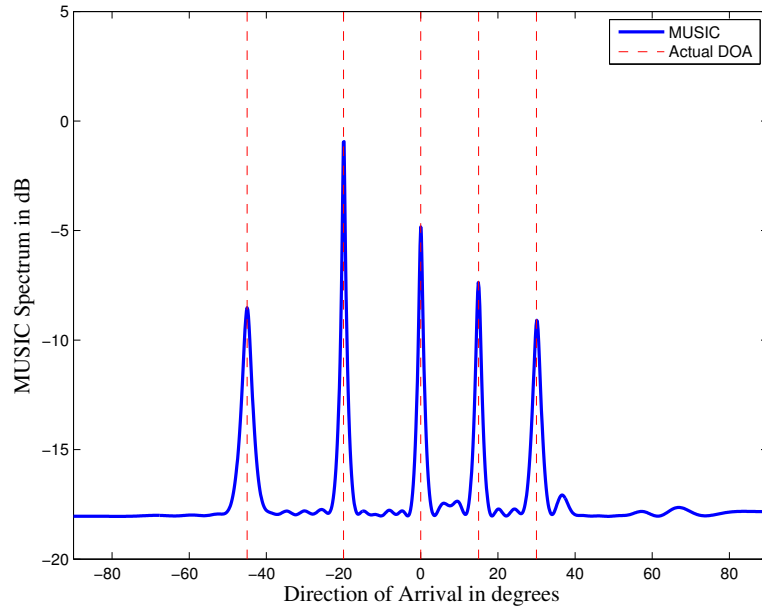
Figure 22. The MUSIC spectrum of scenario 1 formed using a coherently focused covariance matrix showing the DOA for the four interference sources and the SOI.
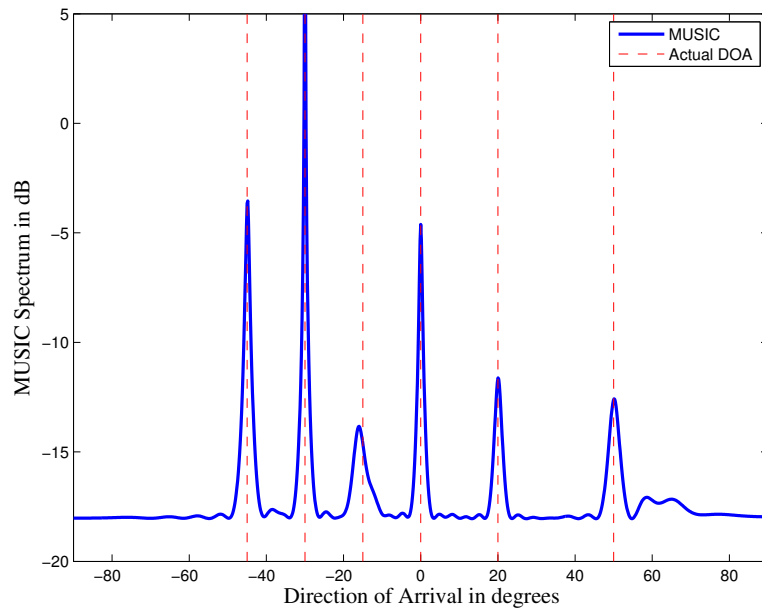

Figure 23. The MUSIC spectrum of scenario 2 formed using a coherently focused covariance matrix showing the DOA for the five interference sources and the SOI.
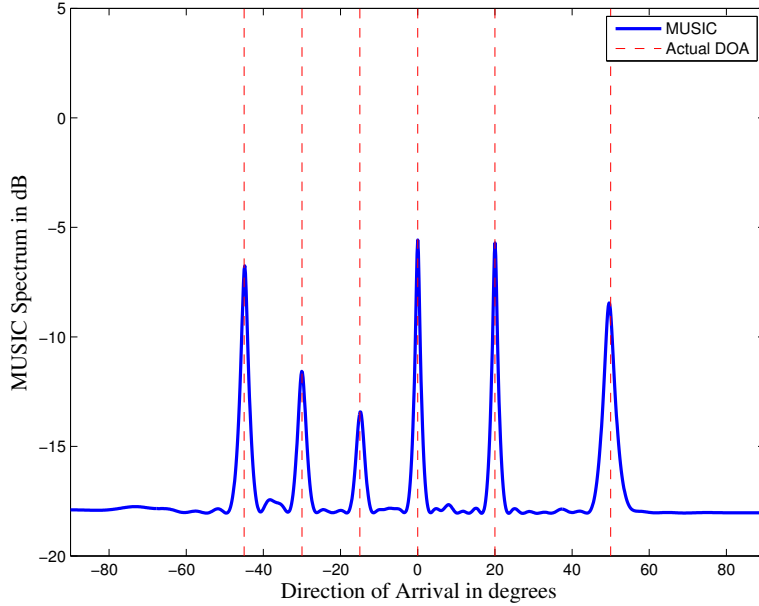
131

Figure 24. The MUSIC spectrum of scenario 3 formed using a coherently focused covariance matrix showing the DOA for the five interference sources and the SOI.

linearly constrained minimum variance (LCMV). Verification that the RM chooses the correct adaptive DBF algorithm is given by Table 8 that provides the SINR output for each of the five implemented adaptive DBF algorithms when applied to each of the three wideband SOI verification scenarios. When a SINR threshold of 10 dB is considered for adaptive DBF selection, as was considered in LUT generation, the first row indicates that all algorithms except for the narrowband LCMV provide an adequate level of SINR. Of the four algorithms the wideband LCMV has the lowest computational complexity and is the optimal algorithm for scenario 1.

Similarly to the output from scenario 1, the SINR output from Table 7 indicates that scenario 2 has greater than five narrowband interference sources where the LUT provides the narrowband LCMV as the most optimal algorithm. The SINR output for all adaptive DBF algorithms except the generalized discrete Fourier transform (GDFT) provide adequate SINR out; the narrowband LCMV algorithm has the lowest computational complexity indicating that the RM chooses the *best* DBF from the

LUT for scenarios containing only narrowband interference sources. Performance of the RM is also verified against a scenario with wideband and narrowband sources as can be shown again looking at the SINR output numbers from Table 8. As with the output for scenario one, all algorithms except the narrowband LCMV provide SINR output levels above the required 10 dB threshold. The wideband LCMV has the lowest computational complexity of the four adaptive DBF algorithms and is therefore the *best*. The RM chooses the wideband LCMV algorithm for mixed bandwidth scenarios with five or greater interference signals completing the verification.

Table 8. SINR in dB output for each adaptive DBF algorithm when applied to each of the three interference scenarios where the boldface quantities are those chosen by the resource manager.

Scenario	WB LCMV	GDFT	TRM	LSSB	NB LCMV
1	**22.484**	22.068	19.054	45.674	4.064
2	12.257	5.754	20.269	33.047	**13.062**
3	**19.065**	15.612	17.481	37.841	3.787

5.1.1.2   Wideband Signal of Interest Detection.

The SOI detection functional block is designed to detect any signals of interest in the electromagnetic environment, and if signals are detected to determine the DOA for each SOI. The presence of any SOI and their respective DOA are included in the environment estimation functional block results. When the environment was parameterized, however, no association was made between signals and the measured DOA. Only the reported environment parameters are required to choose the *best*[2] adaptive DBF algorithm from the LUT precluding the requirement to associate a signal with a DOA. Implementing the adaptive DBF algorithm chosen from the LUT requires knowledge of the DOA for each SOI requiring the additional processing of the SOI detection functional block.

---

[2]Algorithm performance is in terms of algorithm SINR improvement and computational complexity

133

The array data is first passed through a bandpass filter to isolate the spectral region where the SOI is known to exist. Figures 25-27 show the MTM spectral estimates of the spatially filtered array data for each of the three wideband SOI interference scenarios. In all three wideband SOI scenarios spectral content exists in the *a priori* known SOI spectral region and thus the SOI is declared to be present by applying a GLRT as was shown in the discussion of the environment estimation functional block.
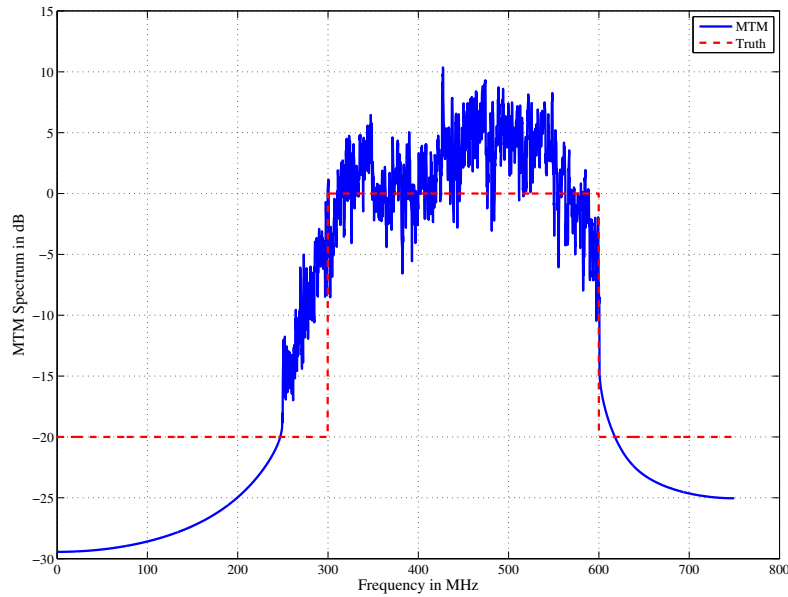

Figure 25. The MTM power spectrum estimate of the array data bandpass filtered between 300 MHz and 600 MHz to include only the spectral region occupied by the SOI for scenario 1.

As discussed in Chapter 3, if only a single DOA is found in the filtered array data then a single SOI is declared to exist and processing continues. If multiple DOA are found, the signals corresponding to each DOA must be disambiguated from each other. The results of applying the DOA estimation algorithm of Kaveh [122] to the filtered array data for each scenario are given in Figures 28-30. In all three wideband SOI scenarios, multiple DOA are found, requiring the RM to perform signal
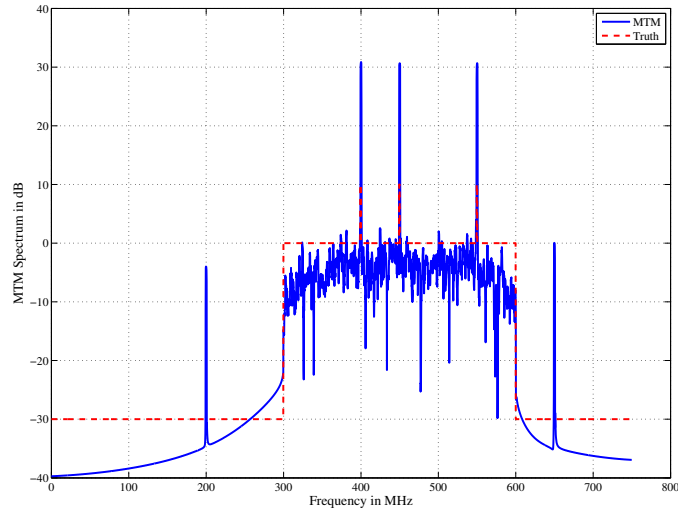
134

Figure 26. The MTM power spectrum estimate of the array data bandpass filtered between 300 MHz and 600 MHz to include only the spectral region occupied by the SOI for scenario 2.
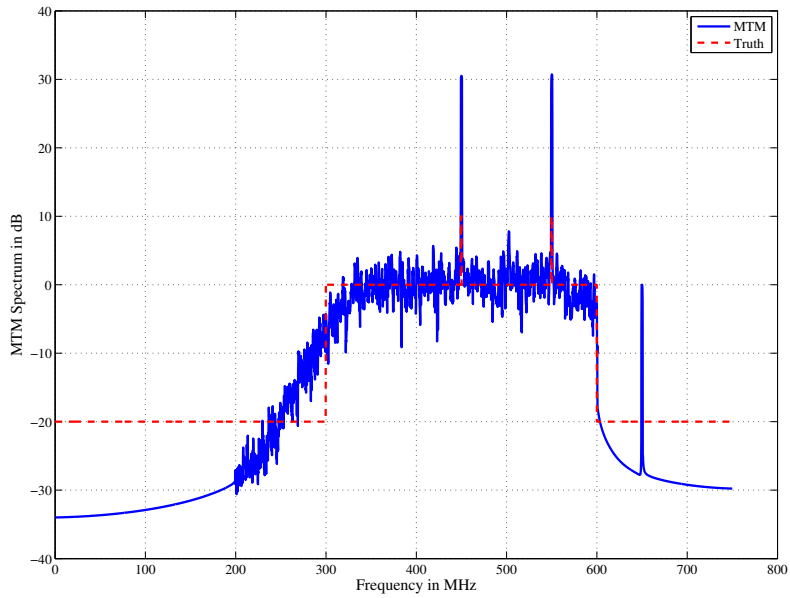

Figure 27. The MTM power spectrum estimate of the array data bandpass filtered between 300 MHz and 600 MHz to include only the spectral region occupied by the SOI for scenario 3.
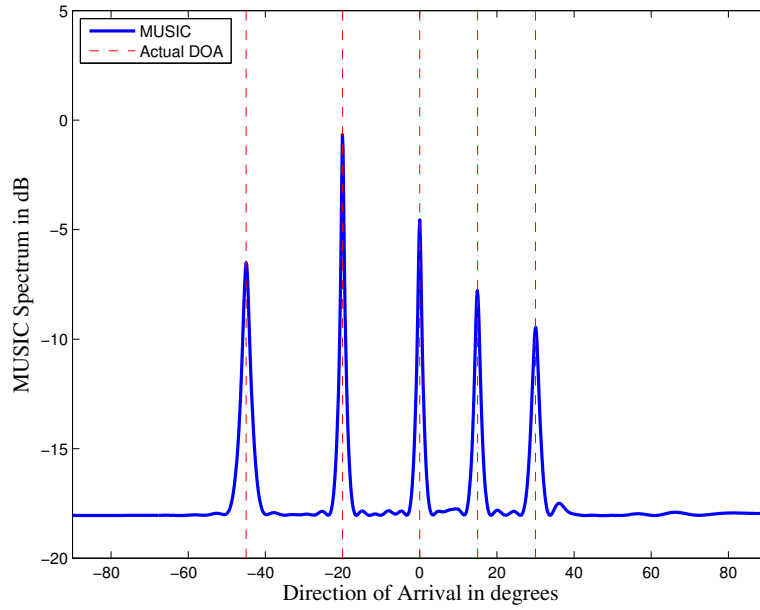
disambiguation.

Figure 28. The MUSIC spectrum of scenario 1 where the data has been bandpass filtered to only contain the SOI occupied spectral region from 300 MHz to 600 MHz for scenario 1. The MUSIC spectrum is formed from a coherently focused wideband covariance matrix and shows five DOA as each interference signal has spectral content in the 300 MHz to 600 MHz spectral region.

Signal disambiguation spatially sub-bands the filtered array data and then applies the three-of-three detection algorithm discussed in Section 3.2.2.1 to each spatial sub-band. Each sub-band consists of one array half-power beamwidth about the estimated DOA for the SOI under consideration. Three-of-three detection algorithm output is based upon spectral content being present in each third of the SOI spectral region. Figures 31-34 provide a MTM spectral estimate of each spatial sub-band[3] for the wideband interference scenario. The vertical dashed lines divide the spectral region into thirds and the horizontal dashed line provides the threshold level for signal detection. Only the first spatial sub-band, corresponding to the SOI, has spectral

---

[3] Each spatial sub-band is formed to correspond to a direction from the DOA estimate. Each sub-band covers one half-power beamwidth which for a 64 element array with an inter-element spacing of 0.1 meter is 3° for a midpoint frequency of 375 MHz.
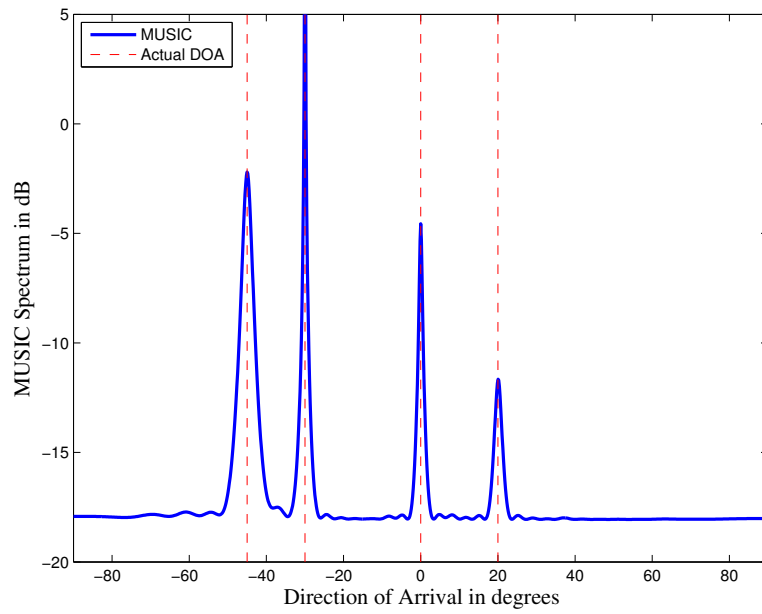
Figure 29. The MUSIC spectrum of scenario 2 where the data has been bandpass filtered to only contain the SOI occupied spectral region from 300 MHz to 600 MHz for scenario 2. The MUSIC spectrum is formed from a coherently focused wideband covariance matrix and shows four DOA as only three interference signals have spectral power in the 300 MHz to 600 MHz spectral region.
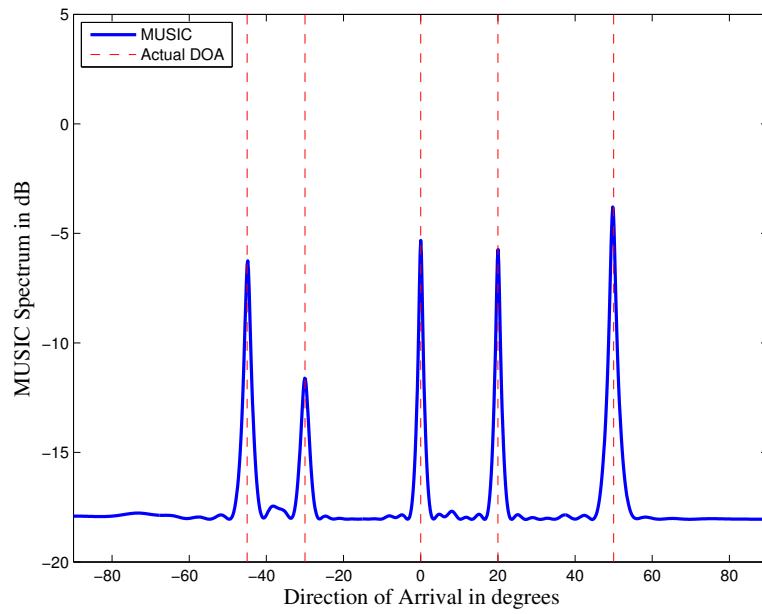
Figure 30. The MUSIC spectrum of scenario 3 where the data has been bandpass filtered to only contain the SOI occupied spectral region from 300 MHz to 600 MHz for scenario 3. The MUSIC spectrum is formed from a coherently focused wideband covariance matrix and shows five DOA where four interference signals have spectral power in the 300 MHz to 600 MHz spectral region

content in each third of the spectral region. When a GLRT is applied to each of the spatial sub-sections in the three-of-three detection algorithm, only the first sub-band returns a positive indication for all three spectral regions and detects the SOI. A complete breakout of the three-of-three detection GLRT outcomes is given in Table 9 where a one indicates that a signal is present and a zero indicates that no signal is present.
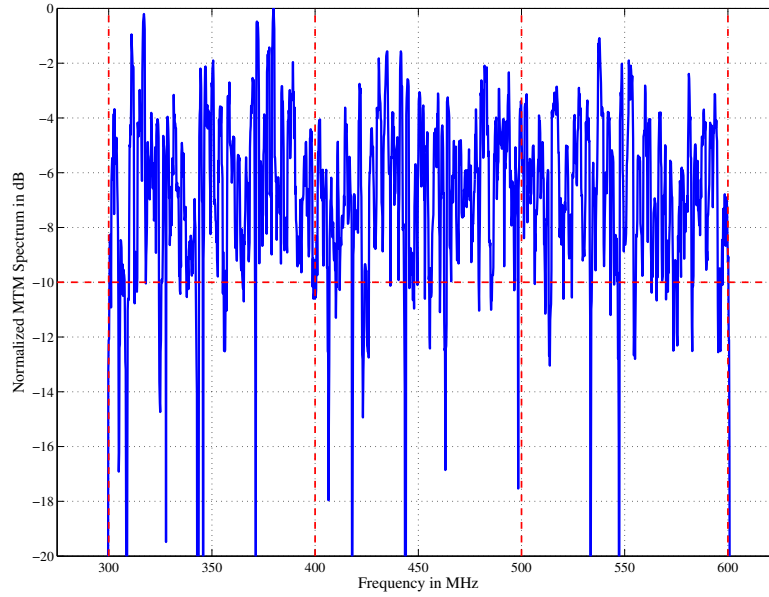

Figure 31. The MTM spectral estimate of the signal in the first spatial sub-band for signal disambiguation in scenario 1. There is power located in each third of the spectral region from 300 MHz to 600 MHz. Spectral power in all three regions indicates that the signal in the first sub-band is an SOI.

Table 9. Scenario 1 Thee-of-three detection algorithm results showing that only the first sub-band contains an SOI and that the other three sub-bands contain interference signals. A one indicates that a signal is present in the given sub-band and a zero indicates that no signal is present.

Spatial Beam	sub-band 1	sub-band 2	sub-band 3
1	1	1	1
2	1	0	0
3	1	1	0
4	0	1	1

139

Figure 32. The MTM spectral estimate of the signal in the second spatial sub-band for signal disambiguation in scenario 1. There is only spectral power in the first third of the 300 MHz to 600 MHz spectral region indicating that the signal in the second sub-band is an interference signal.

Figure 33. The MTM spectral estimate of the signal in the third spatial sub-band for signal disambiguation in scenario 1. There is only spectral power in the first two-thirds of the 300 MHz to 600 MHz spectral region indicating that the signal in the third sub-band is an interference signal.
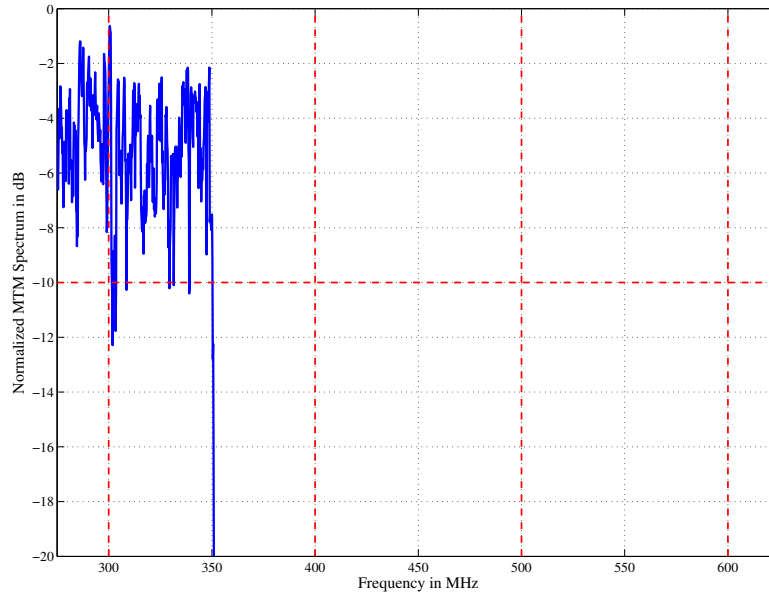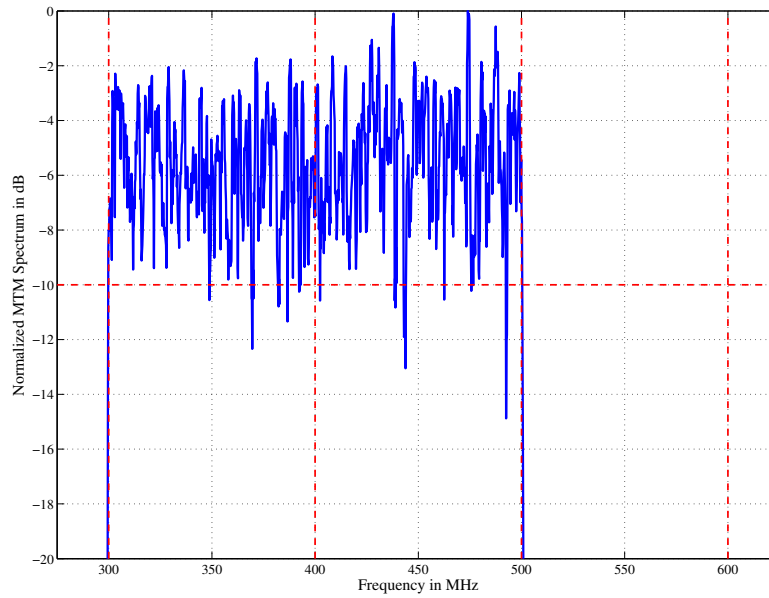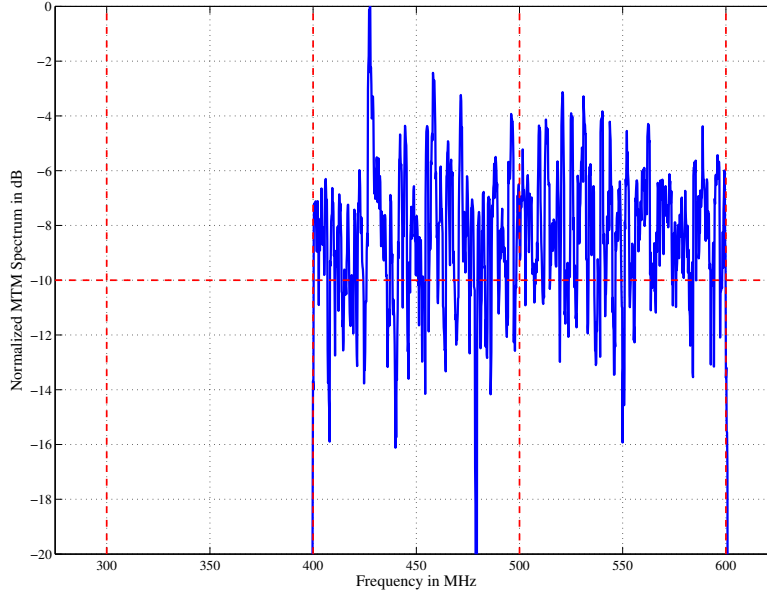
Figure 34. The MTM spectral estimate of the signal in the fourth spatial sub-band for signal disambiguation in scenario 1. There is only spectral power in the last two-thirds of the 300 MHz to 600 MHz spectral region indicating that the signal in the fourth sub-band is an interference signal.

Figures 35-38 plot the spectral estimates for each spatial sub-band in the three-of-three detection algorithm for the narrowband interference case. Figures 39-43 likewise are the three-of-three spectral estimate plots for the mixed bandwidth interference scenario. As with the wideband interference scenario, in the narrowband and mixed bandwidth scenarios only the spatial sub-band corresponding to the SOI has spectral content returning a signal's SOI present in each scenario. The three-of-three detection GLRT outcomes for the narrowband scenario and the mixed bandwidth scenario are given in Table 10 and Table 11 respectively. Differences in the number of sub-bands processed by the three-of-three algorithm are due to the number of signals removed from consideration by the initial band-pass filter applied at the start of the signal detection functional block.
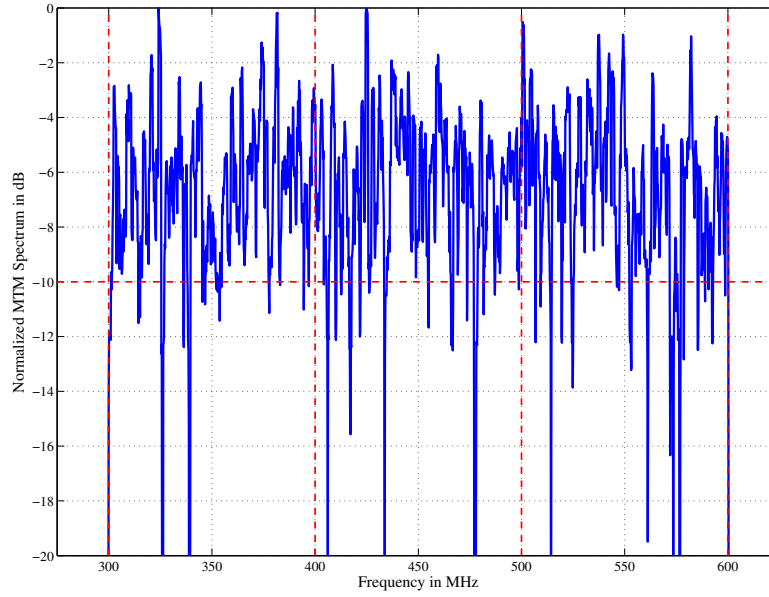
141

Figure 35. The MTM spectral estimate of the signal in the first spatial sub-band for signal disambiguation in scenario 2. There is power located in each third of the spectral region from 300 MHz to 600 MHz. Spectral power in all three regions indicates that the signal in the first sub-band is an SOI.

Table 10. Scenario 2 Thee-of-three detection algorithm results showing that only the first sub-band contains an SOI and that the other three sub-bands contain interference signals. A one indicates that a signal is present in the given sub-band and a zero indicates that no signal is present.

Spatial Beam	sub-band 1	sub-band 2	sub-band 3
1	1	1	1
2	0	0	0
3	0	0	0
4	0	0	0

Table 11. Scenario 3 Thee-of-three detection algorithm results showing that only the first sub-band contains an SOI and that the other four sub-bands contain interference signals.

Spatial Beam	sub-band 1	sub-band 2	sub-band 3
1	1	1	1
2	0	1	1
3	0	0	0
4	0	0	0
5	1	0	0

142

Figure 36. The MTM spectral estimate of signal in the second spatial sub-band for signal disambiguation in scenario 2. The signal is narrowband at 400 MHz with lesser energies for other narrowband signals with energy reduced by the spatial filter creating the spatial sub-band. There is not enough energy in any third of 300 MHz to 600 MHz to return a signal indicating that the signal is an interference signal.

Figure 37. The MTM spectral estimate of signal in the third spatial sub-band for signal disambiguation in scenario 2. The signal is narrowband at 550 MHz with lesser energies for other narrowband signals with energy reduced by the spatial filter creating the spatial sub-band. There is not enough energy in any third of 300 MHz to 600 MHz to return a signal indicating that the signal is an interference signal.
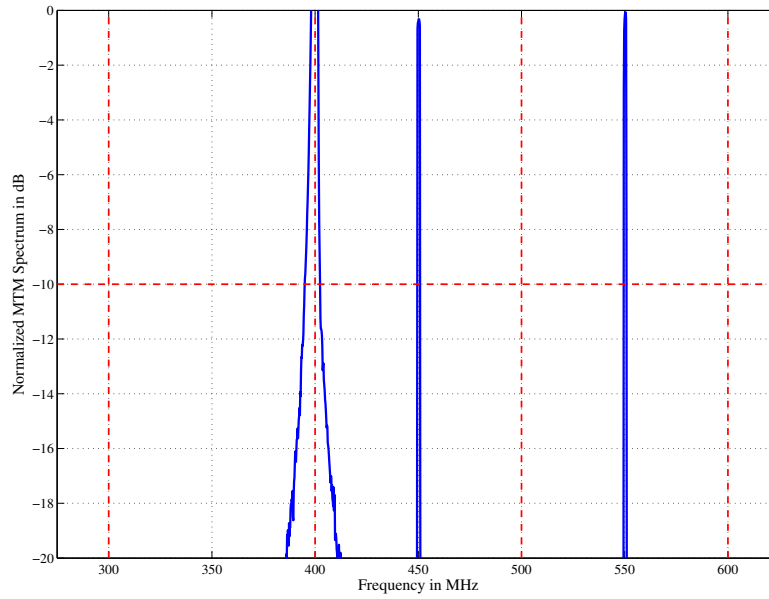
144

Figure 38. The MTM spectral estimate of signal in the fourth spatial sub-band for signal disambiguation in scenario 2. The signal is narrowband at 450 MHz with lesser energies for other narrowband signals with energy reduced by the spatial filter creating the spatial sub-band. There is not enough energy in any third of 300 MHz to 600 MHz to return a signal indicating that the signal is an interference signal.
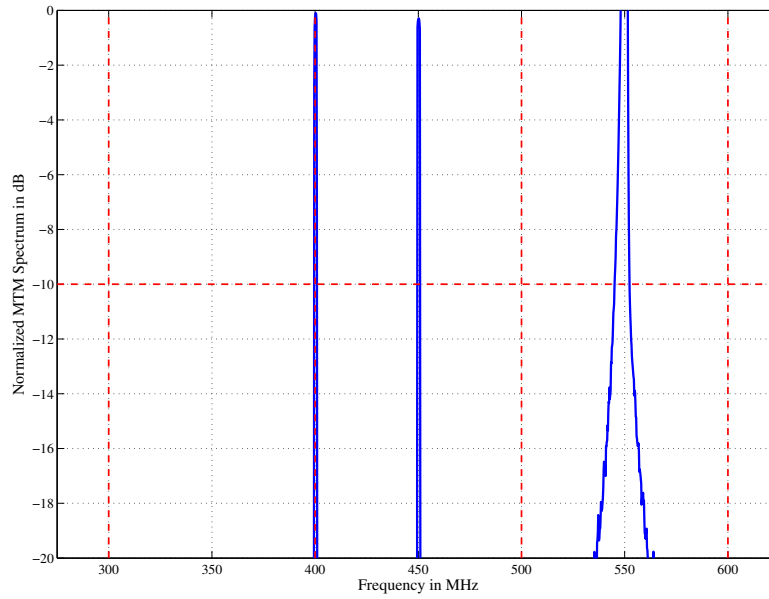
Figure 39. The MTM spectral estimate of the signal in the first spatial sub-band for signal disambiguation in scenario 3. There is power located in each third of the spectral region from 300 MHz to 600 MHz. Spectral power in all three regions indicates that the signal in the first sub-band is an SOI

Figure 40. The MTM spectral estimate of the signal in the second spatial sub-band for signal disambiguation in scenario 3. There is only spectral power in the last two-thirds of the 300 MHz to 600 MHz spectral region indicating that the signal in the second sub-band is an interference signal.

146
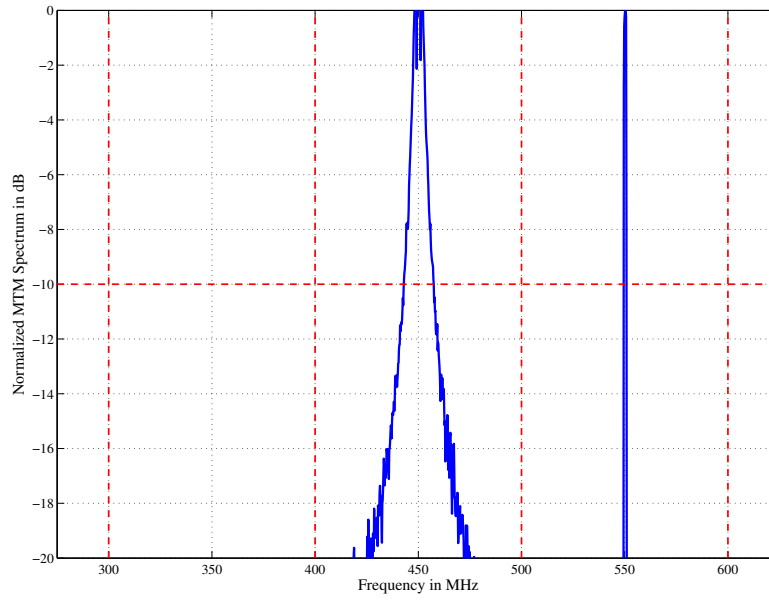
Figure 41. The MTM spectral estimate of signal in the third spatial sub-band for signal disambiguation in scenario 3. The signal is narrowband at 550 MHz and there is lesser energy from the other wideband and narrowband interference sources with power reduced by spatial filtering. There is not enough energy in any third of 300 MHz to 600 MHz to return a signal indicating that the signal is an interference signal.
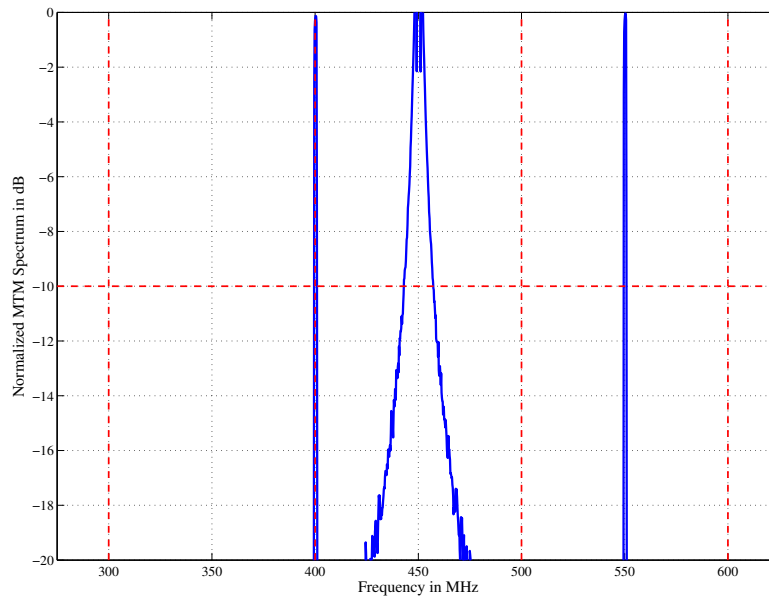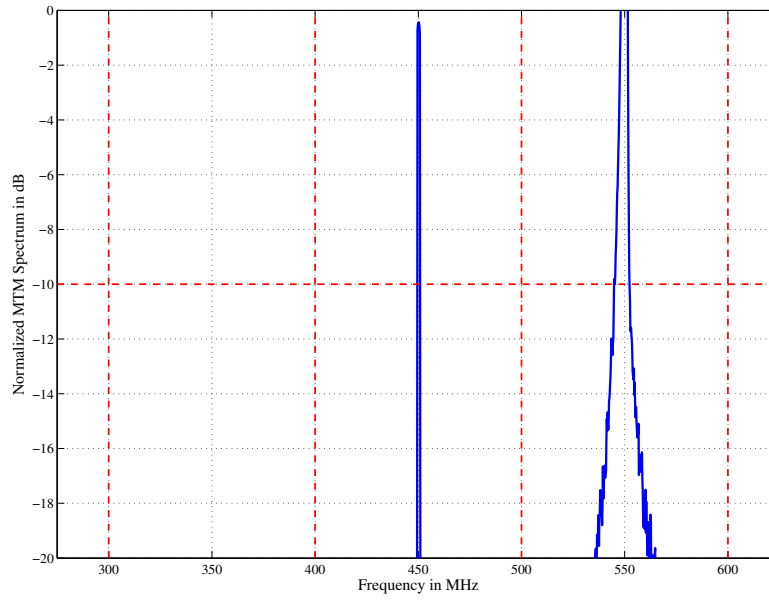
Figure 42. The MTM spectral estimate of signal in the fourth spatial sub-band for signal disambiguation in scenario 3. The signal is narrowband at 450 MHz and there is lesser energy from the other wideband and narrowband interference sources with power reduced by spatial filtering. There is not enough energy in any third of 300 MHz to 600 MHz to return a signal indicating that the signal is an interference signal.
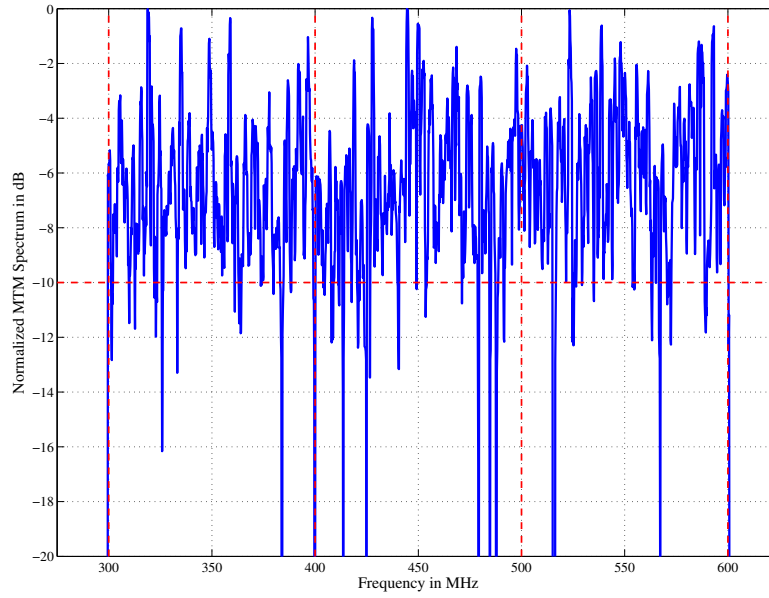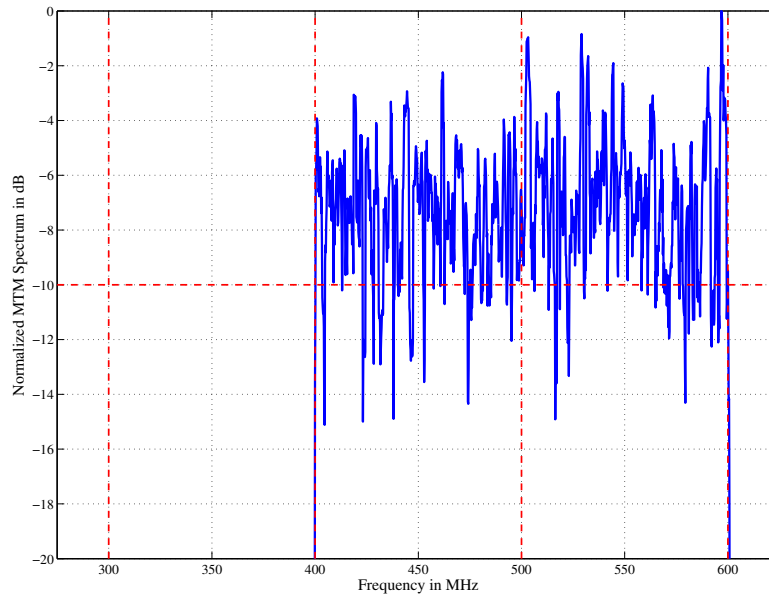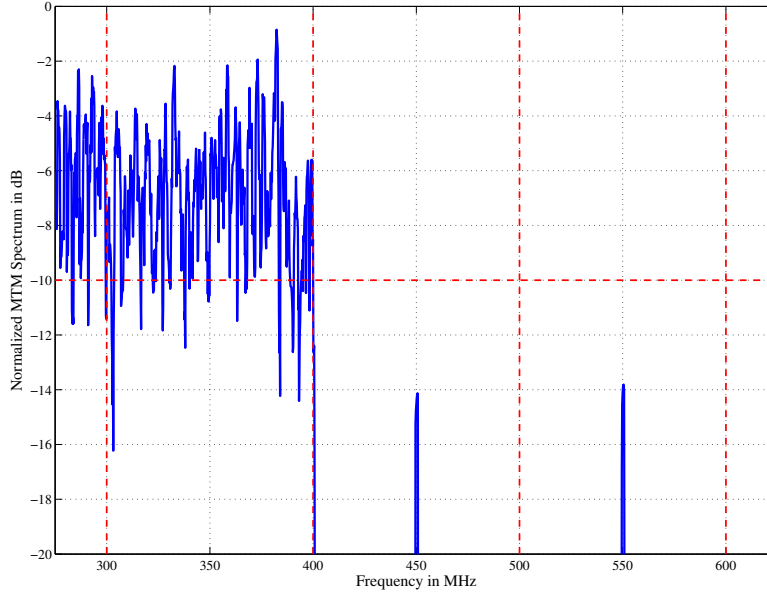
Figure 43. The MTM spectral estimate of the signal in the fifth spatial sub-band for signal disambiguation in scenario 3. There is only spectral power in the first third of the 300 MHz to 600 MHz spectral region indicating that the signal in the fifth sub-band is an interference signal.

5.1.2 Narrowband SOI Scenario Performance.

The narrowband SOI verification scenario contains a continuous wave (CW) SOI at $f_c = 375$ MHz incident from broadside (direction of arrival of 0 degrees). The wideband interference signals are again pseudo noise signals with an ISR of 10 dB. Narrowband interference sources are again 20 dB ISR continuous wave signals. Table 12 provides the bandwidths, center frequencies, and DOA for all interference signals.

5.1.2.1 Narrowband SOI Environment Estimation.

Figure 44 is the MTM spectral estimate of the EM environment for the narrowband SOI verification scenario. The SOI is present as a peak above the wideband interference sources at 375 MHz. The narrowband interference sources are also present

149

Table 12. Frequency and DOA listing for the baseband signals implemented in the Narrowband SOI RM verification scenario.

Scenario 4	Bandwidth	f_c	DOA
Signal 1	200 MHz	500 MHz	-45°
Signal 2	10 MHz	550 MHz	-30°
Signal 3	10 MHz	450 MHz	20°
Signal 4	200 MHz	300 MHz	50°
Signal 5	10 MHz	650 MHz	-15°

as peaks at 450 MHz, 550 MHz, and 650 MHz respectively. The RM detects signal energy at the *a priori* known SOI frequency of 375 MHz as well as across multiple other frequencies indicating both narrowband and wideband interference sources as shown in the GLRT output of Figure 45. The DOA of all the signals in the environment, as well as the exact number of signals in the environment is determined through wideband DOA estimation and application of the Akaike information criteria (AIC). The DOA estimation result is plotted in Figure 46. There are six DOA in Figure 46 which is the number of signals in the environment corroborated by the AIC algorithm output. The DOA estimation completes the environment parameter estimation summarized in Table 13.

Table 13. Output of the environment estimation functional block for the RM applied to scenario 4 showing the relative bandwidth of the signals in the environment and the DOA estimates for each signal in the environment to include the SOI and interference signals .

Scenario	Bandwidth	# Signals	DOA
4	mixed	6	-44.82^o, -30.06^o, -14.94^o, 0°, 20.03^o, 49.59^o

The output of the RM environmental estimation functional block presented in Table 13, for a wideband SOI causes the RM selection algorithm to choose the wideband LCMV from the LUT. The SOI in scenario four, however, is narrowband. For narrowband SOI the RM chooses the narrowband LCMV algorithm for all scenarios because the narrowband algorithm is designed to estimate narrowband signals even with wideband interference sources. This choice is confirmed by the data in Table 14

150
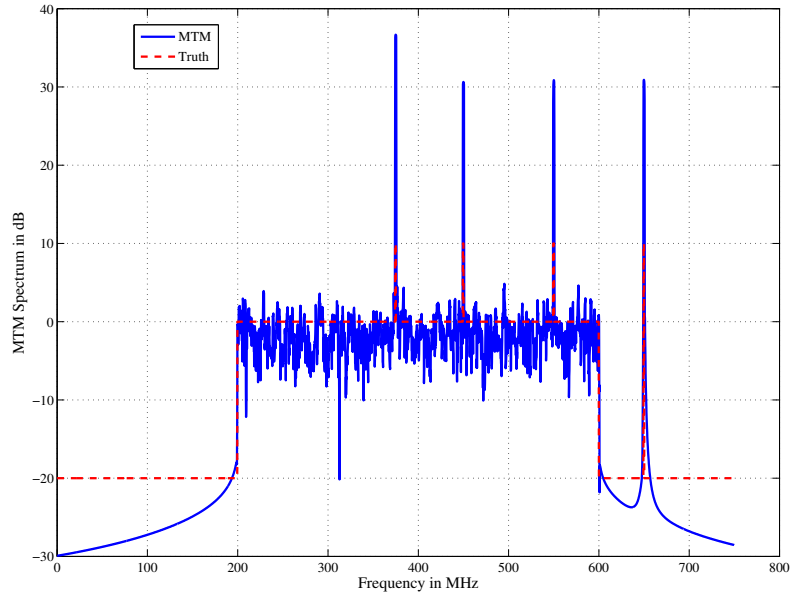
Figure 44. The MTM power spectral estimate of the two wideband interference sources, three narrowband interference sources, and the narrowband SOI in interference scenario 4.
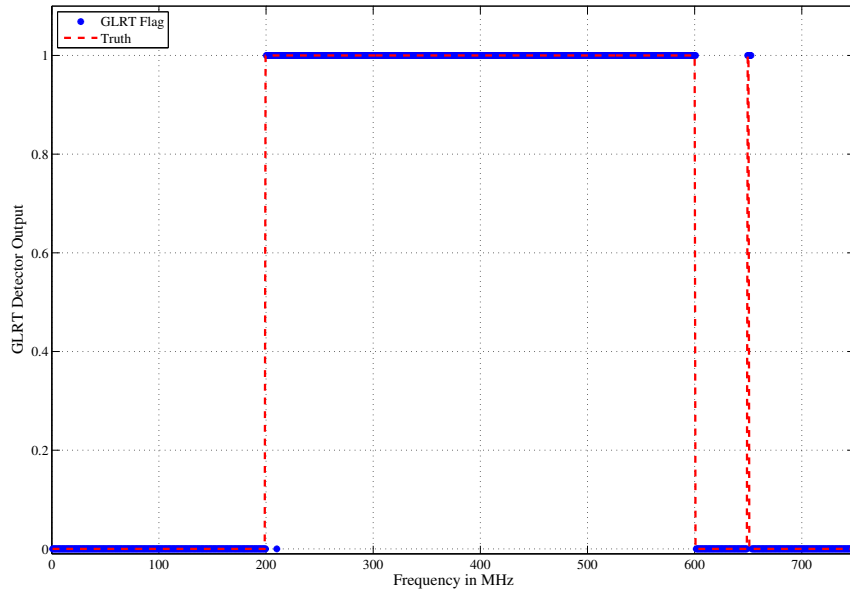
Figure 45. The GLRT output of the RM for interference scenario 4 indicating that there are wideband signals present from 200 MHz to 600 MHz as well as narrowband signals indicated by the spike at 650 MHz. The SOI is considered present as there is signal energy present at 375 MHz; if this energy is due to an interference source or an actual SOI is determined by the disambiguation algorithm.

151
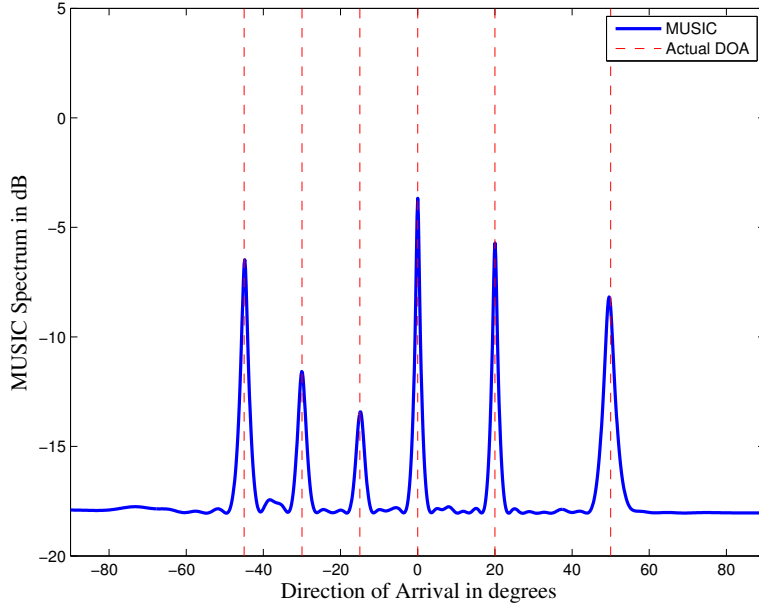
Figure 46. The MUSIC spectrum of interference scenario 4 formed using a coherently focused covariance matrix showing the DOA for the five interference sources and the SOI.

that indicates that all adaptive DBF algorithms implemented in the LUT are capable of providing an adequate level of SINR improvement; however, the narrowband LCMV algorithm has the lowest computational complexity of all algorithms and is therefore *best* for scenario four.

Table 14. SINR improvement in dB for each of the five adaptive DBF algorithms applied to scenario four containing a narrowband SOI, two wideband interference sources, and three narrowband interference sources where the boldface quantities are those chosen by the resource manager.

WB LCMV	GLRT	TRM	LSSB	NB LCMV
26.45	31.42	23.85	53.75	**14.06**

5.1.2.2   Narrowband Signal of Interest Detection.

As was performed for SOI detection in the scenarios having wideband SOI the first step in detection is spectrally filtering the array data. The MTM spectral estimate for the bandpass filtered scenario 4 data is given in Figure 47. Both the filtered

wideband interference signal present at 375 MHz and the SOI are present in the data. Performing a DOA estimation confirms that only two signals are present in the filtered data as shown in Figure 48.

Because the SOI is narrowband the three-of-three detection algorithm in practice divides a 50 MHz spectral region into thirds. As the data used in the scenario is simulated, there is a narrow peak covering only a couple of MHz. The entire 50 MHz region that would nominally be considered is shown between the vertical dashed lines in Figures 49 and 50. Each of the figures is a spatial sub-band corresponding to a DOA from Figure 48. If only the three-of-three detection criteria is applied, both sub-bands return a SOI present as energy is present across the entire *a priori* known SOI spectral region for each spatial sub-band. If, however, further *a priori* knowledge about the signal bandwidth is applied, i.e. that the SOI is narrowband, a determination that the signal present in one of the two spatial sub-bands is wideband is used to reject the interference source returning only the narrowband SOI and its DOA.

5.1.3 RM Validation Review.

Sections 5.1.1 and 5.1.2 demonstrated the ability of the RM for the proposed receiver framework to properly parameterize the electromagnetic environment for adaptive DBF selection from the LUT and to detect and disambiguate signals of interest in the environment across four different interference environments. The four environments are chosen to represent a wide variety of possible RF interference environments. All environments contain a wideband or a narrowband SOI. All scenarios also contain either wideband interference sources, narrowband interference sources, or a combination of both. The RM is able to properly parameterize the environment against the basis set and therefore against all possible scenarios. The RM for the proposed receiver architecture is therefore a valid structure for ES receiver implemen-
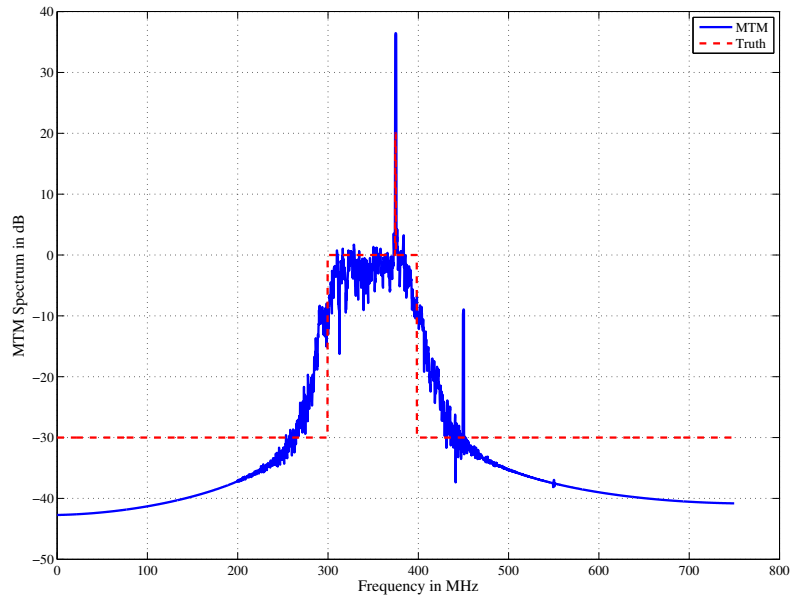
Figure 47. The MTM power spectrum estimate of the array data for scenario 4 band-pass filtered between 350 MHz and 400 MHz to include only the spectral region occupied by the SOI.
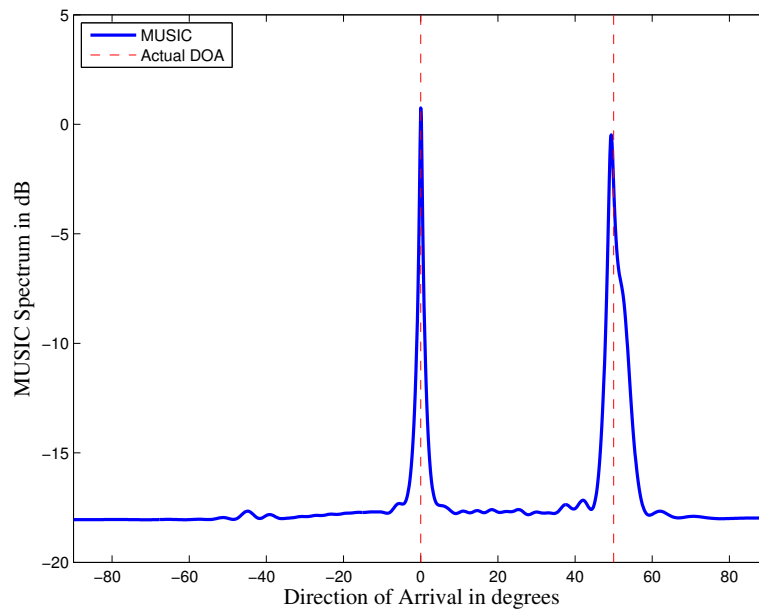
Figure 48. The MUSIC spectrum of scenario 4 where the data has been bandpass filtered to only contain the SOI occupied spectral region from 350 MHz to 400 MHZ.

154
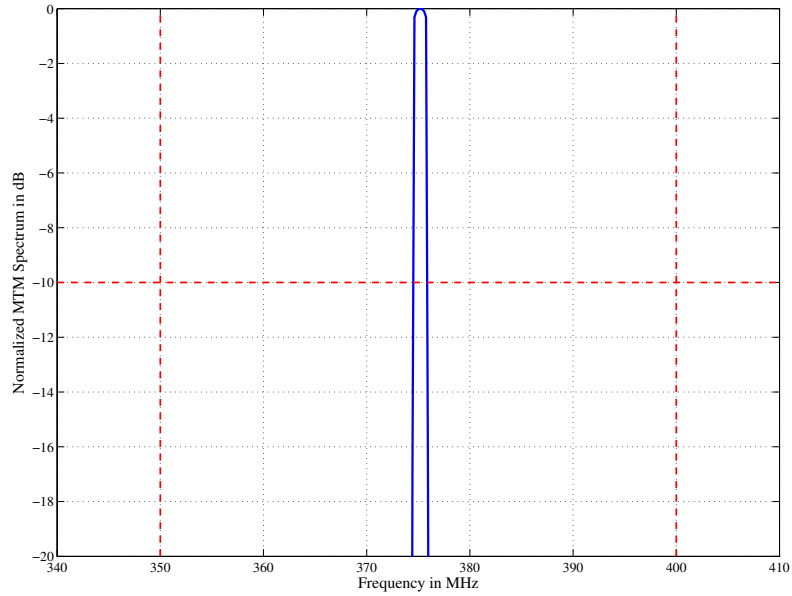
Figure 49. The MTM power spectral estimate of the signal in the first spatial sub-band for signal disambiguation in scenario 4. The power is present only at 375 MHz indicating a narrowband signal at the SOI frequency.
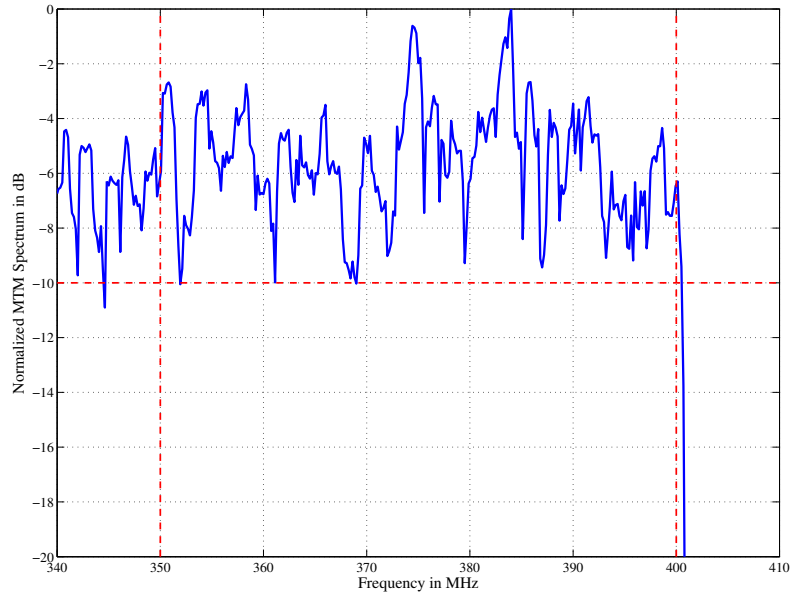
Figure 50. The MTM power spectral estimate of the signal in the second spatial sub-band for signal disambiguation in scenario 4. The power is present across the entire 50 MHZ region and is classified as an SOI. The *a priori* knowledge of a narrowband SOI is used to reject the second spatial sub-band as containing an SOI.

155

tation.

5.2 Receiver Framework Verification

Verification of the receiver framework uses measured data from the McWESS and MUD-WASP receiver test beds. The first verification scenario creates a SOI and interference signals from a data set collected on the McWESS receiver testbed, provided by AFRL Sensors Directorate. The data set contains continuous wave signals incident from -60° to 60° in one degree increments for signals transmitted at 5.0 GHz, 5.1 GHz, and 5.2 GHz. The signals were all collected during the same array test with the receiver at thermal equilibrium. From linear systems theory the environment is a superposition of all signals in the environment [83]. To verify the receiver framework a scenario is created by summing one 5.0 GHz signal incident at broadside and two 5.1 GHz signals incident from -45^0 and 30° forming a superposition equivalent to an environment containing all three signals. The McWESS array downconverts the frequency of 5.0 GHz to an intermediate frequency (IF) of 1 GHz and 5.1 GHz to an IF of 1.1 GHz before sampling at 1.33 Gsamp/sec. The 1.33 Gsamp/sec sampling rate provides a 666 MHz instantaneous bandwidth. As a result of the processing the signals at 5.0 GHz are aliased to 333 MHz and the signals at 5.1 GHz are aliased to 233 MHz in the data [39, 57].

The second verification scenario uses a data set from the MUD-WASP receiver testbed, also provided by AFRL. MUD-WASP is designed to form multiple independent simultaneous beams across multiple frequency sub-bands. The receiver array has 64-elements where there are four independent sub-arrays that can be applied to different frequency ranges. This verification effort uses data from one set of 16-elements. The center frequency of the array is 9.49 GHz which is downconverted to an IF of 1125 MHz. The array data is sampled at 1.5 Gsamp/sec giving the receiver

an instantaneous bandwidth of 750 MHz. The MUD-WASP verification scenario has three signals all consideredSOIs. The signals are all narrowband signals with the same frequency of 9.55 GHz. The signals are incident from -20°, 0°, and 50°. After downconversion and digitization, the signals are aliased to 315 MHz in the array data. The environment of the three SOIs is created using the same superposition technique as with the McWESS scenario data.

Both the McWESS array and the MUD-WASP array data are digitized using real measurements of the signal amplitude. Because of this "real" sampling all phase data from the signals are lost. This loss of phase data causes beamforming algorithms and DOA estimation algorithms to form beams/peaks in both the actual direction where the signal exists as well as the negative of the actual arrival angle. To eliminate the false signals from the McWESS data only the positive frequencies from the data are used. No manipulation was performed on the MUD-WASP data and so both the actual DOA are shown along with their negative values.

5.2.1 McWESS Environment Estimation.

Processing of the verification scenario data follows that of the three scenarios used for receiver validation. The environment estimation functional block is considered first. An MTM spectral estimate of the verification scenario is presented in Figure 51. The spectral estimate shows that signals with both of the two expected aliased frequencies of 233 MHz and 333 MHZ are present in the data. Signals at the two frequencies are detected by the GLRT as evidenced in Figure 52. Because the GLRT output contains "spikes" only narrowband interference sources are declared present in the environment corresponding to the actual signals in the environment.

The DOA estimates for the McWESS data are given in Figure 53. All three signals' DOA are represented in the figure. The accuracy of the estimates are within
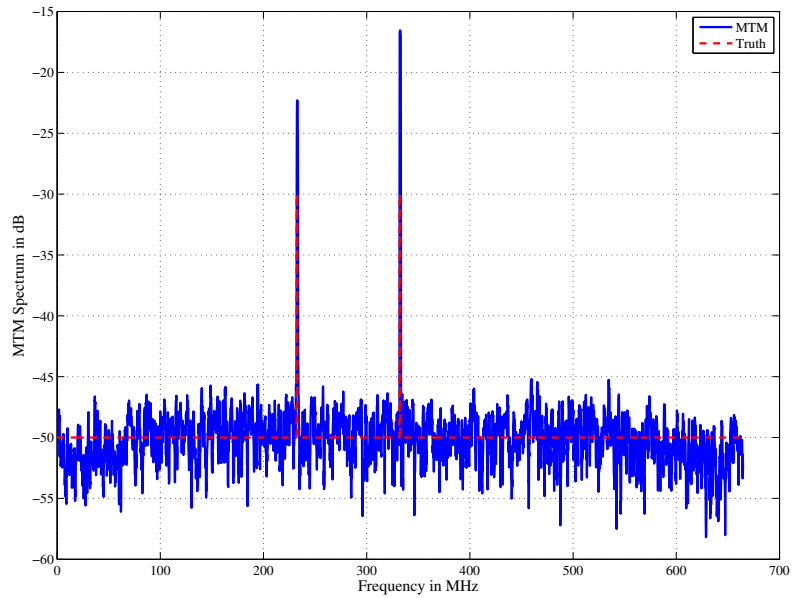
Figure 51. MTM power spectral estimate of the McWess data validation scenario showing the two narrowband spectra corresponding to the SOI and interference signals.
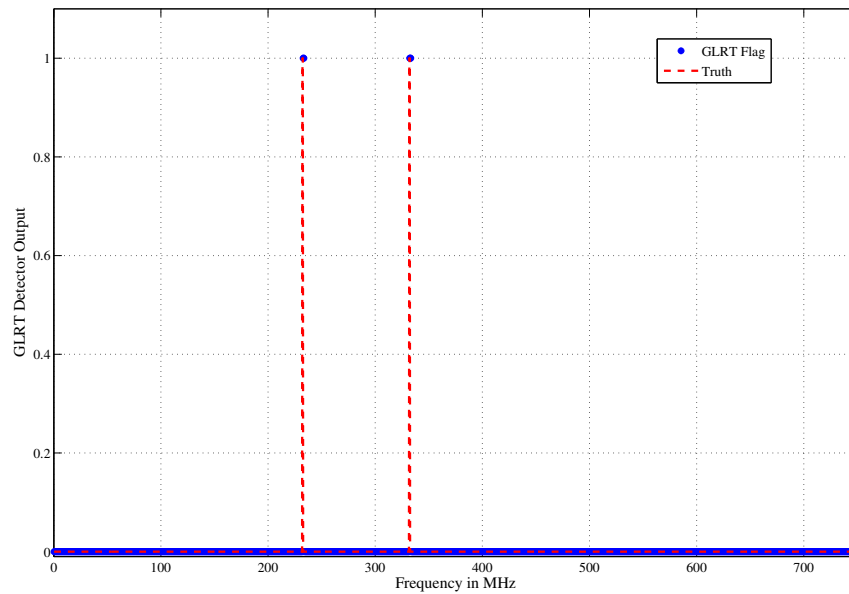
Figure 52. McWess validation scenario GLRT output showing the SOI at 333 MHz and the interference signals at 233 MHz.

158

two degrees of the DOA indicated in the data collection test matrix. This accuracy is less than produced by the RM using the simulated data. Such a decrease in accuracy, however, is expected as the McWESS scenario has the effects of an imperfect array embedded in the data. Furthermore, the McWESS array has highly coupled elements which can reduce the accuracy of DOA estimation methods like MUSIC used in the RM. The accuracy of within two degrees is therefore considered adequate. As with the simulated data, the AIC determines the correct number of signals in the environment. This completes the processing of the environmental estimation functional block. The estimated parameters of the functional block are given in Table 15. As with the simulated data the RM is again able to correctly parameterize the electromagnetic environment and thus select the *best* adaptive DBF from the provided LUT.
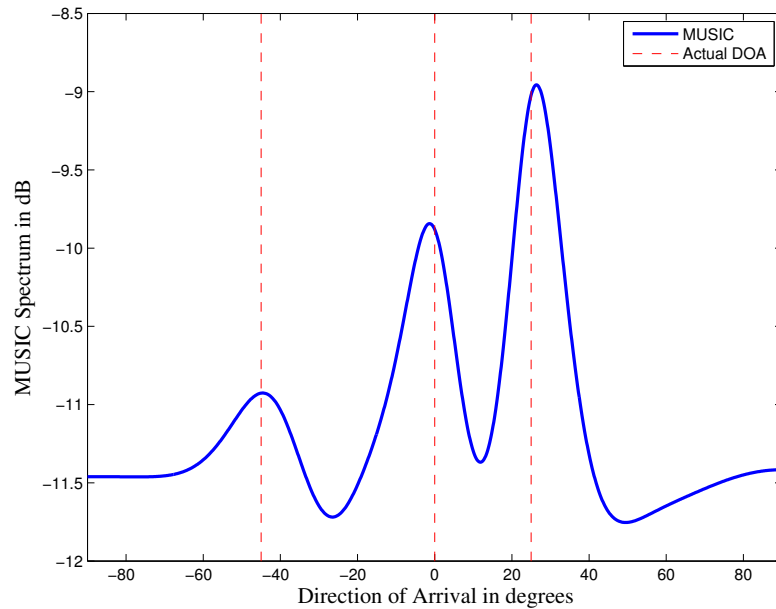
Figure 53. MUSIC spectrum of the McWess validation scenario using a coherently focused covariance matrix showing three DOA.

The RM output of Table 15 shows that the McWess data scenario has less than five interference signals and all interference sources are narrowband. For this output the RM selects the narrowband LCMV algorithm according to Table 5. As the exact

159

Table 15. Output of the environment estimation functional block for the McWess validation scenario providing the bandwidth and DOA for all three signals in the scenario.

# of signals	signal bandwidths	DOA
3	narrowband	-45.18^o, -0.90^o, 26.01^o

signal and noise powers incident upon the receiver are not known for the McWess receiver data a SINR comparison for each adaptive DBF algorithm is not possible; however, for a scenario with all narrowband sources the narrowband algorithm is proven to provide adequate SINR output from the verification scenarios. Furthermore, the narrowband LCMV algorithm is known to have the lowest computational complexity and thus is the optimal algorithm to apply to the McWess scenario data.

5.2.2   McWESS Signal of Interest Detection.

The signal of interest detection functional block again begins with applying a GLRT to the MTM spectral estimate of the array data. Actual processing uses the MTM spectral estimate of Figure 51, where the signal is determined to be present as indicated in Figure 52. The MTM spectral estimate of the spectrally filtered array data, following the processing of the signal of interest functional block, is given as Figure 54 where the SOI is again shown and detected at the correct frequency of 333 MHz.

DOA estimation of the spectrally filtered data provides the MTM spectrum of Figure 55. There is only one DOA in the MUSIC spectrum indicating a single SOI.

At this point the processing for the RM algorithm is complete. As there is only a single DOA present in the MUSIC spectrum only one signal is declared to exist as the SOI and the DOA is returned for further ES receiver processing. It is possible that the single DOA corresponds to an interference signal with the same spectral content as the SOI. In a situation where an interference signal has the exact frequency coverage of the SOI the three-of-three detection method classifies the interference signal as a SOI.

160
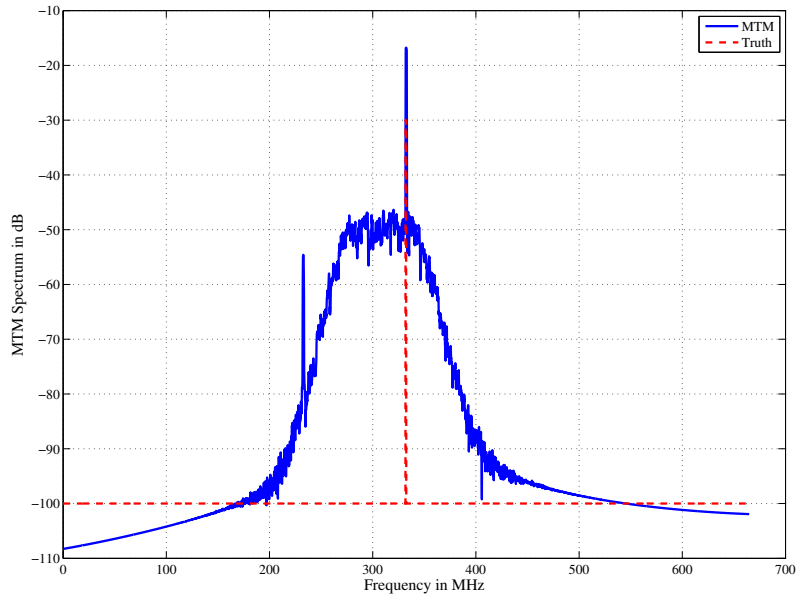
Figure 54. MTM power spectral estimate for the McWess validation scenario data bandpass filtered to only include the RF frequency of 5.0 GHz. The McWess SOI is downconverted to a baseband frequency of 233 MHz.
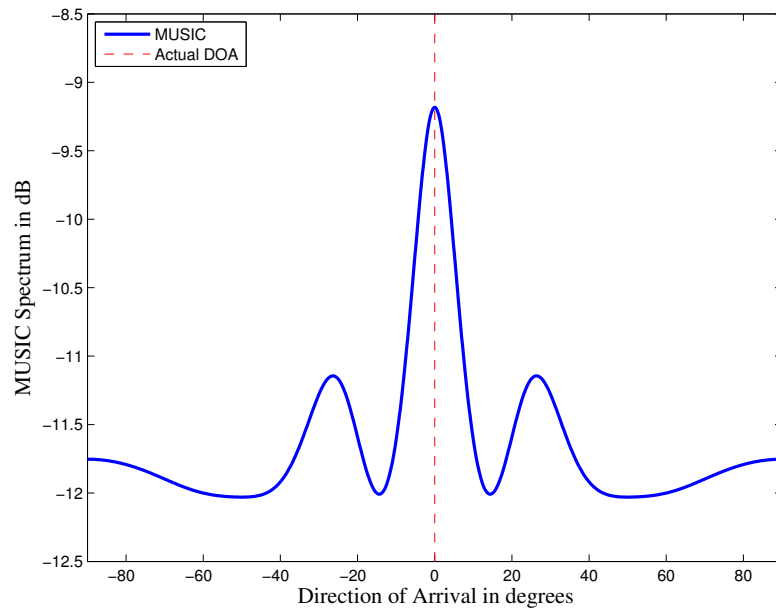
Figure 55. MUSIC spectrum of the McWess validation scenario data bandpass filtered to include only the baseband SOI frequency of 233 MHz. The MUSIC spectrum is generated using a coherently focused covariance matrix and shows only a single signal.

161

This is not a failure of the receiver framework as the algorithms employed separate the SOI from the interference signals based upon their spectral content. If an interference signal is classified as a SOI it is left to the post adaptive DBF algorithm processing to reject the interference signals.

5.2.3 MUD-WASP Environment Estimation.

Real receiver systems such as McWESS and MUD-WASP do not have ideal arrays nor ideal receiver hardware. Physical influences such as mutual coupling, array channel imbalances, and nonlinearities corrupt the collected data such that DOA estimation algorithms and adaptive DBF algorithms have difficulty resolving the different signals in the environment. The effect of the non-ideal receiver structure is shown in Figure 55 where the MUSIC spectrum for a single signal produces sidelobes that could be mistaken for signals.

The deleterious effects of an actual array are mitigated by using the time reversal method (TRM). As opposed to removing the channel delays to a signal arriving from off array broadside, however, the TRM is used to remove any effect of the physical array. Determining the impulse response of the array hardware and RF channels allows for the inverse channel response to be determined. Applying the inverse channel response to the sampled array data removes the effects of physical array processing and provides the sampled array data that would be present if the RF environment were sampled at the front of the array. AFRL determined the inverse response for the MUD-WASP receiver and this inverse response is applied to the sampled MUD-WASP array data prior to application of the RM algorithms.

Figure 56 is the resulting MUSIC spectrum for DOA estimation using the MUD-WASP data. There are five peaks in the MUSIC spectrum. Three peaks are in the correct positions for the three signals at -20°, 0°, and 50°. The other two peaks are

at -50° and 20° due to the strictly real sampled array data; there is no sixth signal present as $-0^o = 0^o$ and only appears once in the MUSIC spectrum. The algorithm is able to find three angles as expected from the scenario composition. Figure 57 shows the MTM spectral estimate of the MUD-WASP scenario data. There is only one narrowband frequency represented in the estimate. This is because all three signals in the scenario are considered narrowband SOI and have the same frequency. As there is only spectral content at one frequency the GLRT is able to detect that a narrowband SOI is present in the data. The GLRT results are shown in Figure 58, presenting a line at the frequency sub-band corresponding to 333 MHz where the MTM estimate of Figure 57 indicates the SOI in the data exists.
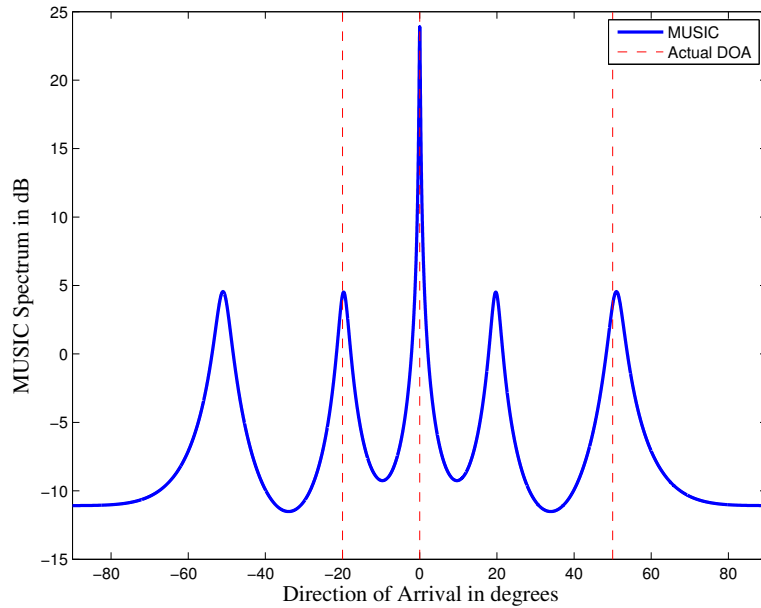
Figure 56. MUD-WASP validation scenario MUSIC spectrum indicating direction of arrival of the three SOI in the MUD-WASP data scenario.

The last parameter required of the RM environment estimation functional block is the number of signals in the environment. Because of the strictly real array data, the number of non-noise eigenvectors and eigenvalues in the covariance matrix of the data is twice that of the true number of signals. Because the AIC criterion is based upon

163
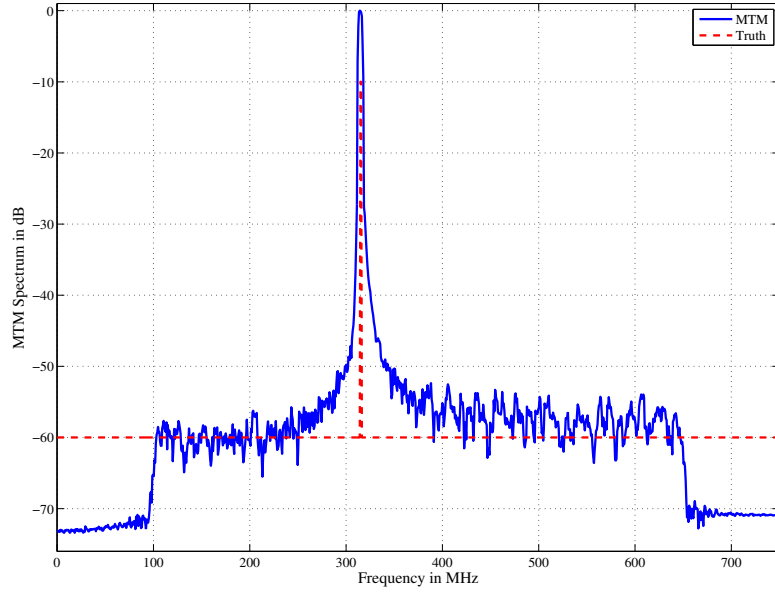
Figure 57. MTM power spectral estimate of the MUD-WASP data validation scenario showing the single narrowband spectrum corresponding to the SOI and interference signals.
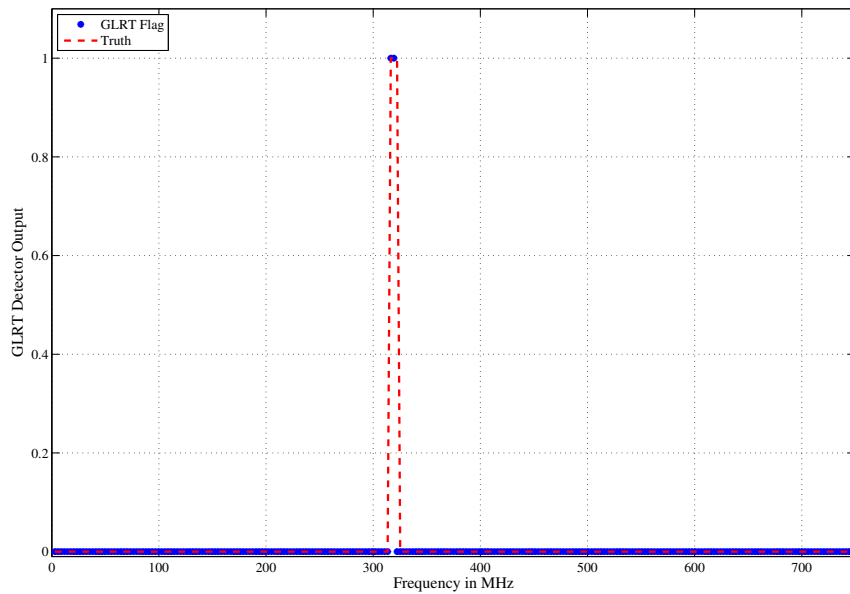
Figure 58. The GLRT output from the MUD-WASP MTM spectral estimate indicating that only narrowband signals exist in the data.

the eigenvalues and eigenvectors of the array data covariance matrix it incorrectly doubles the number of signals present. The digitization scheme of the receiver is known *a priori* to receiver implementation. It is incumbent upon the receiver designer to take this into consideration and when the number of signals present is even, half that number of signals. If the number of signals is odd, than a signal is present at zero degrees and only has a single eigenvalue used in the AIC model order selection. The correct number of signals present from the AIC model order selection is found through $\left(\frac{N_{sig}-1}{2}\right) + 1$ where N_{sig} is the number of signals returned from the AIC model order selection algorithm. There is no simple method for determining which of the estimated are the true DOA and which are the "phantom" signals. In practice all five angles are passed to the SOI estimation functional block and the correct DOA are determined by the signal disambiguation algorithm.

The estimated parameters for the MUD-WASP verification scenario are summarized in Table 16. The correct number of signals is indicated due to knowledge of the type of receiver digitization. The DOA, however, are listed as $+/-$ to indicate the true polarity of the DOA is unknown at this point in the RM processing. All DOA estimates are within 1° of actual indicating good performance of the DOA estimation algorithm.

Table 16. Output of the environment estimation functional block for the MUD-WASP validation scenario providing the bandwidth and DOA for all three signals in the scenario.

# of signals	signal bandwidths	DOA
3	narrowband	$\pm 50.97^o$, $\pm 0^o$, $\pm 19.70^o$

Similar to the McWess verification scenario, the RM environment estimation algorithm returns an environment with less than five signals where all signals are narrowband. From Table 5, the RM is known to select the narrowband LCMV algorithm for this environment. Also as discussed for the McWess scenario, the exact signal and

interference powers are not known for the MUD-WASP verification scenario preventing a by SINR comparison; however, also similar to the McWess verification scenario in narrowband environment the narrowband LCMV algorithm is known to produce adequate SINR output levels and has the lowest computational complexity making it the most optimal algorithm for the MUD-WASP verification scenario.

5.2.4 MUD-WASP Signal of Interest Detection.

All three signals in the environment are considered SOI. Because the signals have the same frequency, filtering the array data in the frequency domain does not eliminate any of the signals. Therefore, when the DOA estimation algorithm is applied to the filtered data the result is the same as Figure 56. The signal disambiguation algorithm separates the data into five spatial sub-bands corresponding to the five estimated DOA. Two of the spatial sub-bands contain noise and are discarded when the three-of-three detection algorithm is applied. Figure 59 plots the MTM spectral estimate of the three signal-containing sub-bands, showing that the spectral content of the three sub-bands are similar as expected. When a GLRT is applied to these spectra the correct number of SOI are detected. The end result from the RM is the correct identification of the three SOI with their correct relative bandwidth and DOA.

5.2.5 RM Verification Review.

The purpose of the RM verification is to ensure that the proposed receiver framework not only applies the implemented algorithm as designed, i.e. are valid, but that the receiver is capable of performing the task that it is designed to perform. Indeed the RM is able to correctly parameterize the electromagnetic environment collected by a physical receiver. The RM is able to use the estimated environment parameters to correctly choose the *best*[4] adaptive DBF algorithm for each scenario. Also, the

---

[4]Performance is determined by SINR improvement and computational complexity
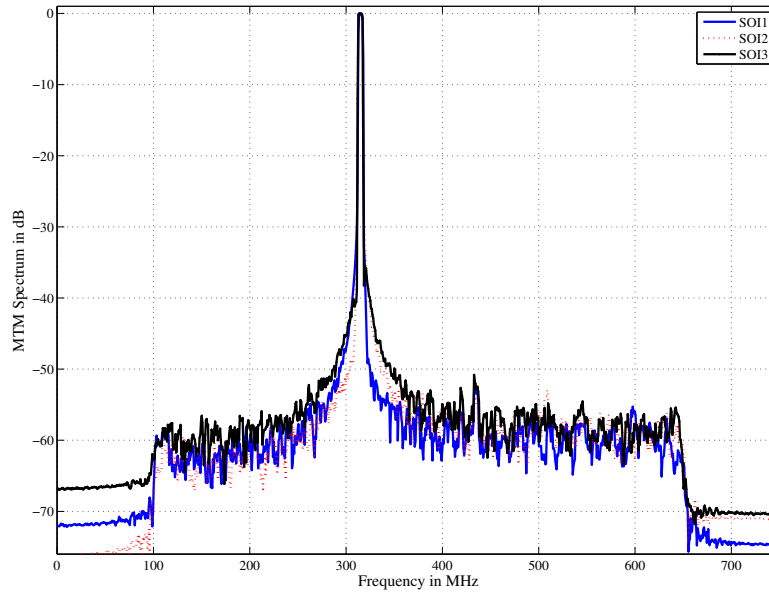
Figure 59. MTM power spectra of the three spatial sub-bands containing signals from the MUD-WASP array data. The signals in all three sub-bands have the same spectral content and are therefore all considered SOI.

RM is able to detect the signals of interest and perform any required signal disambiguation on the signals present in the measured array data. The RM is thus able to perform the tasks it was designed to perform using measured array data and is verified.

VI. Conclusions

Electronic support (ES) receivers are designed to detect and estimate signals-of-interest (SOIs) in a congested electromagnetic (EM) interference environment. Traditional ES receivers apply a single adaptive digital beamforming (DBF) algorithm in all interference environments. The adaptive DBF algorithm implemented by the ES receiver is chosen *a priori* to receiver operation based upon the receiver's operational requirements. Pre-selection of the adaptive DBF algorithm limits the types of interference environments the receiver is able to accurately operate in. Regardless of the severity of the interference environment the receiver is only able to apply a limited number of simultaneous beams. In interference environments with multiple wideband interference sources the algorithm may be unable to improve the signal-to-interference-plus-noise ratio (SINR) by an acceptable amount.

This dissertation presented a new receiver framework designed to intelligently select an adaptive DBF algorithm from a set of algorithms chosen by the receiver designer. Algorithm choice is made based upon the interference environment in which the SOIs are embedded. The interference environment is parameterized with regard to the relative bandwidths of the signals in the environment and their directions-of-arrival (DOAs). An adaptive DBF algorithm is chosen for each SOI from a look-up-table (LUT). Selection from the LUT is based upon the estimated environment parameters.

Chapter 3 presented the design and implementation of a resource manager (RM) used to estimate the environment parameters and determine the number of SOIs and estimate their respective DOA. The algorithm is labeled a RM because the output of the algorithm has a direct impact on the receiver resources used to estimate the SOIs. The output of the RM is an adaptive DBF algorithm choice for each SOI. The number of SOI present and the adaptive DBF algorithm chosen to estimate each SOI

determine the amount of computational resources the receiver is required to employ.

The set of adaptive DBF algorithms contained in the LUT are determined by the receiver designer. Algorithms are chosen based upon the type of SOI and the type of interference environments incident upon the receiver's array. The receiver designer develops the LUT based upon a selection rule that ensures the designer's goals are met. Demonstration of the receiver framework requires a representative LUT of adaptive DBF algorithms be created. Chapter 4 created a LUT of algorithms based upon the performance criteria of SINR improvement and computational complexity. The decision rule chose for inclusion in the LUT the adaptive DBF algorithm for each radio frequency (RF) environment that met a required SINR threshold while having the lowest computational complexity of all algorithms that provided the required SINR improvement.

Chapter 5 determined the performance of the receiver framework against both simulated RF environments and data collected on two receiver testbeds at Air Force Research Laboratory (AFRL). The simulated RF environments demonstrated that proposed receiver framework algorithms were mathematically correct and provided the expected output. The collected RF data demonstrated that the receiver framework is able to process actual signals and provide the *best* adaptive DBF algorithm, from the pre-selected set of algorithms, for estimating the SOI.

6.1 Future Research

The receiver architecture described in this dissertation employs only a limited set of adaptive DBF algorithms. Algorithms are chosen from the LUT based on their SINR improvement and computational complexity. Future research should focus on considering additional adaptive DBF algorithms for the LUT. The study should include the development of new selection rules. In this research only three algorithms

of five are included in the LUT. Work should be conducted to determine if a new selection rule would include more algorithms in the LUT. Inclusion of new algorithms should allow for inclusion of more algorithms in the LUT with the current selection rule. The new rule with old algorithms should be compared with designs using the old rule with new algorithms as well as the new rule with new algorithms.

In conjunction with the additional DBF algorithms, additional environment parameters should be investigated. A further extension of considering more environment parameters is to determine the sensitivity of the adaptive DBF algorithms to changing more than one interference environment parameter at once. The addition of an interference parameter and the inclusion of changing combinations of interference environment parameters expands the types of interference environments the RM has to identify. This, in turn, should allow for a greater variety of adaptive DBF algorithms to be considered optimal for a given environment and allow for the meaningful inclusion of more adaptive DBF algorithms.

The additional parameter that should be considered first is the power of the interference sources. An empirical study shown in Chapter 4 indicated a definite sensitivity of adaptive DBF performance with regard to interference signal power. Signal power was not chosen as a parameter for the initial study as the addition would have added computational complexity to the environment estimation functional block of the RM. Any additional interference parameter considered by the RM of adaptive DBF selection requires additional computations in the RM that have to be considered when determining the benefits of the new receiver architecture.

An additional area for future research is implementing the RM framework on the AFRL MUD-WASP receiver testbed. This additional research task requires the rewriting of the chosen adaptive DBF algorithms in a language that can be implemented on an field programmable gate array (FPGA). The research also involves

interfacing a computing system with existing MUD-WASP hardware to host the RM architecture and pass the adaptive DBF algorithm selected from the LUT, along with any required data and parameters, to the MUD-WASP for filter weight implementation. A first step toward MUD-WASP implementation is to create formulations of the adaptive DBF algorithms that work, independent of each other, on the MUD-WASP architecture. From there the development of the RM on a separate computational platform can commence.

One other possible future research area is to improve the structure of the RM algorithms. The formulations of the estimators in the RM implementation are chosen for ease of implementation and applicable background literature. There are other possible algorithmic implementations of all portions of the RM and another implementation could reduce the complexity of the RM or increase the accuracy of the estimation algorithms used. This line of research can also carry over to the choice of adaptive DBF algorithms used in the LUT. The adaptive DBF formulations chosen for this dissertation were the standard versions found in the literature for each algorithm. Within the literature there are various versions of each adaptive DBF that are more robust, more accurate, less complex, or have some other improvement over the standard form. Research would implement each algorithm and test the new implementation against all the scenarios used for LUT generation. If the algorithm was considered optimal for any scenario it would be included in the LUT. This line of reasoning should be extend to testing the algorithms developed in a computing language other than MATLAB. The speed of the algorithm implementations should increase when coded in a language such as C, however, there could be new implementation issues that occur in the new language.

6.2 Final Thoughts

Radar and communication systems research is progressing toward more dynamic systems. Cognitive radios are used to make better use of the limited RF spectrum [31]. Likewise, research is progressing towards more "aware" radar systems such that transmit and receiver patterns are amended real time to account for changing environment conditions [31]. This research presents a method for ES receivers to become more aware of their electromagnetic environment and use this knowledge to improve the receiver performance. The RM has only knowledge of the desired signal type and is otherwise operating blind. The ability to intelligently select an appropriate adaptive DBF algorithm for a given electromagnetic environment is of use in its own right. It also provides a starting place to attempt to use information other than the environment parameters to improve the selection of receive weight patterns.

Appendix A. MUSIC

The DOA of the SOI and any interference sources are estimated using the Multiple Signal Classification (MUSIC) method. MUSIC is a subspace processing method first described by Schmidt in [91]. In the notation of Schmidt, MUSIC assumes the data model

$$
\begin{bmatrix} \mathbf{x}_1 \\ \mathbf{x}_2 \\ \vdots \\ \mathbf{x}_M \end{bmatrix} = \begin{bmatrix} \mathbf{v}(\phi_1)\,\mathbf{v}(\phi_2)\cdots\mathbf{v}(\phi_D) \end{bmatrix} \begin{bmatrix} \mathbf{f}_1 \\ \mathbf{f}_2 \\ \vdots \\ \mathbf{f}_D \end{bmatrix} + \begin{bmatrix} \mathbf{n}_1 \\ \mathbf{n}_2 \\ \vdots \\ \mathbf{n}_M \end{bmatrix} \tag{144}
$$

where the D waveforms $\{f_1, \cdots, f_D\}$ are received by an M element array. Each of the $\mathbf{n}$ are vectors of noise samples. The data model can be rewritten as

$$
\mathbf{X} = \mathbf{VF} + \tilde{\mathbf{N}}. \tag{145}
$$

Each of the column vectors $\mathbf{v}(\phi_i)$ are steering vectors of the transmitted data. The covariance matrix of the received data is found by

$$
\mathbf{R} = E\left[\mathbf{X}\mathbf{X}^H\right] = \mathbf{V}E\left[\mathbf{F}\mathbf{F}^H\right]\mathbf{V}^H + E\left[\tilde{\mathbf{N}}\tilde{\mathbf{N}}^H\right] \tag{146}
$$

where $E[\cdot]$ indicates the expected value of the enclosure.

The form of (146) illuminates that the covariance matrix is composed of the sum of signal and noise subspaces. A spectral decomposition of $\mathbf{R}$ is given by

$$
\mathbf{R} = \sum_{m=1}^{M} \lambda_m \boldsymbol{\Phi}_m \boldsymbol{\Phi}_m^H, \tag{147}
$$

where the $\{\lambda_1, \cdots, \lambda_M\}$ are the M eigenvalues of $\mathbf{R}$ and the $\{\boldsymbol{\Phi}_m\}$ are the corresponding eigenvectors corresponding to eigenvalues λ_m. The spectral decomposition

of $\mathbf{R}$ presents the covariance matrix as the sum of M orthogonal subspaces. Furthermore, there are D subspaces associated with the signals in $\mathbf{X}$ and $M - D$ noise subspaces. MUSIC development proceeds by splitting the M eigenvectors $\boldsymbol{\Phi}_m$ into two groupings representing a basis for the signal subspace and a separate basis for the noise subspace. The two subspace eigenvector matrices are written as

$$\mathbf{U}_{signal} \triangleq \left[\boldsymbol{\Phi}_1 \vdots \boldsymbol{\Phi}_2 \vdots \cdots \vdots \boldsymbol{\Phi}_D \right], \tag{148}$$

and

$$\mathbf{U}_{noise} \triangleq \left[\boldsymbol{\Phi}_{D+1} \vdots \boldsymbol{\Phi}_{D+2} \vdots \cdots \vdots \boldsymbol{\Phi}_M \right], \tag{149}$$

Because the noise subspace is orthogonal to the signal subspace, the projection of any vector from the signal subspace onto the noise subspace returns zero. MUSIC forms a set of steering vectors $\mathbf{v}\left(\phi\right)$ spanning the possible range of signal directions of arrival and projects each signal onto the noise subspace. The result of all projections as a function of direction is referred to as the *null spectrum* of the correlation matrix $\mathbf{R}$. Then null spectrum is formed using the noise eigenvector matrix of (149) and an angle dependent steering vector as

$$\mathbf{Q}_{MU} = \mathbf{v}^H\left(\phi\right) \mathbf{U}_{noise} \mathbf{U}_{noise}^H \mathbf{v}\left(\phi\right), \tag{150}$$

where the MU subscript indicates that this is the MUSIC null spectrum. In theory all signal projections into the null space would result in exactly zero output, in reality due to imperfect sensors and having to estimate the covariance matrix $\mathbf{R}$ the null spectrum never reaches zero. Nevertheless, the minima of the null spectral result at the angles corresponding to the directions of arrival of all signals in the environment. The MUSIC spectrum, which is the final result of the MUSIC algorithm, is found by

taking one over the null spectrum

$$MUSIC\left(\phi\right) = \frac{1}{\mathbf{Q}_{MU}\left(\phi\right)}.$$

(151)

Appendix B. SINR as a Metric

Receivers apply beamformers to estimate a signal-of-interest (SOI) embedded in noise and interference sources. Beamformers operate by forming spatial-temporal beams that increase the gain of a signal of interest while forming nulls to reduce the gain of interference signals and noise. The resource manager (RM) is designed to estimate parameters characterizing the electromagnetic (EM) environment incident upon the array and choosing the most optimal adaptive digital beamforming (DBF) algorithm for the estimated environment parameters from a look-up-table (LUT) of adaptive DBF algorithms. Algorithm optimality is determined by a decision rule where the two criteria are algorithm performance and algorithm computational complexity.

The first decision rule criteria is algorithm performance. There are multiple methods for measuring adaptive DBF performance. The primary performance measurements in the literature are signal-to-interference-plus-noise ratio (SINR) improvement, mean square error (MSE), integrated sidelobe ratio (ISLR), and peak sidelobe ratio (PSLR). Both of the sidelobe ratio performance measures are applied to synthetic aperture radar (SAR) performance and pulse compressed radar waveform performance but are not usually applied to beamformer performance [76, 104]. In a survey of beamforming literature presented in Chapter 2 the SINR output of a beamformer was the most commonly used measure of beamformer performance.

Given that the purpose of the adaptive DBF algorithm is to estimate a SOI embedded in white Gaussian noise and directional interference sources the most natural performance measure is MSE. The requirement for post processing algorithms such as pulse descriptor word (PDW) generation algorithms and communication decoding algorithms are given in terms of SINR output. This difference between the most natural, i.e. the most logical performance measure, and the performance measure

176

most widely used is remedied by Goldstein *et al.* in [25]. Goldstein shows mathematically that the performance measures of SINR out and MSE are equivalent for constrained beamformers. For this research effort the five chosen adaptive DBF algorithms - wideband linearly constrained minimum variance (LCMV), generalized discrete Fourier transform (GDFT), time reversal method (TRM), and narrowband LCMV - are constrained beamformers. Therefore, the SINR metric is an appropriate metric to used for beamformer performance in the RM.

The algorithm chosen by the RM for each wideband scenario of Chapter 5 is verified as being the correct algorithm based upon both SINR improvement and MSE using Table 17. The table provides the SINR improvement and MSE for the three beamformer types contained in the LUT. From Table 6, scenario one had multiple wideband interference sources and the RM chose the wideband LCMV[1] algorithm for beamforming. Table 17 shows that the wideband LCMV algorithm had a higher SINR improvement and lower MSE than the narrowband LCMV algorithm. The TRM method had a lower SINR than the wideband LCMV algorithm, but also lower MSE which appears to contradict the notion that MSE and SINR are equivalent metrics. This difference is attributable to the TRM method applying a pre-steering algorithm to the data before application of a constrained beamformer. This implies that the analysis of Goldstein is only strictly valid when only purely constrained beamformers are being compared.

For the current analysis, both the wideband LCMV and the TRM meet the SINR out threshold. At first it appears that the RM chooses the wrong algorithm as the TRM has slightly lower MSE, although both are of the same order of magnitude and an order of magnitude lower than the narrowband LCMV. The algorithm selection, however, is based on two performance criteria and the computational complexity must

---

[1]The wideband LCMV applied is Frost's algorithm and the two terms are used synonimously.

be considered. The complexity of the TRM is higher than the wideband LCMV and so the failure of the SINR-MSE equivalence does not affect the RM choice. This indicates that if two SINR and MSE are of the same order of magnitude, as for the case of scenarios one and three where the best SINR does not equate to the best MSE, SINR output/improvement is still the correct choice as both algorithms will provide the required SINR out threshold and the computational complexity objective will allow for proper selection between the two.

The idea that the order of magnitude of the SINR and MSE are equivalent for all constrained beamformers and choosing either allows for correct algorithm selection is corroborated with the output of scenario two as given in Table 17. For the particular scenario the TRM SINR and MSE are an order of magnitude better than either LCMV algorithm. The two LCMV algorithms (purely constrained algorithms) have comparable SINR out and MSE values where the algorithm with the better SINR out has the better MSE as predicted by Goldstein [25]. In this case the RM selects the narrowband LCMV algorithm as all algorithms have an SINR out that meets the threshold and the narrowband LCMV has the lowest computational complexity. The results from scenario one are repeated for scenario three where the wideband LCMV algorithm provides the best MSE and SINR of the constrained algorithms. Once again the TRM has a lower SINR and MSE with the difference attributable to the the algorithm not being a purely constrained beamformer. The results again, i.e. choosing the wideband LCMV algorithm, are correct because the wideband LCMV algorithm has a lower computational complexity than the TRM algorithm.

The analysis of the data from the three scenarios given above demonstrates that SINR out is an appropriate metric for comparing adaptive DBF performance. This is because the post processing algorithms that use the beamformer output require a given SINR output level to properly operate, which may justify the use of SINR out-

178

Table 17. A comparison of the MSE and SINR improvement metrics for use in evaluating adaptive DBF performance.

	Scenario 1		
	WB Frost	TRM	NB Frost
MSE	3.785×10^{-3}	1.657×10^{-3}	7.199×10^{-2}
SINR	22.48	16.08	4.06
	Scenario 2		
	WB Frost	TRM	NB Frost
MSE	7.140×10^{-3}	4.793×10^{-4}	3.221×10^{-3}
SINR	12.26	20.01	13.06
	Scenario 3		
	WB Frost	TRM	NB Frost
MSE	4.416×10^{-3}	1.528×10^{-3}	6.440×10^{-2}
SINR	19.07	15.77	3.78

put as a metric by itself. When MSE and SOI estimate accuracy are considered, the work of Goldstein taken with the above empirical results indicate that the algorithm with the highest SINR output will provide and estimate with the lowest possible order of magnitude MSE compared to all other algorithms. When used for algorithm selection the second objective of computational complexity ensures the correct adaptive DBF algorithm is chosen when the other criteria is SINR improvement even when Goldstein's analysis is not applicable.

Acronyms

ADC . . . . analog to digital converter

AFRL . . . . Air Force Research Laboratory

AIC . . . . Akaike information criteria

ASP . . . . algorithm selection problem

CR . . . . cognitive radio

CRLB . . . . Cramer-Rao lower bound

CW . . . . continuous wave

DBF . . . . digital beamforming

DFT . . . . discrete Fourier transform

DOA . . . . direction-of-arrival

DPSS . . . . discrete prolate spheroidal sequence

DSP . . . . digital signal processing

EM . . . . electromagnetic

ES . . . . electronic support

FFT . . . . fast Fourier transform

FIB . . . . frequency invariant beamformer

FIR . . . . finite impulse response

FOV   . . . . field-of-view

FPGA   . . . . field programmable gate array

GDFT   . . . . generalized discrete Fourier transform

GLRT . . . . generalized likelihood ratio test

GPU   . . . . graphics processing unit

GSM   . . . . global system for mobile

HVT   . . . . high value target

IADS   . . . . integrated air defense system

IF   . . . . intermediate frequency

IFFT   . . . . inverse fast Fourier transform

IFT   . . . . inverse Fourier transform

INR   . . . . interference-to-noise-ratio

ISLR   . . . . integrated sidelobe ratio

ISR   . . . . interference-to-signal-ratio

LCMV   . . . . linearly constrained minimum variance

LMS . . . . least mean squares

LRT . . . . likelihood ratio test

LS . . . . least squares

LSSB . . . . least squares space-time beamformer

LUT . . . . look-up-table

MIMO . . . . multiple-input multiple-output

MLE . . . . maximum likelihood estimator

MMSE . . . . minimum mean squared error

MSE . . . . mean square error

MTM . . . . multi-taper method

MUSIC . . . . multi-signal classification

MVDR . . . . minimum variance distortionless response

PDW . . . . pulse descriptor word

PSD . . . . power spectral density

PSLR . . . . peak sidelobe ratio

RF . . . . radio frequency

RM . . . . resource manager

RWR . . . . radar warning receiver

SAR . . . . synthetic aperture radar

SDP . . . . semi-definite programming

SINR . . . . signal-to-interference-plus-noise ratio

SMI . . . . sample matrix inversion

SNR . . . . signal-to-noise-ratio

SOI . . . . signal-of-interest

SV . . . . spatial variation

TOT . . . . three-of-three

TRM . . . . time reversal method

ULA . . . . uniform linear array

Bibliography

[1] M. Agrawal and S. Prasad, "Robust adaptive beamforming for wide-band, moving, and coherent jammers via uniform linear arrays," *IEEE Transactions on Antennas and Propagation*, vol. 47, no. 8, pp. 1267–1275, 1999.

[2] S. Applebaum, "Adaptive arrays," *IEEE Transactions on Antennas and Propagation*, vol. 24, no. 5, pp. 585–598, 1976.

[3] J.-H. Baek, H.-J. Oh, and S.-H. Hwang, "Improved reliability of spectrum sensing using energy detector in cognitive radio system," in *10th International Conference on Advanced Communication Technology (ICACT 2008)*, vol. 1, 2008, pp. 575–578.

[4] Z. Bai, *Templates for the Solution of Algebraic Eigenvalue Problems: A Practical Guide*, ser. SIAM e-books. Society for Industrial and Applied Mathematics, 2000.

[5] C. Balanis, *Antenna Theory: Analysis and Design.* John Wiley, 2005.

[6] S. Boll, "Suppression of acoustic noise in speech using spectral subtraction," *IEEE Transactions on Acoustics, Speech and Signal Processing*, vol. 27, no. 2, pp. 113–120, 1979.

[7] S. Boyd and L. Vandenberghe, *Convex Optimization.* Cambridge University Press, 2004.

[8] J. A. Cadzow, "Multiple source location-the signal subspace approach," *IEEE Transactions on Acoustics, Speech and Signal Processing*, vol. 38, no. 7, pp. 1110–1125, 1990.

[9] J. A. Cadzow, "Multiple source location: The signal subspace approach," in *Twenty-Third Asilomar Conference on Signals, Systems and Computers*, vol. 2, 1989, pp. 777–781.

[10] J. Capon, "High-resolution frequency-wavenumber spectrum analysis," *Proceedings of the IEEE*, vol. 57, no. 8, pp. 1408–1418, 1969.

[11] T.-W. Chiang, J.-M. Lin, and H.-P. Ma, "Optimal detector for multitaper spectrum estimator in cognitive radios," in *IEEE Global Telecommunications Conference (GLOBECOM 2009)*, Dec. 2009, pp. 1–6.

[12] M. Coker and E. Ferrara, "A new method for multiple source location," in *IEEE International Conference on Acoustics, Speech, and Signal Processing, ICASSP '82.*, vol. 7, May 1982, pp. 411– 415.

[13] J. Compton, R. T., "The relationship between tapped delay-line and fft processing in adaptive arrays," *IEEE Transactions on Antennas and Propagation*, vol. 36, no. 1, pp. 15–26, 1988.

[14] T. Cormen, C. Leiserson, R. Rivest, and C. Stein, *Introduction to Algorithms*. Mit Press, 2009.

[15] R. C. Davis, L. E. Brennan, and L. S. Reed, "Angle estimation with adaptive arrays in external noise fields," *IEEE Transactions on Aerospace and Electronic Systems*, vol. AES-12, no. 2, pp. 179–186, 1976.

[16] K. Dong, N. Prasad, X. Wang, and S. Zhu, "Adaptive antenna selection and Tx/Rx beamforming for large-scale MIMO systems in 60 GHz channels," *EURASIP Journal on Wireless Communications and Networking*, no. 1, pp. 1–14, 2011.

[17] M. A. Doron and A. J. Weiss, "On focusing matrices for wide-band array processing," *IEEE Transactions on Signal Processing*, vol. 40, no. 6, pp. 1295–1302, 1992.

[18] W. P. du Plessis, P. F. Potgieter, M. Gouws, and E. Malan, "Initial results for compressive sensing in electronic support receiver systems," in *2011 Saudi International Electronics, Communications and Photonics Conference (SIECPC)*, Apr. 2011, pp. 1–6.

[19] A. Elnakib, G. Gimel'farb, T. Inanc, and A. El-Baz, "Modified Akaike information criterion for estimating the number of components in a probability mixture model," in *19th IEEE International Conference on Image Processing (ICIP)*, 2012, pp. 2497–2500.

[20] M. H. Er, "Linear antenna array pattern synthesis with prescribed broad nulls," *IEEE Transactions on Antennas and Propagation*, vol. 38, no. 9, pp. 1496–1498, 1990.

[21] O. L. Frost, "An algorithm for linearly constrained adaptive array processing," *Proceedings of the IEEE*, vol. 60, no. 8, pp. 926–935, 1972.

[22] W. F. Gabriel, "Adaptive arrays an introduction," *Proceedings of the IEEE*, vol. 64, no. 2, pp. 239–272, 1976.

[23] A. Gangi, "The active adaptive antenna array system," *IEEE Transactions on Antennas and Propagation*, vol. 11, no. 4, pp. 405–414, 1963.

[24] R. Ghose, "Electronically adaptive antenna systems," *IEEE Transactions on Antennas and Propagation*, vol. 12, no. 2, pp. 161–169, 1964.

[25] J. S. Goldstein and I. S. Reed, "Performance measures for optimal constrained beamformers," *IEEE Transactions on Antennas and Propagation*, vol. 45, no. 1, pp. 11–14, 1997.

[26] L. J. Griffiths, "A comparison of multidimensional Wiener and maximum-likelihood filters for antenna arrays," *Proceedings of the IEEE*, vol. 55, no. 11, pp. 2045–2047, 1967.

[27] L. J. Griffiths, "A simple adaptive algorithm for real-time processing in antenna arrays," *Proceedings of the IEEE*, vol. 57, no. 10, pp. 1696–1704, 1969.

[28] M. Harteneck, J. M. Paez-Borrallo, and R. W. Stewart, "Filterbank design for oversampled filter banks without aliasing in the subbands," *Electronics Letters*, vol. 33, no. 18, pp. 1538–1539, 1997.

[29] M. Harteneck and R. W. Stewart, "An oversampled filter bank with different analysis and synthesis filters for the use with adaptive filters," in *Conference Record of the Thirty-First Asilomar Conference on Signals, Systems and Computers*, vol. 2, 1997, pp. 1274–1278.

[30] M. Harteneck and R. W. Stewart, "A subband adaptive filter," in *IEE Colloquium on Adaptive Signal Processing for Mobile Communication Systems*, 1997, pp. 1–6.

[31] S. Haykin, *Cognitive Dynamic Systems: Perception-Action Cycle, Radar and Radio.* Cambridge University Press, 2012.

[32] S. Haykin, D. J. Thomson, and J. H. Reed, "Spectrum sensing for cognitive radio," *Proceedings of the IEEE*, vol. 97, no. 5, pp. 849–877, May 2009.

[33] S. Haykin, *Adaptive Filter Theory*, 4th ed. Upper Saddle River, N.J.: Prentice Hall, 2002.

[34] S. Haykin, "Cognitive radio: Brain-empowered wireless communications," *IEEE Journal on Selected Areas in Communications*, vol. 23, no. 2, pp. 201–220, 2005.

[35] S. Haykin, "Cognitive radar: A way of the future," *IEEE Signal Processing Magazine*, vol. 23, no. 1, pp. 30–40, 2006.

[36] W. Herbordt, H. Buchner, S. Nakamura, and W. Kellermann, "Multichannel bin-wise robust frequency-domain adaptive filtering and its application to adaptive beamforming," *IEEE Transactions on Audio, Speech, and Language Processing*, vol. 15, no. 4, pp. 1340–1351, 2007.

[37] W. Hong and A. H. Tewfik, "Focusing matrices for wideband array processing with no a priori angle estimates," in *IEEE International Conference on Acoustics, Speech, and Signal Processing, ICASSP-92*, vol. 2, 1992, pp. 493–496.

[38] Y.-J. Hong, S. M. Kim, and D. K. Sung, "Adaptive random beamforming with interference suppression and beam selection in cellular networks," in *IEEE Global Telecommunications Conference, GLOBECOM 2009*, 2009, pp. 1–6.

[39] Z. Hu, N. Guo, R. Qiu, J. Bonior, L. Liou, D. Lin, M. Longbrake, P. Buxa, T. Dalrymple, S. Hary, and J. Tsui, "Robust wideband beamforming," in *Proceedings of the IEEE 2010 National Aerospace and Electronics Conference (NAECON)*, Jul. 2010, pp. 60–64.

[40] Z. Hu, N. Guo, R. Qiu, J. Bonior, L. Liou, D. Lin, M. Longbrake, P. Buxa, T. Dalrymple, S. Hong, S. Hary, and J. Tsui, "Design of look-up table based architecture for wideband beamforming," in *2010 International Waveform Diversity and Design Conference (WDD)*, Aug. 2010, pp. 1–5.

[41] H. Hung and M. Kaveh, "A new class of focussing matrices for coherent signal-subspace method," in *1988 International Conference on Acoustics, Speech, and Signal Processing, ICASSP-88.*, 1988, pp. 2284–2287.

[42] N. K. Jablon, "On the complexity of frequency-domain adaptive filtering," *IEEE Transactions on Signal Processing*, vol. 39, no. 10, pp. 2331–2334, 1991.

[43] M. K. Jataprolu, R. D. Koilpillai, and S. Bhashyam, "Optimal MTM spectral estimation based detection for cognitive radio in HDTV," in *2012 National Conference on Communications (NCC)*, Feb. 2012, pp. 1–5.

[44] S. Kay, "Broadband detection of signals with unknown spectra," in *IEEE International Conference on Acoustics, Speech, and Signal Processing, ICASSP '85.*, vol. 10, 1985, pp. 1263–1265.

[45] S. M. Kay, *Fundamentals of Statistical Signal Processing: Detection theory.* Prentice-Hall PTR, 1998.

[46] S. Kay, *Intuitive Probability and Random Processes using MATLAB®.* Springer, 2006.

[47] S. M. Kay, *Modern spectral estimation : Theory and Application*, ser. Prentice-Hall signal processing series. Englewood Cliffs, N.J.: Prentice Hall, 1988.

[48] J. M. Khalab and M. S. Woolfson, "Efficient multirate adaptive beamforming technique," *Electronics Letters*, vol. 30, no. 25, pp. 2102–2103, Dec. 1994.

[49] R. W. Klein, M. A. Temple, and M. J. Mendenhall, "Application of wavelet-based RF fingerprinting to enhance wireless network security," *Journal of Communications and Networks*, vol. 11, no. 6, pp. 544–555, 2009.

[50] J. Kleinberg and É. Tardos, *Algorithm Design.* Pearson/Addison-Wesley, 2006.

[51] L. Kotthoff, "Algorithm selection for combinatorial search problems: A survey," *Computing Research Repository, CoRR*, 2012.

[52] H. J. Landau and H. O. Pollak, "Prolate spheroidal wave functions, fourier analysis and uncertainty-ii," *Bell System Technical Journal*, vol. 40, pp. 65–84, Jan. 1961.

[53] H. J. Landau and H. O. Pollak, "Prolate spheroidal wave functions, fourier analysis and uncertainty-iii: The dimension of the space of essentially time and band-limited signals," *Bell System Technical Journal*, vol. 41, pp. 1295–1336, Jul. 1962.

[54] A. Lee, L. Chen, A. Song, J. Wei, and H. K. Hwang, "Simulation study of wideband interference rejection using adaptive array antenna," in *2005 IEEE Aerospace Conference*, 2005, pp. 1–6.

[55] N. Levanon and E. Mozeson, *Radar Signals.* J. Wiley, 2004.

[56] D. M. Lin, L. L. Liou, and J. B. Y. Tsui, "Directional wide band time reversal digital beam forming FIR filter design using bore-sight calibration data," in *Proceedings of the IEEE 2010 National Aerospace and Electronics Conference (NAECON)*, 2010, pp. 215–222.

[57] L. L. Liou, D. M. Lin, M. Longbrake, P. Buxa, J. McCann, T. Dalrymple, J. B. Tsui, R. Qiu, H. Zhen, and G. Nan, "Digital wideband phased array calibration and beamforming using time reversal technique," in *2010 IEEE International Symposium on Phased Array Systems and Technology (ARRAY)*, 2010, pp. 261–266.

[58] W. Liu and S. Weiss, *Wideband Beamforming: Concepts and Techniques*, ser. Wireless Communications and Mobile Computing. Wiley, 2010.

[59] W. Liu, D. C. McLernon, and M. Ghogho, "Design of frequency invariant beamformer without temporal filtering," *IEEE Transactions on Signal Processing*, vol. 57, no. 2, pp. 798–802, Feb. 2009.

[60] W. Liu and S. Weiss, "New class of broadband arrays with frequency invariant beam patterns," in *IEEE International Conference on Acoustics, Speech, and Signal Processing Proceedings. (ICASSP '04).*, vol. 2, May 2004, pp. 185–188.

[61] W. Liu and S. Weiss, "Design of frequency-invariant beamformers employing multi-dimensional Fourier transforms," in *The Fourth International Workshop on Multidimensional Systems, NDS 2005.*, Jul. 2005, pp. 19–23.

[62] W. Liu and S. Weiss, "Design of frequency invariant beamformers for broadband arrays," *IEEE Transactions on Signal Processing*, vol. 56, no. 2, pp. 855–860, 2008.

[63] W. Liu and S. Weiss, "Design of frequency invariant beamformers for broadband arrays," *IEEE Transactions on Signal Processing*, vol. 56, no. 2, pp. 855–860, Feb. 2008.

[64] W. Liu, S. Weiss, and L. Hanzo, "A novel method for partially adaptive broadband beamforming," in *2001 IEEE Workshop on Signal Processing Systems*, 2001, pp. 361–372.

[65] W. Liu, R. Wu, and R. J. Langley, "Design and analysis of broadband beamspace adaptive arrays," *IEEE Transactions on Antennas and Propagation*, vol. 55, no. 12, pp. 3413–3420, Dec. 2007.

[66] G. Masini, E. Segre, and F. Stella, *Marconi*. Marsilio Publishers, 1998.

[67] J. Mayhan, A. Simmons, and W. Cummings, "Wide-band adaptive antenna nulling using tapped delay lines," *IEEE Transactions on Antennas and Propagation*, vol. 29, no. 6, pp. 923–936, Nov. 1981.

[68] R. Merched and A. H. Sayed, "An embedding approach to frequency-domain and subband adaptive filtering," *IEEE Transactions on Signal Processing*, vol. 48, no. 9, pp. 2607–2619, 2000.

[69] B. Mondal and R. W. Heath, "Channel adaptive quantization for limited feedback MIMO beamforming systems," *IEEE Transactions on Signal Processing*, vol. 54, no. 12, pp. 4717–4729, 2006.

[70] R. A. Monzingo and T. W. Miller, *Introduction to Adaptive Arrays*. Scitech, 2004.

[71] Naval Air Warfare Center Weapons Div Point Mugu, CA, *Electronic Warfare and Radar Systems Engineering Handbook*. Storming Media, 1997.

[72] M. Neinhus and K. Solbach, "Finite impulse response-filter-based RF-beamforming network for wideband and ultra-wideband antenna arrays," *IET Microwaves, Antennas Propagation*, vol. 5, no. 7, pp. 844–851, 2011.

[73] T. Q. Nguyen, "Near-perfect-reconstruction pseudo-QMF banks," *IEEE Transactions on Signal Processing*, vol. 42, no. 1, pp. 65–76, 1994.

[74] K. Nishikawa, T. Yamamoto, K. Oto, and T. Kanamori, "Wideband beamforming using fan filter," in *1992 IEEE International Symposium on Circuits and Systems Proceedings, ISCAS '92.*, vol. 2, 1992, pp. 533–536.

[75] S. Ohno and H. Sakai, "Spectral analysis of subband adaptive digital filters," *IEEE Transactions on Signal Processing*, vol. 48, no. 1, pp. 254–257, 2000.

[76] C. Oliver and S. Quegan, *Understanding Synthetic Aperture Radar Images*, ser. SciTech radar and defense series. SciTech Publ., 2004.

[77] A. V. Oppenheim and R. W. Schafer, *Discrete-Time Signal Processing*. Prentice Hall, 2010.

[78] Y.-H. Pan, B. K. Letaief, and Z. Cao, "Adaptive beamforming with antenna selection in MIMO systems," in *IEEE 60th Vehicular Technology Conference, VTC2004.*, vol. 3, 2004, pp. 1570–1574.

[79] D. B. Percival and A. T. Walden, *Spectral Analysis for Physical Applications*. Cambridge University Press, 1993.

[80] B. Porat, *A Course in Digital Signal Processing*. John Wiley, 1997.

[81] B. Porat and B. Friedlander, "Estimation of spatial and spectral parameters of multiple sources," *IEEE Transactions on Information Theory*, vol. 29, no. 3, pp. 412–425, May 1983.

[82] C. Radhakrishnan and W. K. Jenkins, "Fault tolerant adaptive filters based on modified discrete Fourier transform architectures," in *2011 IEEE International Symposium on Circuits and Systems (ISCAS)*, 2011, pp. 1271–1274.

[83] J. G. Reid, *Linear System Fundamentals: Continuous and Discrete, Classic and Modern*, ser. McGraw-Hill series in electrical engineering: Networks and systems. McGraw-Hill, 1983.

[84] D. R. Reising, M. A. Temple, and M. J. Mendenhall, "Improving intra-cellular security using air monitoring with RF fingerprints," in *2010 IEEE Wireless Communications and Networking Conference (WCNC)*, 2010, pp. 1–6.

[85] J. R. Rice, "The algorithm selection problem," *Advances in Computers*, vol. 15, 1976.

[86] W. E. Rodgers and R. T. Compton, "Adaptive array bandwidth with tapped delay-line processing," *IEEE Transactions on Aerospace and Electronic Systems*, vol. AES-15, no. 1, pp. 21–28, Jan. 1979.

[87] M. Rossi, J.-Y. Zhang, and W. Steenaart, "Iterative least squares design of perfect reconstruction QMF banks," in *Canadian Conference on Electrical and Computer Engineering*, vol. 2, 1996, pp. 762–765.

[88] W. Rotman and R. Turner, "Wide-angle microwave lens for line source applications," *IEEE Transactions on Antennas and Propagation*, vol. 11, no. 6, pp. 623–632, 1963.

[89] D. Ruiyan, W. Jinkuan, L. Fulai, and Z. Qinping, "An effective nulls control method," in *3rd IEEE International Symposium on Microwave, Antenna, Propagation and EMC Technologies for Wireless Communications*, 2009, pp. 666–668.

[90] F. A. Sakarya, G. S. Nagel, L. H. Tran, and J. A. Molnar, "Wideband compressed sensing for cognitive radios," in *Military Communications Conference, MILCOM.*, 2011, pp. 31–36.

[91] R. Schmidt, "Multiple emitter location and signal parameter estimation," *IEEE Transactions on Antennas and Propagation*, vol. 34, no. 3, pp. 276–280, 1986.

[92] T. Sekiguchi and Y. Karasawa, "Wideband beamspace adaptive array utilizing FIR fan filters for multibeam forming," *IEEE Transactions on Signal Processing*, vol. 48, no. 1, pp. 277–284, Jan. 2000.

[93] A. Shaw and R. Kumaresan, "Estimation of angles of arrival of broadband signals," in *IEEE International Conference on Acoustics, Speech, and Signal Processing, ICASSP '87.*, vol. 12, Apr. 1987, pp. 2296–2299.

[94] J. J. Shynk, "Frequency-domain and multirate adaptive filtering," *IEEE Signal Processing Magazine*, vol. 9, no. 1, pp. 14–37, 1992.

[95] S. Sivanand, J. F. Yang, and M. Kaveh, "Focusing filters for wide-band direction finding," *IEEE Transactions on Signal Processing*, vol. 39, no. 2, pp. 437–445, Feb. 1991.

[96] B. Sklar, *Digital Communications: Fundamentals and Applications*, ser. Prentice Hall Communications Engineering and Emerging Technologies Series. Prentice-Hall PTR, 2001.

[97] M. I. Skolnik, *Introduction to Radar Systems*, ser. McGraw-Hill International Editions. McGraw-Hill, 2001.

[98] D. Slepian, "Prolate spheroidal wave functions, fourier analysis and uncertainty-iv: Extensions to many dimensions; generalized prolate spheroidal functions," *Bell System Technical Journal*, vol. 43, pp. 3009–3057, Nov. 1964.

[99] D. Slepian, "Prolate spheroidal wave functions, Fourier analysis, and uncertainty - the discrete case," *ATT Technical Journal*, vol. 57, pp. 1371–1430, Jun. 1978.

[100] D. Slepian and H. O. Pollak, "Prolate spheroidal wave functions, fourier analysis and uncertainty-i," *Bell System Technical Journal*, vol. 40, pp. 43–63, Jan. 1961.

[101] J. S. Soo and K. K. Pang, "Multidelay block frequency domain adaptive filter," *IEEE Transactions on Acoustics, Speech and Signal Processing*, vol. 38, no. 2, pp. 373–376, 1990.

[102] T. Strohmer, M. Emami, J. Hansen, G. Papanicolaou, and A. J. Paulraj, "Application of time-reversal with MMSE equalizer to UWB communications," in *IEEE Global Telecommunications Conference GLOBECOM '04*, vol. 5, 2004, pp. 3123–3127.

[103] G. Su and M. Morf, "Modal decomposition signal subspace algorithms," in *IEEE International Conference on Acoustics, Speech, and Signal Processing, ICASSP '83.*, vol. 8, Apr. 1983, pp. 340–343.

[104] R. Sullivan, *Radar Foundations for Imaging and Advanced Concepts.* SciTech Pub., 2004.

[105] C. Tarran, M. Mitchell, and R. Howard, "Wideband phased array radar with digital adaptive beamforming," in *High Resolution Radar and Sonar IEE Colloquium*, 1999, pp. 1/1–1/7.

[106] J. D. Taylor, *Introduction to Ultra-Wideband Radar systems.* CRC Press, 1995.

[107] J. D. Taylor, *Ultra-Wideband Radar Technology.* CRC Press, 2001.

[108] I. Thng, A. Cantoni, and Y. H. Leung, "Derivative constrained optimum broadband antenna arrays," *IEEE Transactions on Signal Processing*, vol. 41, no. 7, pp. 2376–2388, Jul. 1993.

[109] D. J. Thomson, "Spectrum estimation and harmonic analysis," *Proceedings of the IEEE*, vol. 70, no. 9, pp. 1055–1096, Sep. 1982.

[110] D. J. Thomson, "An overview of multiple-window and quadratic-inverse spectrum estimation methods," in *IEEE International Conference on Acoustics, Speech, and Signal Processing, ICASSP-94.*, vol. vi, Apr. 1994, pp. 185–194.

[111] Z. Tian and G. B. Giannakis, "A wavelet approach to wideband spectrum sensing for cognitive radios," in *1st International Conference on Cognitive Radio Oriented Wireless Networks and Communications*, Jun. 2006, pp. 1–5.

[112] J. Tsui, *Digital Techniques for Wideband Receivers.* SciTech Publishing, Incorporated, 2004.

[113] H. L. Van Trees, *Detection, Estimation, and Modulation Theory*, ser. Detection, Estimation, and Modulation Theory. John Wiley & Sons, 2004, no. pt. 1.

[114] H. L. Van Trees, *Detection, Estimation, and Modulation Theory, Optimum Array Processing*, ser. Detection, Estimation, and Modulation Theory. Wiley, 2004.

[115] J. L. Vicario, R. Bosisio, and U. Spagnolini, "Adaptive beam selection techniques for opportunistic beamforming," in *IEEE 17th International Symposium on Personal, Indoor and Mobile Radio Communications*, 2006, pp. 1–5.

[116] F. W. Vook and J. Compton, R. T., "Bandwidth performance of linear adaptive arrays with tapped delay-line processing," *IEEE Transactions on Aerospace and Electronic Systems*, vol. 28, no. 3, pp. 901–908, 1992.

[117] R. H. Walden, "Analog-to-digital converter technology comparison," in *16th Annual Gallium Arsenide Integrated Circuit (GaAs IC) Symposium Technical Digest*, 1994, pp. 217–219.

[118] F. Wang, V. Balakrishnan, P. Zhou, J. Chen, R. Yang, and C. Frank, "Optimal array pattern synthesis using semidefinite programming," in *Acoustics, Speech, and Signal Processing, 2001. Proceedings. (ICASSP '01). 2001 IEEE International Conference on*, vol. 5, 2001, pp. 2925 –2928 vol.5.

[119] F. Wang, J. Litva, and T. Lo, "Performance analysis of broadband adaptive digital beamforming," in *Antennas and Propagation Society International Symposium AP-S. Digest*, 1993, pp. 1884–1887.

[120] F. Wang, V. Balakrishnan, P. Zhou, J. Chen, R. Yang, and C. Frank, "Optimal array pattern synthesis using semidefinite programming," *Signal Processing, IEEE Transactions on*, vol. 51, no. 5, pp. 1172 – 1183, may 2003.

[121] F. Wang, J. Litva, and T. Lo, "Performance of broadband adaptive digital beamforming in communication," in *23rd European Microwave Conference*, 1993, pp. 113–115.

[122] H. Wang and M. Kaveh, "Coherent signal-subspace processing for the detection and estimation of angles of arrival of multiple wide-band sources," *IEEE Transactions on Acoustics, Speech and Signal Processing*, vol. 33, no. 4, pp. 823–831, 1985.

[123] J. Wang and Q. T. Zhang, "A multitaper spectrum based detector for cognitive radio," in *IEEE Wireless Communications and Networking Conference, WCNC 2009.*, 2009, pp. 1–5.

[124] M. Wax and T. Kailath, "Optimum localization of multiple sources by passive arrays," *IEEE Transactions on Acoustics, Speech and Signal Processing*, vol. 31, no. 5, pp. 1210–1217, Oct. 1983.

[125] M. Wax and T. Kailath, "Detection of signals by information theoretic criteria," *IEEE Transactions on Acoustics, Speech and Signal Processing*, vol. 33, no. 2, pp. 387–392, 1985.

[126] S. Weiss, M. Harteneck, and R. W. Stewart, "On implementation and design of filter banks for subband adaptive systems," in *1998 IEEE Workshop on Signal Processing Systems, SIPS 98.*, 1998, pp. 172–181.

[127] S. Weiss, R. W. Stewart, M. Schabert, I. K. Proudler, and M. W. Hoffman, "An efficient scheme for broadband adaptive beamforming," in *Conference Record of the Thirty-Third Asilomar Conference on Signals, Systems, and Computers*, vol. 1, Oct. 1999, pp. 496–500.

[128] S. Weiss, R. Stewart, M. Harteneck, and A. Stenger, "Polyphase analysis of subband adaptive filters," in *Conference Record of the Thirty-Third Asilomar Conference on Signals, Systems, and Computers*, vol. 2, 1999, pp. 903–907.

[129] B. Widrow, P. E. Mantey, L. J. Griffiths, and B. B. Goode, "Adaptive antenna systems," *Proceedings of the IEEE*, vol. 55, no. 12, pp. 2143–2159, 1967.

[130] R. G. Wilson, "Digitally controlled receiver," *IEEE Transactions on Aerospace and Electronic Systems*, vol. 2, no. 5, pp. 544–549, 1966.

[131] S.-P. Wu, S. Boyd, and L. Vandenberghe, "FIR filter design via semidefinite programming and spectral factorization," in *Proceedings of the 35th IEEE Conference on Decision and Control*, vol. 1, 1996, pp. 271–276.

[132] M. Zatman and E. Baranoski, "Time delay steering architectures for space-time adaptive processing," in *Antennas and Propagation Society International Symposium*, vol. 4, 1997, pp. 2426–2429.

[133] Q. T. Zhang, "Multitaper based spectrum sensing for cognitive radio: Design and performance," in *IEEE 73rd Vehicular Technology Conference (VTC Spring)*, 2011, pp. 1–5.

[134] Y. Zhao, W. Liu, and R. Langley, "Application of the least squares approach to fixed beamformer design with frequency-invariant constraints," *IET Signal Processing*, vol. 5, no. 3, pp. 281–291, Jun. 2011.

[135] Y. Zhao, W. Liu, and R. J. Langley, "Subband design of fixed wideband beamformers based on the least squares approach," *Signal Processing*, vol. 91, no. 4, pp. 1060 – 1065, 2011.

[136] Y. Zhao, W. Liu, and R. Langley, "Design of frequency invariant beamformers in subbands," in *IEEE/SP 15th Workshop on Statistical Signal Processing, SSP '09.*, Sep. 2009, pp. 201–204.

[137] Y. Zhao, L. Wei, and R. Langley, "A least squares approach to the design of frequency invariant beamformers," in *17th European Signal Processing Conference*, Glasgow, Scotland, Aug. 2009, pp. 844–848.

REPORT DOCUMENTATION PAGE

Form Approved
OMB No. 0704–0188

1. REPORT DATE (DD–MM–YYYY)	2. REPORT TYPE	3. DATES COVERED (From — To)
27-12-2013	Dissertation	Aug 2010 – 26 Dec 2013

4. TITLE AND SUBTITLE

Development of a Resource Manager Framework for Adaptive Beamformer Selection

5a. CONTRACT NUMBER

5b. GRANT NUMBER

5c. PROGRAM ELEMENT NUMBER

6. AUTHOR(S)

Stringer, Jeremy P, Maj

5d. PROJECT NUMBER

5e. TASK NUMBER

5f. WORK UNIT NUMBER

7. PERFORMING ORGANIZATION NAME(S) AND ADDRESS(ES)

Air Force Institute of Technology
Graduate School of Engineering and Management (AFIT/ENY)
2950 Hobson Way
WPAFB OH 45433-7765

8. PERFORMING ORGANIZATION REPORT NUMBER

AFIT-ENG-DS-13-D-01

9. SPONSORING / MONITORING AGENCY NAME(S) AND ADDRESS(ES)

AFRL/RYDR
Peter Buxa
2241 Avionics Circle
Area B Bldg 620
WPAFB, OH 45433-7301

10. SPONSOR/MONITOR'S ACRONYM(S)

AFRL/RYDR

11. SPONSOR/MONITOR'S REPORT NUMBER(S)

12. DISTRIBUTION / AVAILABILITY STATEMENT

APPROVED FOR PUBLIC RELEASE; DISTRIBUTION UNLIMITED

13. SUPPLEMENTARY NOTES   This material is declared a work of the U.S. Government and is not subject to copyright protection in the United States.

14. ABSTRACT

Adaptive digital beamforming (DBF) algorithms are designed to mitigate the effects of interference and noise in the electromagnetic (EM) environment encountered by modern electronic support (ES) receivers. Traditionally, an ES receiver employs a single adaptive DBF algorithm that is part of the design of the receiver system. While the traditional form of receiver implementation is effective in many scenarios it has inherent limitations.

This dissertation proposes a new ES receiver framework capable of overcoming the limitations of traditional ES receivers. The proposed receiver framework is capable of forming multiple, independent, simultaneous adaptive digital beams toward multiple signals of interest in an electromagnetic environment. The main contribution of the research is the development, validation, and verification of a resource manager (RM) algorithm. The RM estimates a set of parameters that characterizes the electromagnetic environment and selects an adaptive digital beam forming DBF algorithm for implementation toward all each signal of interest (SOI) in the environment. Adaptive DBF algorithms are chosen by the RM based upon their signal to interference plus noise ratio (SINR) improvement ratio and their computational complexity. The proposed receiver framework is demonstrated to correctly estimate the desired electromagnetic parameters and select an adaptive DBF from the LUT.

15. SUBJECT TERMS

Adaptive Arrays, Beamforming

16. SECURITY CLASSIFICATION OF:			17. LIMITATION OF ABSTRACT	18. NUMBER OF PAGES	19a. NAME OF RESPONSIBLE PERSON
a. REPORT	b. ABSTRACT	c. THIS PAGE	UU	208	LtCol Geoffrey A Akers, AFIT/ENG
U	U	U			19b. TELEPHONE NUMBER (Include Area Code) (937)255-3636, 4659

Standard Form 298 (Rev. 8–98)
Prescribed by ANSI Std. Z39.18